

Smart crowding in poly-Acrylamide/Poly(N-isopropylacrylamide) composite hydrogels, studied by two-focus fluorescence correlation spectroscopy

Von der Fakultät für Mathematik, Informatik und Naturwissenschaften der
RWTH Aachen University zur Erlangung des akademischen Grades eines
Doktors der Naturwissenschaften genehmigte Dissertation

vorgelegt von

Diplomphysiker

Swen Lehmann

aus Düsseldorf

1. Bericht: Universitätsprofessor Dr. Walter Richtering
2. Bericht: Universitätsprofessor Dr. Alexander Böker

Tag der mündlichen Prüfung: 15. April 2015

Diese Dissertation ist auf den Internetseiten der Hochschulbibliothek online
verfügbar.

Erstgutachter: Universitätsprofessor Dr. Walter Richtering

Zweitgutachter: Universitätsprofessor Dr. Alexander Böker

Die vorliegende Arbeit entstand im Zeitraum von April 2008 bis Dezember 2014 am Institut für Physikalische Chemie der RWTH Aachen University.

Teile dieser Arbeit sind bereits veröffentlicht:

The role of the N-terminal domain in dimerization and nucleocytoplasmic shuttling of latent STAT3, *J. Cell Sci.* 2011

M. Vogt, T. Domszalai, D. Kleshchanok, S. Lehmann, A. Schmitt, V. Poli, W. Richtering, G. Müller-Newen

DOI: 10.1242/jcs.072520

Spatially Resolved Tracer Diffusion in Complex Responsive Hydrogels, *JACS* 2012

S. Lehmann, S. Seiffert, W. Richtering

DOI: 10.1021/ja306808j

Temperature-Sensitive Composite Hydrogels: Coupling Between Gel Matrix and Embedded Nano- and Microgels, *Prog. Colloid Polym. Sci.* 2013

J. Meid, S. Lehmann, W. Richtering

DOI: 10.1007/978-3-319-01683-2_8

Diffusion of mesoscopic actives within sensitive core–shell micogel carriers, *J. Colloid Interface Sci.* 2014

S. Lehmann, S. Seiffert, W. Richtering

DOI: 10.1016/j.jcis.2014.06.014

Refractive index mismatch can misindicate anomalous diffusion in single-focus fluorescence correlation spectroscopy, *Macromol. Chem. Phys.* 2014

S. Lehmann, S. Seiffert, W. Richtering

DOI: 10.1002/macp.201400349

Danksagung

Ich möchte mich zuallererst bei Herrn Prof. Dr. Walter Richtering bedanken. Ich danke ihm für sein Vertrauen, das sich nicht nur auf meine wissenschaftliche Arbeit, sondern auch auf die mir anvertraute Tätigkeit als Systemadministrator der Arbeitsgruppe erstreckte. Ich danke ihm ferner für die große Unterstützung, für die vielen wissenschaftlichen Diskussionen und für die Möglichkeit an Tagungen und Workshops teilnehmen zu können.

Ich danke Herrn Prof. Dr. Sebastian Seiffert von der Freien Universität Berlin für die Synthese der Beads und Kern-Schale-Teilchen und für den regen Austausch während der Erstellung der gemeinsamen Artikel. Ich konnte viel von dir lernen und auch die Anregungen und Diskussionen bei der Spezifikation der Teilcheneigenschaften haben mir sehr geholfen.

Außerdem bedanke ich mich bei Herrn Prof. Dr. Alexander Böker für die Übernahme der Begutachtung meiner Arbeit.

Ein weiterer großer Dank geht an die Mitglieder des Arbeitskreises, sowohl ehemalige als auch aktuelle. Ohne euch wäre das Arbeitsklima nicht so angenehm und die Zeit insgesamt nicht so schön gewesen. Ich danke euch für die vielen Diskussionen, Kickerspiele und die sehr schönen Grillabende. Ganz besonders bedanken möchte ich mich dabei bei Judith, Jochen, Bastian und Ting Ting, die mir vor allem zu Beginn meiner Arbeit, aber auch im späteren Verlauf, immer mit einem guten Rat oder einer guten Erklärung für mich da waren. Bei Ralph möchte ich mich ganz herzlich für die tolle Atmosphäre im Büro bedanken. Thomas, Stephan Felix und Christian danke ich für die Schnitzelrunde, die wir eine ganze Zeit lang pflegten. Die kurze Auszeit in der Mitte der

Woche hat immer viel neue Kraft gegeben. Felix und Christian danke ich auch für die Unterstützung bei der Fertigstellung meiner Dissertation, danke, dass ihr euch fürs Korrekturlesen Zeit genommen habt. Stephan und dem Rest vom Praktikumsteam danke ich für die tolle technische Unterstützung während der Versuchstage. Ihr habt mir die Betreuung der Studenten wirklich sehr erleichtert. Sonja Keimes danke ich für die hervorragende Zusammenarbeit bei der Administration der Arbeitsgruppe und dass du mir auch in der Zeit, nachdem ich nichtmehr im Arbeitskreis angestellt war, immer mit Rat und Tat zur Seite standest. Ohne dich hätte ich so manches Telefonat mit dem Rechenzentrum mehr führen müssen, um das zu erreichen, was du dort in einem Anruf erledigen konntest.

Ich möchte mich auch bei allen Mess-Gästen bedanken, bei Tamas, Katrin, Konstantina und all den anderen. Ihr habt mir mit euren Messungen und den Einblicken in eure Arbeiten, die ich genießen durfte, immer wieder neue Ideen und Blickwinkel ermöglicht.

Zu guter Letzt gilt mein ganz besonderer Dank meiner Familie, meinen Eltern, die mich in allem immer unterstütz haben und mich meinen Weg haben finden lassen. Meiner Frau Marina danke ich dabei besonders für ihre Unterstützung und den Ansporn, den sie mir immer wieder gab, wenn ich ins Stocken geraten bin. Du hast immer die richtigen Worte gefunden und mir den Halt gegeben, um meine Dissertation fertig zu stellen. Du hast immer an mich geglaubt und mir den Rücken gestärkt. Meinen Kindern Tobi und Tim danke ich, dass sie da sind und mich jeden Morgen die Welt mit anderen Augen sehen lassen. Ihr lasst mich weiter Fragen stellen und nach Antworten suchen, auch wenn es manchmal um ganz alltägliche Kleinigkeiten geht.

Allen, die ich bis hierhin vergessen habe, sei gesagt, ich danke auch euch, jeder Einzelne von euch hat seinen Beitrag geleistet, damit ich der geworden bin, der ich bin und das geschafft habe, was ich bis jetzt erreicht habe.

für Tobias, Tim und Marina

Abstract

The diffusion in complex media is of high interest for a broad range of applications. Fluorescence correlation spectroscopy (FCS) is often used to study diffusion in complex media, such as semi diluted polymer solutions, living cells or complex, heterogeneous hydrogel structures. In these media the refractive index usually differs from that of the immersion medium and is potentially changing across the sample. The two-focus fluorescence correlation spectroscopy (2fFCS) is known to be robust against the refractive index mismatch. In this work the 2fFCS is used to measure the diffusion in such complex media and the results are compared to single-focus FCS measurement results on the same samples to demonstrate the potential impact of the refractive index mismatch on the single-focus FCS measurement results. The diffusion of tagged dextran tracers in water, dilute dextran solutions, acrylamide monomer solutions, polyacrylamide polymer solutions, and a cross-linked polyacrylamide hydrogel is probed by 2fFCS. In these experiments, both the refractive index and the potential topological constraint and thermodynamic interaction to the probe diffusion is varied, and pairs of samples with same refractive indexes but different compositions are compared. Whereas 2fFCS shows no anomalous diffusion in any of them, single-focus FCS indicates anomalous diffusion. In particular, the values of the stretching exponent of the fluorescence autocorrelation function, which is often interpreted to reflect the extent of anomaly of diffusion, does not vary systematically with the extent of topological or thermodynamic complexity of the different matrixes, but with their refractive index. This shows that apparent anomalous diffusion in FCS is at risk to be the result of refractive index mismatch rather than reflecting truly complex diffusion.

Furthermore the 2fFCS has been used in a spatial resolved mode to study the diffusion in core-shell particles and thermo-responsive composite hydrogels.

The diffusion of payloads within core-shell carrier particles is of major relevance for drug-delivery applications. We use spatially resolved two-focus fluorescence correlation spectroscopy to quantify the diffusivity of different dextran molecules and colloids within carrier particles composed of a temperature-responsive poly(*N*-isopropylacrylamide) (PNIPAM) shell that surrounds a temperature-insensitive poly(acrylamide) (PAAM) core. The deswelling of the shell that occurs upon heating above the lower critical solution temperature of PNIPAM slightly slows down the diffusion of these tracer oligomers near the core-shell interface. By contrast, the mobility of the tracers inside the core is not affected by deswelling of the shell. This finding assures absence of artifacts such as adsorption of the guests to the amphiphilic shell polymer, supporting the utility of these microgel carriers in encapsulation and controlled release applications. Thermosensitive composite hydrogels that consist of a PAAM hydrogel matrix with embedded micrometre-sized PNIPAM microgel beads are promising models for complex, heterogeneous gels and living cells. The coupling of the microgel beads with the gel matrix and the formation of interpenetrating networks inside the microgels had been investigated by 2fFCS. This technique serves to study the effects of the heterogeneous structure of the composite hydrogels on the diffusive mobility of nanoscopic dextran tracers within the gels. The investigations reveal that the formation of interpenetrating networks inside the embedded microgel beads depends on their cross-link density: whereas interpenetrating networks are formed inside weakly cross-linked beads, they are not formed inside strongly cross-linked beads. If the formation of interpenetrating networks occurs, the temperature-dependent swelling and deswelling of the beads is

obstructed. In addition, the mobility of dextran tracers inside the embedded microgel beads is hindered compared to those in free beads and in the surrounding gel matrix. Surprisingly, the surrounding PAAM hydrogel matrix swells inhomogeneously when the embedded PNIPAM beads collapse upon heating. This indicates the formation of pores near the surface of the collapsed beads, offering promising means to tailor composite hydrogels for applications such as membranes with tunable permeability. This experiment also demonstrates the utility of 2fFCS to study spatially resolved diffusion in complex environments, which is of great interest in biomaterials research.

Kurzfassung

Die Diffusion in komplexen Medien ist von großem Interesse für eine breite Palette von Anwendungen. Fluoreszenzkorrelationsspektroskopie (FCS) wird oft verwendet, um eine Diffusion in komplexen Medien, wie halb verdünnten Polymerlösungen, lebenden Zellen oder komplexen, heterogenen Hydrogelen zu untersuchen. In diesen Medien unterscheidet sich in der Regel der Brechungsindex von dem des Immersionsmediums und möglicherweise ändert der Brechungsindex sich innerhalb der Probe. Die zwei-Focus-Fluoreszenzkorrelationsspektroskopie (2fFCS) ist bekannt dafür, gegenüber der Brechungsindex-Fehlanpassung unempfindlich zu sein. In dieser Arbeit wurden die Ergebnisse aus 2fFCS-Messungen mit den Ergebnissen aus Einzelfokus-FCS-Messungen in denselben Proben verglichen, um die möglichen Auswirkungen der Brechungsindex-Fehlanpassung auf die Einfokus-FCS-Messergebnisse zu demonstrieren. Die Diffusion von markierten Dextran-Tracern in Wasser, verdünnten Dextranlösungen, Acrylamid-Monomer-Lösungen, Polyacrylamid-(PAAM)-Polymerlösungen und ein vernetztes Polyacrylamid-Hydrogel wurden durch 2fFCS-Messungen sondiert. In diesen Experimenten sind sowohl der Brechungsindex, als auch die potentiellen topologischen Einschränkungen der thermodynamischen Wechselwirkung der Diffusion der Sondenmoleküle verändert worden und Probenpaare mit gleichem Brechungsindex, aber unterschiedlichen Zusammensetzungen verglichen worden. In allen gemessenen Proben zeigt die 2fFCS keine anomale Diffusion, wohingegen die Einfokus-FCS anomale Diffusion zeigt. Insbesondere haben sich die Werte des Exponenten der Fluoreszenzautokorrelationsfunktion, die oft interpretiert wird, um das Ausmaß der Anomalie der

Diffusion zu beschreiben, nicht systematisch mit dem Ausmaß der topologischen oder thermodynamischen Komplexität der verschiedenen Matrizen verändert, sondern abhängig vom Brechungsindex. Dies zeigt, dass das Auftreten von nicht ausreichend berücksichtigten Brechungsindexunterschieden die Gefahr birgt, als anomale Diffusion in FCS Messungen fehlinterpretiert zu werden.

Ferner wurde die 2fFCS in einem orts aufgelösten Modus verwendet, um die Diffusion in Kern-Schale-Partikel und temperaturabhängigen Verbund-Hydrogelen zu untersuchen. Die Diffusion von Wirkstoffmolekülen, sowohl innerhalb als auch hinein und hinaus, Kern-Schale-Trägerpartikel ist von großer Bedeutung für Wirkstofffreisetzungsanwendungen. Die Diffusion verschiedener Dextranmoleküle und Kolloide im Trägerpartikel wurde untersucht. Die Trägerpartikel bestehen dabei aus einer temperaturempfindlichen Poly(N-isopropylacrylamid)(PNIPAM)-Schale und einem temperaturunempfindlichen Poly(acrylamid)(PAAM)-Kern. Die Entquellung der Schale, welche beim Erhitzen der Probe oberhalb der unteren kritischen Entmischungstemperatur(LCST) von PNIPAM auftritt, verlangsamt die Diffusion dieser Tracer-Oligomere in der Nähe der Kern-Schale-Schnittstelle leicht. Im Gegensatz dazu ist die Beweglichkeit der Tracer im Kern nicht durch die Entquellung der Schale beeinflusst. Dieses Ergebnis verdeutlicht die Abwesenheit von Artefakten in den Messungen, wie die Adsorption der Gastmoleküle an der amphiphilen Polymerhülle, und verdeutlicht den Nutzen dieser Mikrogelpartikel bei der Verkapselung und kontrollierten Freisetzung in der Anwendung.

Temperaturabhängige Verbundhydrogele, die aus einer PAAM-Hydrogelmatrix mit eingebetteten Mikrometer großen PNIPAM Mikrogelpartikeln bestehen, sind vielversprechende Modelle für komplexe, heterogene Gele und lebende Zellen. Die

Kopplung der Mikrogelpartikel an die Gel-Matrix und die Bildung von durchdringenden Netzwerken (IPN) innerhalb der Mikrogele wurden untersucht. Die Ortsauflösung dient dazu, die Auswirkungen der heterogenen Struktur der zusammengesetzten Hydrogele auf die Diffusionsmobilität von nanoskopischen Dextran-Tracer innerhalb der Gele zu studieren. Die Untersuchungen zeigen, dass die Bildung von sich durchdringenden Netzwerken innerhalb der eingebetteten Mikrogelpartikel von ihrer Vernetzungsdichte abhängen. Während sich IPNs im Inneren schwach vernetzter Partikel bilden, werden sie in stark vernetzten Partikeln nicht gebildet. Bilden sich IPNs, wird die temperaturabhängige Quellung und Entquellung der Mikrogelpartikel behindert. Außerdem ist die Beweglichkeit von Dextran-Tracern innerhalb der eingebetteten Mikrogelpartikel gehindert, im Vergleich zur Diffusion in freien Mikrogelpartikeln in Wasser oder in der umgebenden Gelmatrix. Überraschenderweise quillt die umgebende PAAM-Hydrogelmatrix inhomogen, wenn die eingebetteten PNIPAM-Partikel beim Erhitzen kollabieren. Dies deutet auf die Bildung von Poren in der Nähe der Oberfläche der kollabierten Partikel hin und bietet vielversprechende Möglichkeiten um Verbundhydrogele für Anwendungen als Membranen mit einstellbarer Permeabilität herzustellen. Diese Experimente zeigen auch die Nützlichkeit von ortsaufgelösten 2fFCS-Messungen um die Diffusion in komplexen Umgebungen, die von großem Interesse für die Biomaterialforschung ist, zu studieren.

Tabel of Contents

Abstract	IX
Kurzfassung.....	XII
1. Motivation and Aim of the Thesis.....	1
2. Theory	5
2.1. Diffusion.....	5
2.2. Brownian motion.....	7
2.3. Fluorescence	10
2.4. Hydrogels.....	12
2.5. Fluorescence Correlation Spectroscopy	14
2.5.1. Basic working principle	15
2.6. Two-focus Fluorescence Correlation Spectroscopy	18
2.6.1. Basic working principle	18
2.6.2. The molecule detection function (MDF) and the resulting correlation functions	19
2.7. References.....	22
3. Refractive index mismatch can misindicate anomalous diffusion in single-focus fluorescence correlation spectroscopy	25
3.1. Introduction	25
3.2. Experimental Part	28
3.2.1 Sample preparation	28
3.2.1.1 Tracer particles	28
3.2.1.2 Matrix polymers.....	29
3.2.2 Experimental techniques	30
3.2.2.1 2fFCS	30
3.2.2.2 FCS data evaluation	32
3.3. Results and Discussion.....	34

3.4. Conclusions	43
3.5. Supporting Information	44
3.6. References	47
4. Diffusion of guest molecules within sensitive core–shell microgel carriers	51
4.1. Introduction.....	51
4.2. Materials and methods.....	53
4.2.1. Microgel synthesis	53
4.2.2. Tracer entrapment.....	54
4.2.3. 2fFCS	56
4.3. Results and discussion.....	58
4.4. Conclusions	64
4.5. References	66
5. Spatially Resolved Tracer Diffusion in Complex Responsive Hydrogels	69
5.1. Introduction.....	69
5.2. Experimental Part.....	72
5.2.1. Sample Preparation	72
5.2.2. Dynamic Light Scattering	74
5.2.3. Spatially Resolved 2fFCS	74
5.3. Results and Discussion	77
5.4. Conclusions	88
5.5. Supporting Information	89
5.6. References	92
6. Summary and Outlook.....	95
6.1. Outlook.....	98
6.1.1. Anomalous diffusion.....	98
6.1.1.1. Detection of anomalous diffusion via 2fFCS	98
6.1.2. Diffusion inside core-shell particles	99

6.1.2.1. Core-shell particle composition	99
6.1.2.2. Core-shell particle architecture	99
6.1.3. Hydrogels with switchable inhomegeneties	100
6.1.3.1. Combining core-shell particles with hydrogels	101
6.2. References.....	101
7. Appendix.....	103
7.1. Quantum dots as tracer particles.....	103
7.1.1 References	110
7.2. Dimerization of STAT3 protein and measurement in living cells.....	111
7.2.1. References	116
7.3. DNA-functionalized gold nano particles (Au-NP).....	116
7.3.1. References	119
7.4. Hydrogels made of star polymers.....	120
7.5. Temperature-sensitive polymers from Renate Messing	123
7.6. Galectin-1 – LacNAc Interaction.....	127
7.6.1. References	129
7.7. Lysozyme labelled with Fluorescein and Rhodamin.....	130
7.8. Curriculum Vitae.....	133

1. Motivation and Aim of the Thesis

In modern life the role of soft materials are getting more and more important. We are surrounded by plastics and gels. Especially stimulus-responsive or smart materials such as thermo-responsive materials are of high interest. The research on such materials is a continuously growing field. The applications for new smart materials are huge and complex smart hydrogels are very interesting for a huge variety of applications, such as tunable membranes in food production, filtering and tissue engineering; as carriers in drug delivery; as “intelligent patches” in medicine and many more. A great advantage of hydrogels is, that they are easy to modify and their properties are tunable. Making heterogeneous hydrogels out of a surrounding gel matrix and incorporating colloidal materials such as microgels or nanoparticles increases the number of tunable properties for hydrogels.

In all mentioned applications the diffusion of small guest molecules inside and through the hydrogel is of mayor importance. Measuring the diffusion is rather tricky. One has to somehow visualize the diffusion. A very common way to do this is to tag the guest molecules with a fluorescent dye. The labeled guest molecules can now be tracked if the label is excited by light and the emitted light is detected. A very simple method to do this is to illuminate the whole gel with the correct wavelength and making a film of the gel which is floated from one side with a solution of labeled molecules. The molecules will form a border inside the gel between the parts of the gel already filled with labeled molecules and the part with no labeled molecules. The border moves across the gel and the speed of the border gives information about the diffusion of the molecules inside the gel.

One well-established method which is based on the described method is the fluorescence recovery after photo bleaching (FRAP) method. In this method a spot inside the gel, which is filled with labeled molecules, is bleached and the vanishing of the bleached spot is measured. These two methods have a big disadvantage, they need rather high concentrations of labeled guest molecules and therefore the molecule concentration is of risk to lower the diffusion of the molecules additionally to the gel.

Another technique which deals with fluorescently labeled molecules is the confocal fluorescence correlation spectroscopy (FCS). This method measures the time a labeled molecule stays inside a small volume determined by a laser focus. This technique has the advantage that the molecule concentration is close to the infinite dilution and no macroscopic concentration gradient is present. A big disadvantage of this technique is that the measured diffusion coefficient is not an absolute value and has to be referenced by a standard. The standard is a molecule with known diffusion coefficient and is used to determine the detection volume. This makes the method fragile to refractive index mismatches, cover slight thickness and the used wavelengths.

A modification of the standard FCS is the rather new two-focus fluorescence correlation spectroscopy (2fFCS). This technique is robust against refractive index mismatch. This is achieved by introducing an external length scale. A detailed description will be given later. With the 2fFCS absolute diffusion measurements are possible and make it to the technique of choice for investigating complex hydrogels.

In complex heterogeneous hydrogels with stimulus-responsive additives the diffusion of guest molecules is dependent on the position inside the complex hydrogel.

The aim of this thesis is to introduce the spatially resolved 2fFCS measurements. This method will then be applied to core-shell particles and in hydrogels with switchable

inhomogeneities. The question to answer is: How does the diffusion in these samples react on external stimuli? In these environments the aspect of anomalous diffusion will be investigated by comparing FCS and 2fFCS results on different samples to answer the question of possible artifacts in the detection of anomalous diffusion caused by the refraction index mismatch.

2. Theory

2.1. Diffusion

One approach, to describe the diffusion was established by Adolf Fick in 1855[1]. Fick started with a macroscopic observation of the diffusion.

If one puts a drop of liquid soap into a glass of water, the soap drop will dissolve and the drop of liquid soap will vanish, meaning that the opaque soap drop will become more and more transparent, whereas the transparent water will become slightly opaque if the soap concentration in water gets high enough. In other words the density gradient of the soap surfactant is very high in the beginning and will drop during time until the gradient is zero in equilibrium state. This effect is called diffusion. A cartoon of the process is shown in Figure 2.1.

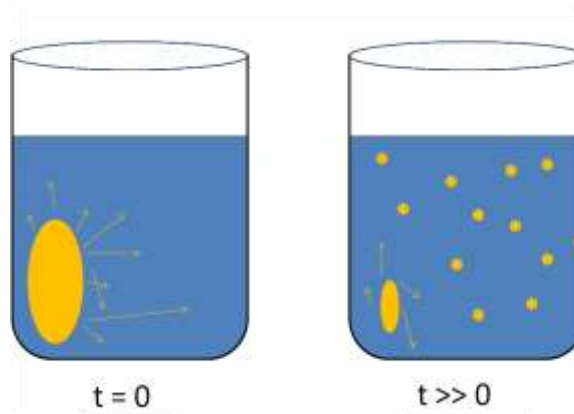


Figure 2.1 A schematic draw of the diffusion of soap from the soap droplet (yellow) into the surrounding water (blue).

The diffusion can be seen by naked eye, if the process is not too fast.

The number of particles that moves through a defined unit area into a second is called particle flux density \vec{j}_n which is a vector.

The particle flux density is given by Fick's first law for one dimension:

$$j_x = -\frac{L \langle v \rangle}{3} \frac{dn}{dx} \quad (2.1)$$

L is the mean free path, $\langle v \rangle$ is the mean velocity and dn/dx is the one dimensional particle density gradient.

The first factor on the right side is obviously a particle-specific constant. So we can define

$$\frac{L \langle v \rangle}{3} = D \quad (2.2)$$

And call D the diffusion coefficient.

Due to entropy more particles of the higher concentrated species will diffuse out of the volume. In other words the particle density will be reduced in the volume of high concentration:

$$\dot{n} = -\text{div} \vec{j}_n \quad (2.3)$$

Where \vec{j}_n is a vector.

Including Fick's first law we get:

$$\dot{n} = D \text{div grad } n = D \Delta n \quad (2.4)$$

The diffusion coefficient D is constant.

Another path to determine the diffusion coefficient more mathematically is discussed in the next part.

2.2. Brownian motion

Particles in a system with a temperature T move with an undirected movement. The mean kinetic energy of such particles is given by $E_{\text{kin}} = 3/2 k_B T$. The motion was first observed by Robert Brown in 1827 on pollen grains in water under a microscope. This was the first direct evidence of kinetic energy theory of matter [2, 3]. In 1905, Albert Einstein published a paper about the origin of the motion Brown found in 1827 [4]. An example for Brownian motion in two dimensions is shown in Figure 2.2.

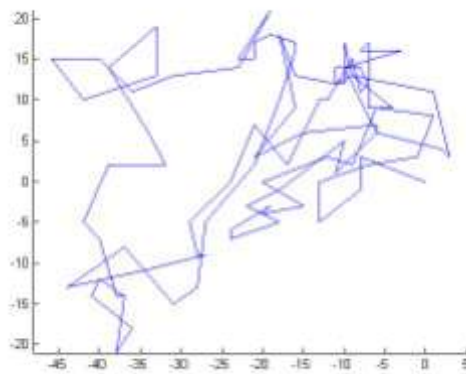


Figure 2.2 Sketch of a trace of a particle under Brownian motion, using a self defined matlab routine with 1000 steps of moving.

He considered that the pollen grains were moved by the collision with the water molecules. This motion can be described by a random walk. The particle moves straight for a certain length L between two individual collisions. Averaging over all L_i , leads to the mean free path L . The mean free path is dependent on the density of particles in a

liquid. Einstein showed, for one dimension, that if $\rho(x,t)$ is the particle density at a point x at a time t , the movement can be described by

$$\frac{\partial \rho}{\partial t} = D \frac{\partial^2 \rho}{\partial x^2} \quad (2.5)$$

D is the diffusion coefficient. The equation is equivalent to equation (2.4).

Solving the equation, using the initial conditions:

$$\rho(x, t) = 0 \quad (2.6)$$

For $x \neq 0, t = 0$.

And

$$\int_{-\infty}^{+\infty} \rho(x, t) dx = \rho_0 \quad (2.7)$$

Leads to:

$$\rho(x, t) = \frac{\rho_0}{\sqrt{4 \pi D t}} e^{-\frac{x^2}{4 D t}} \quad (2.8)$$

Now the moments can be calculated directly. The first moment is zero, which is equivalent to no preferred direction for the particle movement. This is expected for random walk. The second moment gives us the mean square displacement $\langle x^2 \rangle$:

$$\langle x^2 \rangle = 2 D t \quad (2.9)$$

And for three dimensions:

$$\langle x^2 \rangle = 6 D t \quad (2.10)$$

In 1908 Jean-Baptist Perrin got the Nobel Prize for proving Einstein's theory in an experiment[5].

As a direct consequence, the diffusion coefficient of particles with a thermal energy of $E_{\text{kin}} = 3/2 k_B T$ in a solution can be described by the mobility of the particle inside the solution:

$$D = \mu k_B T \quad (2.11)$$

For low Reynolds numbers μ is the inverse of the flow coefficient γ .

With

$$\gamma = 6 \pi \eta r_h \quad (2.12)$$

Where r_h is the hydrodynamic radius of the particle and η is the viscosity of the particle.

Combining equation (2.11) and (2.12) we get the well-known Stokes – Einstein equation:

$$D = \frac{k_B T}{6 \pi \eta r_h} \quad (2.13)$$

Now we have a direct relation between the diffusion coefficient and the size of the diffusing particle. Therefore, a change in the diffusion coefficient of the same particle at

the same temperature but in different environments can be described directly by a change of the viscosity or more generally spoken a change of the mobility of the particle.

2.3. Fluorescence

To investigate small particles in different environments, the contrast between the particles of interest and the environment has to be high enough to distinguish between particle and environment. The contrast can be described by a certain attribute of the particle of interest. This attribute can be a special structure for NMR measurements, high scattering potential for neutrons in SANS or many other attributes. In our case we need a photo-physical active particle which shows luminescence under irradiation of light of a defined wave-length. This luminescence can be distinguished between two different categories: Fluorescence and phosphorescence, depending on the physical properties of the excited state in the molecule. The fluorescence takes place on a smaller timescale as the phosphorescence and is the effect of choice for our experiments.

Both effects, fluorescence and phosphorescence, can be explained, using the Jablonski diagram (figure 2.3).

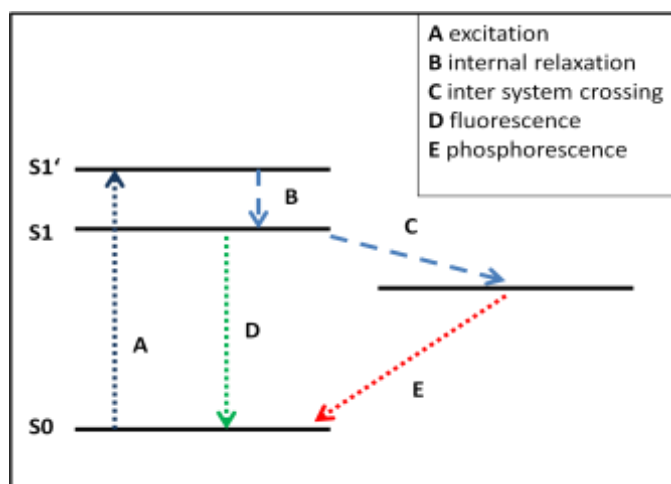


Figure 2.3 Simple Jablonski diagram including fluorescence and phosphorescence.

In 1933 Aleksander Jablonski described the fluorescence and phosphorescence using a scheme equal to that shown in figure 2.3[6].

If a dye is exposed to light with a wavelength equal to the energy difference between the ground state S0 of the dye and an excited state S1' of the same dye and the valence electrons of the dye are in ground state, one electron will be excited by absorbing the energy of a light photon and moves to the state S1'. S1' is one state of the possible states of the S1 states without specifying all other quantum values. If S1' is not equal to S1, the S1 state with lowest energy and all quantum values equal to 0 except the main quantum value of 1, an internal relaxation without irradiation of light takes place. At this point the differentiation between fluorescence and phosphorescence takes place. If the internal conversion of the S1' to S1 state is combined with a spin change of the electron, a return of the excited electron to S0 is not allowed. Then, an inter-system interaction is needed to change the spin of the excited electron again. This is called inter-system crossing. This leads to phosphorescence and needs larger timescales as a direct relaxation of the excited electron with no spin change. The direct relaxation with irradiation of light is called fluorescence.

Due to the internal relaxation of the S1' to S1 state, an energy lost between excitation and fluorescence light occurs. This shift to longer wavelengths from the absorption to the emission is called Stokes shift. The Stokes shift is crucial for the distinction between excitation and emission light and there for the technique used in this work.

2.4. Hydrogels

Hydrogels are a sort of material which is used in a huge variety of applications in modern life. They are used for contact lenses[7, 8], as super absorbers for example in napkins[9], in DNA analysis[10], cosmetics[11], drug delivery[12-14] and many more. The definition of gels is difficult. Up to now no consistent definition exists. The most common definition is "...if it looks like 'Jell-O', it must be a gel!"[15]. There is only one rule that fits to all hydrogels, that it is composed out of at least two components, a liquid and a solid component. The properties of the hydrogel are a composition of the properties of the solid and the properties of the liquid part. This makes the hydrogel being soft matter. They retain their form as a solid and store the liquid inside without floating out of the gel. At the same time, small particles are able to diffuse through the hydrogel as if they were dissolved in a liquid[16].

There are two types of hydrogels known. The first one is the chemically cross-linked hydrogel and the second one is the physically cross-linked one. The chemically bond hydrogels are formed using a cross-linker in the synthesis to form covalently bonds between different polymer chains. These bonds are permanent bonds. Physically cross-linked hydrogels are bonded non-permanently by using interactions like electrostatic

interactions [17-19], entanglements or other intermolecular interactions. The physically cross-linked hydrogels therefore can be influenced by changing the interaction potentials and therefore can be destroyed or changed in their properties easily. Due to the fact, that the polymers have a lot of hydrophilic groups, they can incorporate huge amounts of water inside the hydrogels. Depending on the cross-link density the amount of water inside the hydrogel can be 10 wt% up to nearly 100 wt% in weight of the swollen hydrogel[20]. In cases of the super absorber hydrogels, as used in napkins, the amount of water which can be taken up can be 1000 times of the weight of the polymer network [21, 22].

For a huge variety of applications the swelling and deswelling behaviour of the hydrogels are of major importance. The swelling kinetics of hydrogels strongly depends on the size of the hydrogel [23, 24]. Therefore small gel structures swell and deswell much faster than big gel structures. The fast kinetics is often requested. Therefore hydrogels in the nanometre and micrometre scales are synthesized. These hydrogels are called microgels.

It is also possible to synthesize hydrogels with special properties, as sensitive to external stimuli such as temperature, pH, electro-magnetic fields and many more. These hydrogels are called "smart hydrogels". The sensibility to the external stimuli can be introduced to the hydrogel by using special monomers, for example N-isopropylacrylamide (NIPAM) for the temperature sensibility. PNIPAM has a volume phase transition temperature (VPTT) of 32°C in water[25]. Above the VPTT the polymer becomes hydrophobic and the hydrogel deswells in water. This deswelling is driven by entropy and endothermic[26]. For other sensibilities, additional other components such as magnetic nanoparticles, or charged monomers can be used.

Combining the fast swelling kinetics and the stimuli sensitivity is quite easy by synthesizing microgels with the stimuli responsive components inside. But in some applications it is necessary that the macroscopic shape of the hydrogel does not change upon one external stimulus and at the same time the hydrogel should react quite fast on this stimulus. In these cases so-called “composite hydrogels” are needed. Composite hydrogels contain of a microgel which is sensitive to the external stimulus und a surrounding hydrogel which is not. These composites retain their shape and show a reaction on the external stimulus. The reaction of the sensitive microgels, with a size of several nanometre, is almost the same as those the pure microgel shows. Only at very high cross-linker concentrations an effect is visible [27].

A very large number of monomers, cross-linkers and additives is available and makes hydrogels, smart hydrogels and composite hydrogels to a research field of ongoing work of finding new materials with new properties and applications.

2.5. Fluorescence Correlation Spectroscopy

In the 1970's the idea of fluorescence correlation spectroscopy (FCS) was invented by Elson, Magde and Webb [28-34]. The theory for the FCS was developed by Ehrenberg and Rigler [35] from the theory of dynamic light scattering (DLS). In 1976 Hirschfeld succeeded with the first detection of single molecule diffusion in a liquid. This was possible due to the fact that the detection volume of the FCS had been minimized using the confocal technique [36]. In the confocal setup an objective of high numerical

aperture ($NA > 0.9$) was combined with a lens / pinhole setup. With this setup investigation of polymers with only one fluorescent label was possible in a liquid [37-41]. A huge step forward for the FCS was the development of stable and powerful lasers and single avalanche photo multipliers of high accuracy in the early 1990's. The first review articles about the FCS were published 1997-2002 [40]. They mark the point in time where the FCS technique reached their state as it is used nowadays. There are some new modifications of the FCS in use. For example the two-focus fluorescence correlation spectroscopy (2fFCS)[42], total internal reflection fluorescence correlation spectroscopy (TIRFFCS)[43], scanning fluorescence correlation spectroscopy (SFCS)[44] and more. All these modifications try to tackle the problems of the standard FCS, as they are refractive index mismatch, dependency on the cover slight thickness, optical saturation and other optical and photo physical problems which lead to artifacts in the measurement.

2.5.1. Basic working principle

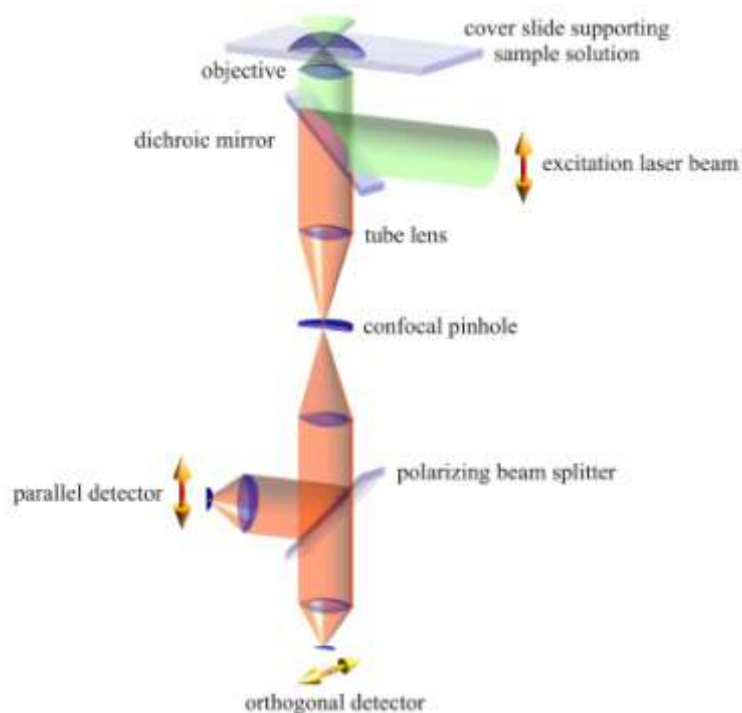


Figure 2.4 Schematic draw of the setup of a confocal fluorescence microscope [42].

In principle the set up of an FCS machine is the same as a standard confocal fluorescence microscope (Figure 2.4). A laser beam of a defined wavelength is coupled into an inverted microscope via a dichroic mirror, which is highly reflective for the wavelength of the laser beam and highly transparent for the other wavelengths. The microscope is focusing the laser beam to a small point with highest laser intensity inside the sample. Fluorescence of the whole focus cone is then detected through the objective, passing the dichroic mirror and is focused by a lens through a pinhole. The pinhole is positioned in the focus of the lens. This leads to a selection of the fluorescence light. Only the light from the focus point inside the sample passes the pinhole. The resulting fluorescence from the very small focus point volume in the sample is then measured by single photon detectors. The resulting signals are measured time resolved and lead to an intensity time trace (Figure 2.5). From this time trace one can calculate the so called auto correlation function (ACF) (Equation 2.14).

$$G(\tau) = \frac{\langle I(t + \tau)I(t) \rangle}{\langle I(t)^2 \rangle} \quad (2.14)$$

$I(t)$ is the intensity at a time t and $I(t + \tau)$ is the intensity at a time $t + \tau$. The angle brackets indicate the time average. The AFC describes the probability to have intensity of a label at the time $t + \tau$ provided that there was intensity at a time t .

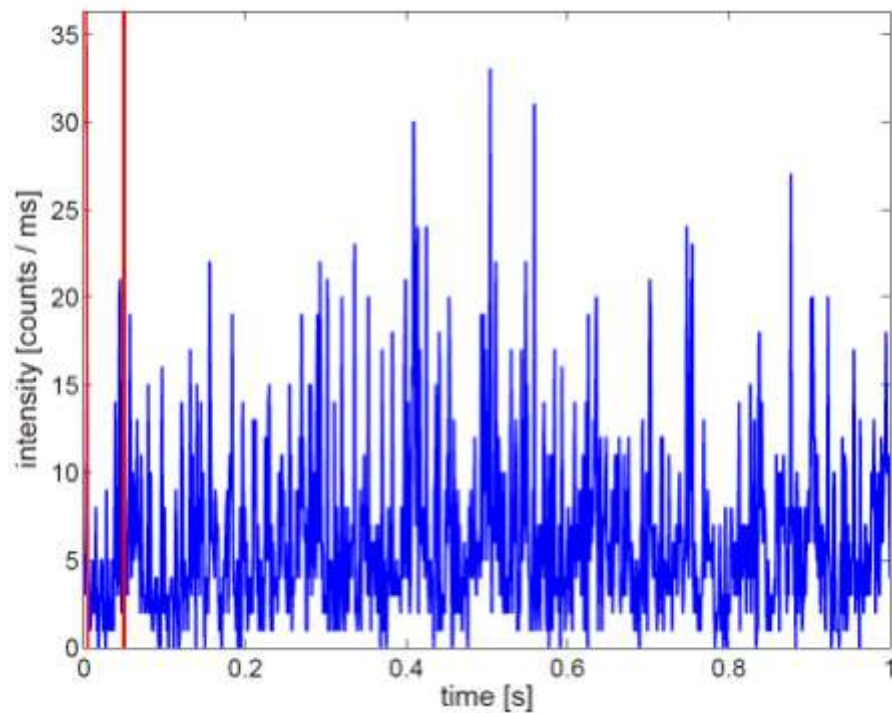


Figure 2.5 Typical time trace recorded by a confocal fluorescence microscope.

To get quantitative data out of the ACF it is necessary to have a precise description of the underlying molecule detection function (MDF). For the MDF the correct shape of the detection volume is needed. In common theory for FCS the shape of the detection volume is assumed to be a three-dimensional, rotationally symmetric Gaussian ellipsoid with a radius $1/e^2$. It had been shown by Dertinger et al.[45] that this is critical because a slight refractive index mismatch changes the shape of the detection volume strongly. This makes it complicated to measure in samples with a different refractive index with respect to the immersion liquid, used in the microscope.

2.6. Two-focus Fluorescence Correlation Spectroscopy

2.6.1. Basic working principle

The knowledge of the correct shape of the detection volume in FCS measurements is needed to have a length scale for the calculation of the diffusion coefficient from the diffusion time τ_D . This is critical due to the fact, that a refractive index mismatch changes the shape of the detection volume from the three dimensional, rotational symmetric Gaussian ellipsoid and makes it difficult to work with. T. Dertinger invented in 2007 the so-called two-focus fluorescence correlation spectroscopy (2fFCS)[42, 45, 46].

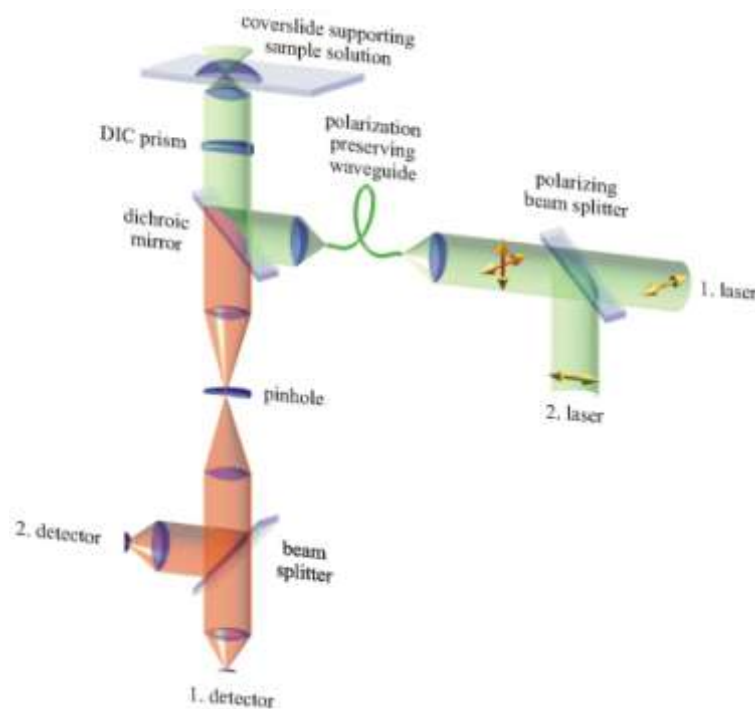


Figure 2.6 Schematic draw of the setup of a confocal fluorescence microscope for 2fFCS measurements. DIC prism denotes the Nomarski prism [42].

This technique is a modification of the standard FCS, where a second laser focus is used in the sample. The both foci are individual foci that overlap. The lateral shift distance is realized by a Nomarski prism. The Nomarski prism displaces the incoming laser beam

depending on the polarization of the beam. Using two perpendicularly polarized laser beams leads to the fixed shift distance between the foci (Figure 2.6). The detection of the signals from the two foci is done with the same setup as in the standard FCS. This is possible if pulsed lasers are used, which are triggered to illuminate the foci fast one after the other. Now the signals of the two foci are separated in time. The laser pulses do have a length of several picoseconds and the time between the two pulses for the different foci is in the order of nanoseconds. The ns scale is needed due to the fact that the life time of the most fluorescence dyes is in that time scale.

2.6.2. The molecule detection function (MDF) and the resulting correlation functions

In contrast to the standard FCS, where the MDF is described using a three-dimensional Gaussian distribution, we use description introduced by T.Dertinger [42]. In this description the MDF is approximated by a modified Gauss-Lorentz distribution, given by equation 2.15.

$$U(\vec{r}) = \frac{\kappa(z)}{w^2(z)} \exp\left[-\frac{2}{w^2(z)}(x^2 + y^2)\right] \quad (2.15)$$

$U(\vec{r})$ denotes the MDF, x, y, z are the Cartesian coordinates with z along the optical axis.

$\kappa(z)$ is given by:

$$\kappa(z) = 2 \int_0^a \frac{\rho}{R^2(z)} \exp\left(-\frac{2\rho^2}{R^2(z)}\right) d\rho = 1 - \exp\left(-\frac{2a^2}{R^2(z)}\right) \quad (2.16)$$

The parameter a denotes the pinhole radius of the confocal optics. The expressions R and w are defined equally:

$$w(z) = w_0 \left[1 + \left(\frac{\lambda_{ex} z}{\pi w_0^2 n} \right)^2 \right]^{1/2} \quad (2.17)$$

and

$$R(z) = R_0 \left[1 + \left(\frac{\lambda_{em} z}{\pi R_0^2 n} \right)^2 \right]^{1/2} \quad (2.18)$$

n is the refractive index, λ_{em} denotes the emission wavelength, λ_{ex} the excitation wavelength and w_0 and R_0 are in principal unknown model parameters.

The auto correlation function for lag time τ and for one focus is given by [47]:

$$g(\tau) = \epsilon^2 \langle c \rangle \int_V \int_V U(\vec{r}_1) \langle \delta c(\vec{r}_1, \tau) \delta c(\vec{r}_2, \tau) U(\vec{r}_2) \rangle d\vec{r}_1 d\vec{r}_2 \quad (2.19)$$

$$+ \left[\epsilon \langle c \rangle \int_V U(\vec{r}) d\vec{r} \right]^2$$

Using Green's probability density function $G(\vec{r}, t | \vec{\rho}, 0)$ for molecular motion from point \vec{r} to point $\vec{\rho}$ in time τ and neglecting uncorrelated background intensity I_{bg} leads to:

$$g(\tau) = \epsilon^2 \langle c \rangle \int_V \int_V U(\vec{r}_1) G(\vec{r}_1, t | \vec{r}_2, 0) U(\vec{r}_2) d\vec{r}_1 d\vec{r}_2 \quad (2.20)$$

$$+ \left[\epsilon \langle c \rangle \int_V U(\vec{r}) I_{bg} d\vec{r} \right]^2$$

With:

$$G(\vec{r}_1, t | \vec{r}_2, 0) = \frac{1}{(4\pi Dt)^{3/2}} \exp\left(-\frac{(\vec{r}_1 - \vec{r}_2)^2}{4Dt}\right) \quad (2.21)$$

The Green function $G(\vec{r}_1, t | \vec{r}_2, 0)$ describes the three dimensional diffusion.

Up to now we have an expression for a single focus experiment. To describe the whole 2fFCS experiment we have to introduce the shift distance \vec{d} and spreading the detection efficiency ϵ to ϵ_1 and ϵ_2 for the different foci in equation 2.20 lead to [47]:

$$g(\tau) = \left(\epsilon_1 c \int_V U(\vec{r}_1) d\vec{r}_1 + I_{bg} \right) \left(\epsilon_2 c \int_V U(\vec{r}_2) d\vec{r}_2 + I_{bg} \right) + \frac{\epsilon_1 \epsilon_2 c}{4} \sqrt{\frac{\pi}{D\tau}}$$

$$\int_{-\infty}^{\infty} \int_{-\infty}^{\infty} \frac{\kappa_{z_1} \kappa_{z_2}}{8 D \tau + w^2(z_1) + w^2(z_2)} \quad (2.22)$$

$$\exp - \frac{(z_2 - z_1)^2}{4D\tau} \frac{2d^2}{8 D \tau + w^2(z_1) + w^2(z_2)} dz_1 dz_2$$

There is no analytical solution for this equation available and a numerical solution of the equation is needed to fit the measurement data (see e.g. Equation 3.2).

2.7. References

1. Fick, A., *On liquid diffusion*. The London, Edinburgh and Dublin Philosophical Magazine and Journal of Science, 1855. **10**: p. 30 - 39.
2. Brown, R., *A brief Account of Microscopical Observations made in the Months of June, July, and August, 1827, on the Particles contained in the Pollen of Plants; and on the general Existence of active Molecules in Organic and Inorganic Bodies*. Philosophical Magazine N. S., 1828(4): p. 161 - 173.
3. Brown, R., *Additional Remarks on Active Molecules*. Philosophical Magazine N. S., 1829. **6**: p. 161 - 166.
4. Einstein, A., *Über die von der molekularkinetischen Theorie der Wärme geforderte Bewegung von in ruhenden Flüssigkeiten suspendierten Teilchen*. Annalen der Physik, 1905. **322**(8): p. 549-560.
5. Perrin, J., *Les atomes*. Félix Alcan, 1913.
6. Jablonski, A., *Efficiency of anti-Stokes fluorescence in dyes*. Nature (London, U. K.), 1933. **131**: p. 839-40.
7. McMahon, T.T. and K. Zadnik, *Twenty-five years of contact lenses - The impact on the cornea and ophthalmic practice*. Cornea, 2000. **19**(5): p. 730-740.
8. Kirschner, C.M. and K.S. Anseth, *Hydrogels in healthcare: From static to dynamic material microenvironments*. Acta Mater., 2013. **61**(3): p. 931-944.
9. Tanaka, T., *Gels*. Sci. Am., 1981. **244**(1): p. 124-36, 138.
10. Seong, G.H., W. Zhan, and R.M. Crooks, *Fabrication of Microchambers Defined by Photopolymerized Hydrogels and Weirs within Microfluidic Systems: Application to DNA Hybridization*. Analytical Chemistry, 2002. **74**(14): p. 3372-3377.
11. Huether, A., et al., *Phase equilibria of hydrogel systems*. Phys. Chem. Chem. Phys., 2002. **4**(6): p. 835-844.
12. Sivakumaran, D., D. Maitland, and T. Hoare, *Injectable Microgel-Hydrogel Composites for Prolonged Small-Molecule Drug Delivery*. Biomacromolecules, 2011. **12**(11): p. 4112-4120.
13. Gurski, L.A., et al., *Hyaluronic acid-based hydrogels as 3D matrices for in vitro evaluation of chemotherapeutic drugs using poorly adherent prostate cancer cells*. Biomaterials, 2009. **30**(30): p. 6076-6085.
14. McGillicuddy, F.C., et al., *Novel "plum pudding" gels as potential drug-eluting stent coatings: Controlled release of fluvastatin*. J. Biomed. Mater. Res., Part A, 2006. **79A**(4): p. 923-933.
15. Weiss, R.G. and P. Terech, *Molecular gels: materials with selfassembled fibrillar networks*. 2006: Springer, Berlin.
16. De Gennes, P.-G., *Soft matter: more than words*. Soft Matter, 2005. **1**(1): p. 16-16.
17. Knobon, W., N.A.M. Besseling, and M.A. Cohen Stuart, *Rheology of a reversible supramolecular polymer studied by comparison of the effects of temperature and chain stoppers*. J. Chem. Phys., 2007. **126**(2): p. 024907/1-024907/9.
18. Aoki, T., et al., *Temperature-Responsive Interpenetrating Polymer Networks Constructed with Poly(acrylic acid) and Poly(N,N-dimethylacrylamide)*. Macromolecules, 1994. **27**(4): p. 947-952.

19. Campoccia, D., et al., *Semisynthetic resorbable materials from hyaluronan esterification*. *Biomaterials*, 1998. **19**(23): p. 2101-27.
20. Hoffman, A.S., *Hydrogels for biomedical applications*. *Advanced Drug Delivery Reviews*, 2002. **54**(1): p. 3-12.
21. Omidian, H., J.G. Rocca, and K. Park, *Advances in superporous hydrogels*. *J. Controlled Release*, 2005. **102**(1): p. 3-12.
22. Gils, P.S., et al., *Designing of new acrylic based macroporous superabsorbent polymer hydrogel and its suitability for drug delivery*. *Int. J. Pharm. Pharm. Sci*, 2009. **1**: p. 43-54.
23. Hirose, H. and M. Shibayama, *Kinetics of Volume Phase Transition in Poly(N-isopropylacrylamide-co-acrylic acid) Gels*. *Macromolecules*, 1998. **31**(16): p. 5336-5342.
24. Tanaka, T. and D.J. Fillmore, *Kinetics of swelling of gels*. *The Journal of Chemical Physics*, 1979. **70**(3): p. 1214-1218.
25. Pelton, R., *Temperature-sensitive aqueous microgels*. *Adv. Colloid Interface Sci.*, 2000. **85**(1): p. 1-33.
26. Heskins, M. and J.E. Guillet, *Solution properties of poly(N-isopropylacrylamide)*. *J. Macromol. Sci., Chem.*, 1968. **2**(8): p. 1441-55.
27. Meid, J., et al., *Composite hydrogels with temperature sensitive heterogeneities: influence of gel matrix on the volume phase transition of embedded poly-(N-isopropylacrylamide) microgels*. *Physical Chemistry Chemical Physics*, 2011. **13**(8): p. 3039-3047.
28. Magde, D., E. Elson, and W.W. Webb, *Thermodynamic Fluctuations in a Reacting System - Measurement by Fluorescence Correlation Spectroscopy*. *Physical Review Letters*, 1972. **29**(11): p. 705-708.
29. Elson, E.L. and D. Magde, *Fluorescence correlation spectroscopy. I. Conceptual basis and theory*. *Biopolymers*, 1974. **13**(1): p. 1-27.
30. Magde, D., E.L. Elson, and W.W. Webb, *Fluorescence correlation spectroscopy. II. Experimental realization*. *Biopolymers*, 1974. **13**(1): p. 29-61.
31. Aragon, S.R. and R. Pecora, *Fluorescence correlation spectroscopy as a probe of molecular dynamics*. *J. Chem. Phys.*, 1976. **64**(4): p. 1791-803.
32. Magde, D., *Chemical kinetics and fluorescence correlation spectroscopy*. *Q. Rev. Biophys.*, 1976. **9**(1): p. 35-47.
33. Webb, W.W., *Applications of fluorescence correlation spectroscopy*. *Q. Rev. Biophys.*, 1976. **9**(1): p. 49-68.
34. Magde, D., W.W. Webb, and E.L. Elson, *Fluorescence correlation spectroscopy. III. Uniform translation and laminar flow*. *Biopolymers*, 1978. **17**(2): p. 361-76.
35. Ehrenberg, M. and R. Rigler, *Rotational brownian motion and fluorescence intensity fluctuations*. *Chem. Phys.*, 1974. **4**(3): p. 390-401.
36. Hirschfeld, T., *Optical microscopic observation of single small molecules*. *Appl. Opt.*, 1976. **15**(12): p. 2965-6.
37. Moerner, W.E. and L. Kador, *Optical detection and spectroscopy of single molecules in a solid*. *Phys. Rev. Lett.*, 1989. **62**(21): p. 2535-8.
38. Shera, E.B., et al., *Detection of single fluorescent molecules*. *Chem. Phys. Lett.*, 1990. **174**(6): p. 553-7.
39. Nie, S. and R.N. Zare, *Optical detection of single molecules*. *Annu. Rev. Biophys. Biomol. Struct.*, 1997. **26**: p. 567-596.

40. Maiti, S., U. Haupts, and W.W. Webb, *Fluorescence correlation spectroscopy: diagnostics for sparse molecules*. Proc. Natl. Acad. Sci. U. S. A., 1997. **94**(22): p. 11753-11757.
41. Weiss, S., *Fluorescence spectroscopy of single biomolecules*. Science (Washington, D. C.), 1999. **283**(5408): p. 1676-1683.
42. Dertinger, T., *Two-Focus Fluorescence Correlation Spectroscopy*. 2007, Cologne.
43. Lieto, A.M. and N.L. Thompson, *Total internal reflection with fluorescence correlation spectroscopy: Nonfluorescent competitors*. Biophys. J., 2004. **87**(2): p. 1268-1278.
44. Petrášek, Z., et al., *Characterization of Protein Dynamics in Asymmetric Cell Division by Scanning Fluorescence Correlation Spectroscopy*. Biophysical Journal, 2008. **95**(11): p. 5476-5486.
45. Dertinger, T., et al., *The optics and performance of dual-focus fluorescence correlation spectroscopy*. Opt. Express, 2008. **16**(19): p. 1435314368.
46. Dertinger, T., et al., *Two-focus fluorescence correlation spectroscopy: A new tool for accurate and absolute diffusion measurements*. Chemphyschem, 2007. **8**(3): p. 433-443.
47. Müller, C.B., *Applications of Two Focus Fluorescence Correlation Spectroscopy in Colloid and Polymer Science*, in *Institut für Physikalische Chemie II*. 2008, RWTH Aachen University: Aachen. p. 154.

3. Refractive index mismatch can misindicate anomalous diffusion in single-focus fluorescence correlation spectroscopy¹

3.1. Introduction

Molecular and particulate diffusion in crowded environments such as cells,[1-3] membranes,[4-6] or gels[7] is a rate-determining factor in dynamic processes in these media,[8-12] including cellular metabolism,[13, 14] transmembrane transport,[15-17] and drug delivery.[18-21] A suitable observable to quantify diffusivities in these media is the time-dependent mean square displacement (MSD); in the simple limit of Brownian motion, this quantity scales linearly with time, as captured by the Einstein–Smoluchowski equation, $MSD \sim t^\alpha$, with $\alpha = 1$. By contrast, diffusion in crowded media is often anomalous, assessed by $\alpha < 1$ and commonly referred to as subdiffusion.[22] This deviation from the simple Brownian limit can be caused by temporal entrapment of the diffusing species due to mechanical constraint or chemical binding imposed by the surrounding matrix.

A suitable method to probe diffusion processes in the Brownian and the anomalous limit is fluorescence correlation spectroscopy (FCS). After initial use in the biophysical field,[23, 24] this technique has gained remarkable popularity in the colloid and polymer sciences.[25-31] In this approach, a determined femtoliter-sized sample volume is irradiated by a focused laser beam, causing autofluorescent or fluorescently tagged

¹ This chapter was published in *Macromol. Chem. Phys.*, 2014. DOI: 10.1002/macp.201400349. The study was performed in collaboration with the co-authors. My contribution was the synthesis of the final samples. Furthermore, I performed the 2fFCS measurements and did the data analysis for single and 2fFCS.

probe molecules to fluoresce. If the probe molecules are present in nanomolar concentrations, only a small number of them occupy the probe volume at a time, causing measurable fluctuation of the fluorescence intensity as probe molecules diffuse in and out of the probe volume. Autocorrelation analysis of these temporal fluctuations of the fluorescence intensity allows the translational diffusion coefficient to be calculated. For this purpose, the autocorrelation data are fitted with suitable mathematical models containing different adjustable parameters;[12] these models differ in detail, depending on whether or not they account for potential complexity such as triplet-state blinking, but they all share the same basic expression. If simple Brownian diffusion is probed, the model consists of a combined reciprocal and inverse square-root function.[12] By contrast, complex subdiffusion requires more sophisticated power-law functions to be applied to obtain confident fitting.[32, 33]

Despite its elegance and excellent sensitivity, FCS is subject to inaccuracy as a result of potential refractive index mismatch between the sample and the microscopy cover slide and immersion fluid that hold the specimen and interface it to the objective lens.[34, 35] If such effects impair an FCS experiment, the resulting autocorrelation data cannot be accurately fitted with standard simple models, [12] but needs sophisticated power-law fitting.[16, 17] As a result, these effects are at risk to be misinterpreted as anomalous diffusion. To overcome this limitation, two-focus fluorescence correlation spectroscopy (2fFCS) is a promising technique.[34, 36, 37] In this approach, two laterally overlapping foci are operated at a determined distance to realize two FCS experiments at a time,[38, 39] followed by cross-correlation analysis. The determined shift distance defines the extent of overlap of the two foci, simultaneously setting the length scale under investigation. As a result, this approach is robust against deviations of the shape of the

laser foci from the ideal Gaussian form, which may arise due to optical effects like refractive index mismatch.[26]

The impact of the refractive index and the ability to probe anomalous diffusion in classical single-focus FCS has been subject to several previous investigations. Aouani et al.[40] showed that refractive index mismatch can be used to minimize the detection volume and therefore optimize the signal to noise ratio in measurements. Harlepp et al.[41] varied the refraction index of RNA (ribonucleic acids) and protein-based samples and took the different refractive indices into account for the data evaluation, demonstrating that such treatment prevents the need for complex power-law fitting. Masuda et al.[42, 43] showed that anomalous diffusion can be measured by evaluating experiments with different sizes of the detection volume, in agreement with theoretical work of Enderlein.[44] These results indicate striking necessity for an in-depth treatment of the impact of refractive index in standard FCS. For the more robust and versatile technique of two-focus FCS, however, no comparable assessment has been made to date. Hence, the role of the refractive index and its potential mismatch, along with the potential benefit of the focal separation in 2fFCS to prevent misinterpretation of seemingly anomalous diffusion, remains elusive.

In this work, we explore to what extent single- and two-focus confocal FCS are influenced by the refractive index of the sample. We use both these techniques to probe the diffusion of fluorescently tagged dextran tracers in different environments, including plain water, dilute dextran solutions, acrylamide monomer solutions, semidilute polyacrylamide polymer solutions, and a crosslinked polyacrylamide hydrogel. With this set of experiments, we vary both the refractive index of the samples and the potential topological constraint and thermodynamic interaction to the dextran tracer diffusion. To

systematically assess the impact of the refractive index, we compare pairs of samples from the upper collection that exhibit the same refractive index but that have completely different compositions. Whereas 2fFCS shows no anomalous diffusion in any of these different samples, single-focus FCS indicates anomalous diffusion in every case that differs from the simplistic scenario of plain tracer diffusion at high dilution in water. In particular, the numerical values of the stretching exponent of the fluorescence autocorrelation function, which is often interpreted as an indicator of the extent of diffusion-anomaly in single-focus FCS,[32, 33] does not vary systematically with the extent of potential topological or thermodynamic complexity of the different matrixes, but with their refractive index. This finding shows that apparent anomalous diffusion in FCS is at risk to be the result of refractive index mismatch rather than truly reflecting complex diffusion. This doesn't mean that anomalous diffusion doesn't exist, but it demonstrates that taking the refractive index mismatch into account is crucial when measuring anomalous diffusion by single focus FCS.

3.2. Experimental Part

3.2.1 Sample preparation

3.2.1.1 Tracer particles

3-kDa dextran labeled with Alexa Fluor 647 ($r_h = 1$ nm, Invitrogen) and 70-kDa dextran labeled with rhodamine B ($r_h = 6.5$ nm, Invitrogen) [45] were dissolved in chromatographic pure water (LiChroSolv, Merck). The hydrodynamic radii of these tracers, r_h , were calculated with the Stokes–Einstein equation (Eq.3.1) from diffusion

coefficients determined at infinite dilution with 2fFCS.

$$D = \frac{k_B T}{6 \pi \eta r_h} \quad (3.1)$$

In this equation, k_B is Boltzmann's constant, T the temperature, η the viscosity of the medium, and r_h the hydrodynamic radius of the diffusing tracer. These experiments were repeated 30 times, respectively, denoting experimental accuracies of the tracer diffusion coefficient of $\pm 5\%$ each.

We choose dextrans as tracers due to their low interactions with other polymers except some specific proteins that are irrelevant here.[46] In most of the former studies, anomalous diffusion of dextran tracers is not reported. This is because in most cases, the correlation data of the dextran diffusion in crowded environments are fitted with two-particle model functions[20] or with model functions additionally accounting for triplet-state blinking.[47] These models can lead to sufficiently low residuals for small refractive index mismatches. At high refractive index mismatches, however, the deformation of the correlation function of the dextran diffusion is marked (Supplemental Information, Fig. S1), and two-particle models or models including triplet blinking are insufficient. Hence, as an alternative, the appearance of anomalous diffusion for dextran tracers has been reported as well.[48]

3.2.1.2 Matrix polymers

One matrix was unlabeled 70-kDa dextran (Invitrogen) dissolved in LiChrioSolv. A second matrix was dimethylmaleimide-functionalized polyacrylamide (p(AAm-co-DMMIAAm), $M_w = 687 \text{ kg mol}^{-1}$, 1 mol-% dimethylmaleimide moieties [49]) dissolved in LiChrioSolv;

the overlap concentration of this polymer is 5 g L^{-1} . As a more complex analogue to the latter type of sample, a third matrix was used in the form of a hydrogel prepared by free-radical crosslinking copolymerization of acrylamide (AAm, Merck) and *N,N'*-methylenebisacrylamide (BIS, Polysciences Inc.) To prepare this gel, a solution of 90 g L^{-1} of pure acrylamide, 3.25 g L^{-1} BIS, and 0.001 g L^{-1} of the UV-cleavable initiator VA-086 (2,2'-azis[2-methyl-*N*-2-hydroxyethyl]propionamide], Wako) in LiChroSolv solvent was irradiated with UV light for 15 minutes at a wavelength of 256 nm with an intensity of 1.5 W cm^{-1} .

3.2.2 Experimental techniques

3.2.2.1 2fFCS

Two-focus FCS was performed on a setup based on an inverted fluorescence microscope of type MicroTime200 (PicoQuant, Berlin, Germany), consisting of a life science microscope XI71 equipped with a water immersion objective UPLAPO 60× W, 1.2 N.A., both from Olympus Europa (Hamburg, Germany). The objective is equipped with a correction collar that was used to compensate for spherical aberration[50]. A pinhole with a diameter of $150 \mu\text{m}$ was used to achieve an ellipsoidal confocal volume of $279 \times 279 \times 693 \text{ nm}$. Measurements were performed at $T = 25 \text{ }^\circ\text{C}$ with a duration of 1 h to obtain proper correlation functions. A large pinhole entails specific requirements to the sample preparation. In this context, Enderlein et al. [35] demonstrated that simulations of FCS measurements with a pinhole of $100 \mu\text{m}$ are reliable if the pinhole is correctly adjusted to the focus plane of the confocal optics and if the tracer concentration is sufficiently low. In addition, Banachowicz et al. [50] recently showed that the pinhole

diameter has to be adjusted to a given tracer concentration to achieve reliable results. In our present work, we account for this by using a tracer concentration adjusted to the pinhole diameter according to these previous insights. We measured with tracer concentrations between 5 nM and 0.5 nM. In this concentration range, it is sufficient to have a rather big detection volume and still have a low number of tracer molecules inside the detection volume. To further assure reliability in our experiments, we used chromatographically clean water, LiChroSolv (Merk, Germany), thereby minimizing the background signals that may originate from the dissolution medium. Both these arrangements lead to a sufficient signal to noise ratio and a sufficiently reliable correlation function. As for the standard FCS setup: the accuracy of this setup has been demonstrated in an earlier publication by the Oppermann-group [51].

The correlation function of the temporally fluctuating fluorescence intensity in 2fFCS is given by:

$$g(\tau, \delta, \nu) = \frac{c}{4} \sqrt{\frac{\pi}{D \tau}} \int dz_1 \int dz_2 \left(\begin{array}{c} \frac{\kappa(z_1)\kappa(z_2)}{8 D \tau + w^2(z_1) + w^2(z_2)} \\ - \frac{(z_2 - z_1 - \nu_z \tau)^2}{4 D \tau} \\ - 2 \frac{(\delta - \nu_x \tau)^2 + \nu_y^2 \tau^2}{8 D \tau + w^2(z_1) + w^2(z_2)} \end{array} \right) \quad (3.2)$$

In this equation, D is the translational diffusion coefficient, τ the lag time of the cross-correlation, c the concentration of the tracer species in molecules per sample volume, and δ the shift distance of the two foci. x and y are the Cartesian coordinates perpendicular to the optical axis, whereas z is the coordinate along the optical axis. Further variables are:

$$w(z) = w_0 \left[1 + \left(\frac{\lambda_{ex} z}{\pi w_0^2 n} \right)^2 \right]^{1/2} \quad (3.3)$$

$$\kappa(z) = 2 \int_0^a \frac{d\rho \rho}{R^2(z)} \exp\left(-\frac{2\rho^2}{R^2(z)}\right) = 1 - \exp\left(-\frac{2\rho^2}{R^2(z)}\right) \quad (3.4)$$

$$R(z) = R_0 \left[1 + \left(\frac{\lambda_{ex} z}{\pi R_0^2 n} \right)^2 \right]^{1/2} \quad (3.5)$$

In these equations, λ_{ex} and λ_{em} are the excitation and emission wavelengths, n is the refractive index, and a is the confocal pinhole radius. R_0 and w_0 are free fitting parameters.

The data analysis in 2fFCS and single-focus FCS measurements was done using a single-particle model. No triplet-state blinking or other photophysical effects were taken into account to keep the model simple. The sufficiency of such a simple model is supported by the obvious absence of low-tau triplet-state blinking contributions to the 2fFCS correlation function, such that the simple function of Eq. (3.2) accurately fits these data.

3.2.2.2 FCS data evaluation

Simple FCS and two-focus FCS data were analyzed with two complimentary approaches. The 2fFCS measurements consist of two independent but equal FCS measurements in each focus, respectively, which are correlated separately and cross-correlated to get the correlation in the cross section of the two foci. In the cross-correlation function, the

detection volume geometry is expressed by the shift distance, which is an external length scale. This makes the cross-correlation function robust against deformation of the detection volume.[26, 36] By contrast, the simple FCS data were fitted with the autocorrelation function of just one of the two independent foci of the 2fFCS measurements, which is identical to the simple correlation function in single-focus FCS. The fitting was performed with two different equations, one not accounting for anomalous diffusion (Equation 3.6) and the other accounting for anomalous diffusion (Equation 3.7).

$$G(\tau) = G(0) \left(1 + \frac{\tau}{\tau_D}\right)^{-1} \left(1 + \frac{\tau}{k^2\tau_D}\right)^{-1/2} \quad (3.6)$$

$$G(\tau) = G(0) \left(1 + \left(\frac{\tau}{\tau_D}\right)^\alpha\right)^{-1} \left(1 + \left(\frac{\tau}{k^2\tau_D}\right)^\alpha\right)^{-1/2} \quad (3.7)$$

In these equations, τ_D is the diffusion time of the fluorescence particle inside the focus, k is the quotient of focus width and diameter, and α is the exponent for stretching the power-law decay of the fit. The value of α is commonly interpreted as the extent of anomaly of diffusion.[32, 33] As a check of consistency, we have conducted FCS experiments on a 70-kDa dextran tracer that diffuses within 80-gL⁻¹ semidilute solutions of aqueous p(AAm-co-DMMIAAm) on both our 2fFCS setup in its single-focus mode of operation and, in addition, on a classical single-focus FCS setup (Institute of Physical Chemistry, Clausthal University of Technology, Germany). This classical setup consists of a confocal laser scanning microscope (Leica TCS SP2) with FCS extension (Leica FCS2) equipped with a 63× objective immersed in water with a numerical aperture of 1.2, a detection pinhole of 100 μm in diameter, and an excitation with a He-Ne laser at 543

nm; to compensate for spherical aberration, a correction collar that is part of the objective lens was used. Both these experiments yielded the same result, assessed by a best-fit value of $\alpha = 0.665$ if fitting to Eq. 3.7 is applied (Supplemental Information Fig. S.3.1).

3.3. Results and Discussion

A simplistic diffusion experiment is performed if fluorescently tagged dextran tracer polymers diffuse in plain water. We conduct such experiments with two different dextran tracers, exhibiting molecular weights of 3 kDa and 70 kDa. In both these cases, classical single-focus FCS shows no indication for anomalous diffusion, and the fluorescence-autocorrelation data can be fitted with a simple decay function according to Eq. 6 to obtain $\tau_{3\text{-kDa}} = 1.13$ ms and $\tau_{70\text{-kDa}} = 1.98$ ms, as shown in Figure 3.1b and f. The same result is obtained in 2fFCS, both qualitatively and quantitatively, as shown in Figure 3.1a and e. A different result is obtained if the medium is supplemented by 30 g L⁻¹ of untagged 70-kDa dextran as an additional matrix. Even though this concentration is below the overlap concentration of 70-kDa dextran ($c^* = 60$ g L⁻¹, calculated according to Ying and Chu[52]), single-focus FCS data can no longer be fitted with a simple decay according to Eq. 3.6 but require fitting with a stretched decay function according to Eq. 3.7, denoting $\alpha = 0.89$ for the 3-kDa dextran tracer and $\alpha = 0.85$ for the 70-kDa dextran tracer, as shown in Figure 1d and h. By contrast, no such effects are detected in 2fFCS. In this case, simple decay functions serve to obtain reliable data fitting,[16] as shown in Figure 3.1c and g. To explain the latter finding in single-focus FCS, it is commonly assumed that chain entanglement or polymer–polymer interactions obstruct the

diffusion.[53, 54] In the present case, however, chain entanglement can be excluded, because the matrix and tracer concentrations are below the overlap threshold. Furthermore, if polymer–polymer interaction is assumed to cause deviation from normal diffusion, then this effect should be more pronounced at higher tracer molecular weight due to greater extent of hypothetical interaction. In our experiment, however, the stretching exponent α is very similar for both the low molecular weight 3-kDa dextran tracer and the high molecular weight 70-kDa tracer, in contradiction to the latter argument. Thus, we assume another reason to cause the above effects: differences in the refractive index of the different samples.[26, 35, 37]

To challenge the preceding hypothesis, we conduct experiments on 3-kDa dextran tracers immersed in a different polymer matrix: dimethylmaleimide-functionalized polyacrylamide, denoted p(AAm-co-DMMIAAm)[49, 55] ($M_w = 687$ kDa). We use different concentrations of this polymer, $c = 28\text{--}84$ g L⁻¹. All these concentrations are *above* the overlap concentration, which is $c^* = 5$ g L⁻¹. These experiments confirm the previous trends observed on dextran matrixes: whereas single-focus FCS denotes anomalous diffusion in all cases, two-focus FCS does not, as shown in Figure 3.2. In single-focus FCS, increase of the matrix concentration from 28 over 56 to 84 g L⁻¹ causes decrease of the best-fit values of the stretching exponent α from 0.83 over 0.57 to 0.43. This effect may be explainable by increasing topological constraint to the tracer motion or by increase of potential matrix–tracer polymer–polymer interactions imparted by increase of the matrix concentration. However, both these potential lines of argument cannot explain why 2fFCS adequately fits to simple decay functions according to Eq. 3.2, thereby not denoting any anomaly of diffusion. Again, this rationale leads us to conclude

that optical artifacts are the true major contributor to deviation from simple decay in single-focus FCS.

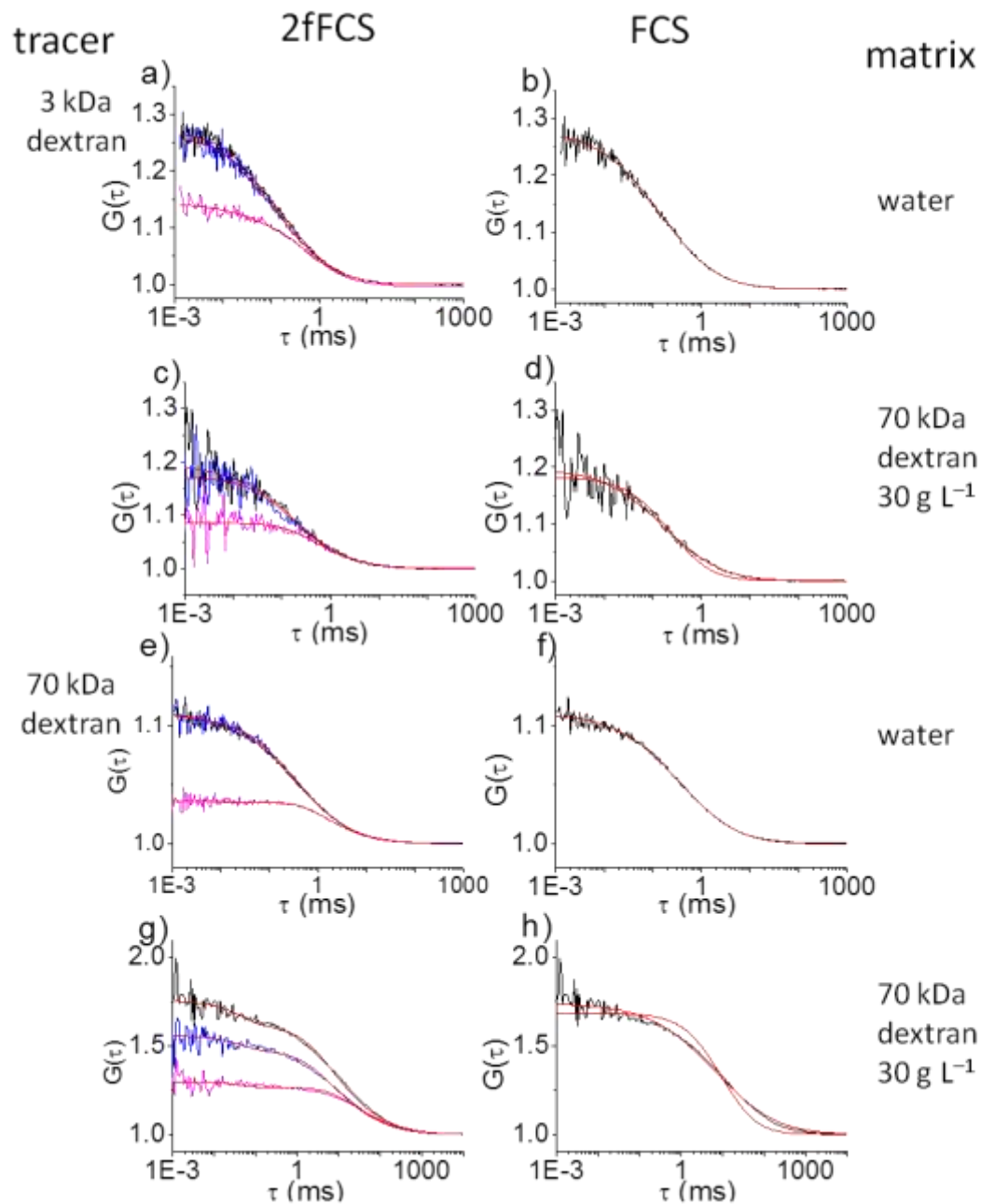


Figure 3.1. 2fFCS and single-focus FCS on fluorescently tagged 3-kDa dextran and 70-kDa dextran tracer polymers, either dissolved in water ((a),(b), (e), (f)) or in a 70-kDa dextran untagged polymer matrix with concentration of 30 g L^{-1} ((c), (d), (g), (h)), which is below the overlap concentration of dextran at this molecular weight ($c^* = 60 \text{ g L}^{-1}$). In single-focus FCS, data fitting (red lines) to a stretched power-law decay function (Eq. 3.7) yields $\alpha = 0.89$ for the 3-kDa dextran tracer and $\alpha = 0.85$ for the 70-kDa dextran tracer ((b), (d), (f), (h)). By contrast, 2fFCS measurements ((a), (c), (e), and (g)) show no anomalous diffusion and can be fitted with a simple decay function (Eq. 3.2). g) We fitted the data with a model including a term that accounts for triplet-state blinking. In the left column, the black and blue lines indicate the auto-correlation functions of the two separate foci, whereas the pink line indicates the cross-correlation function of the two foci. The residuals to the fits can be found in the supplemental information, Fig. S.3.2.

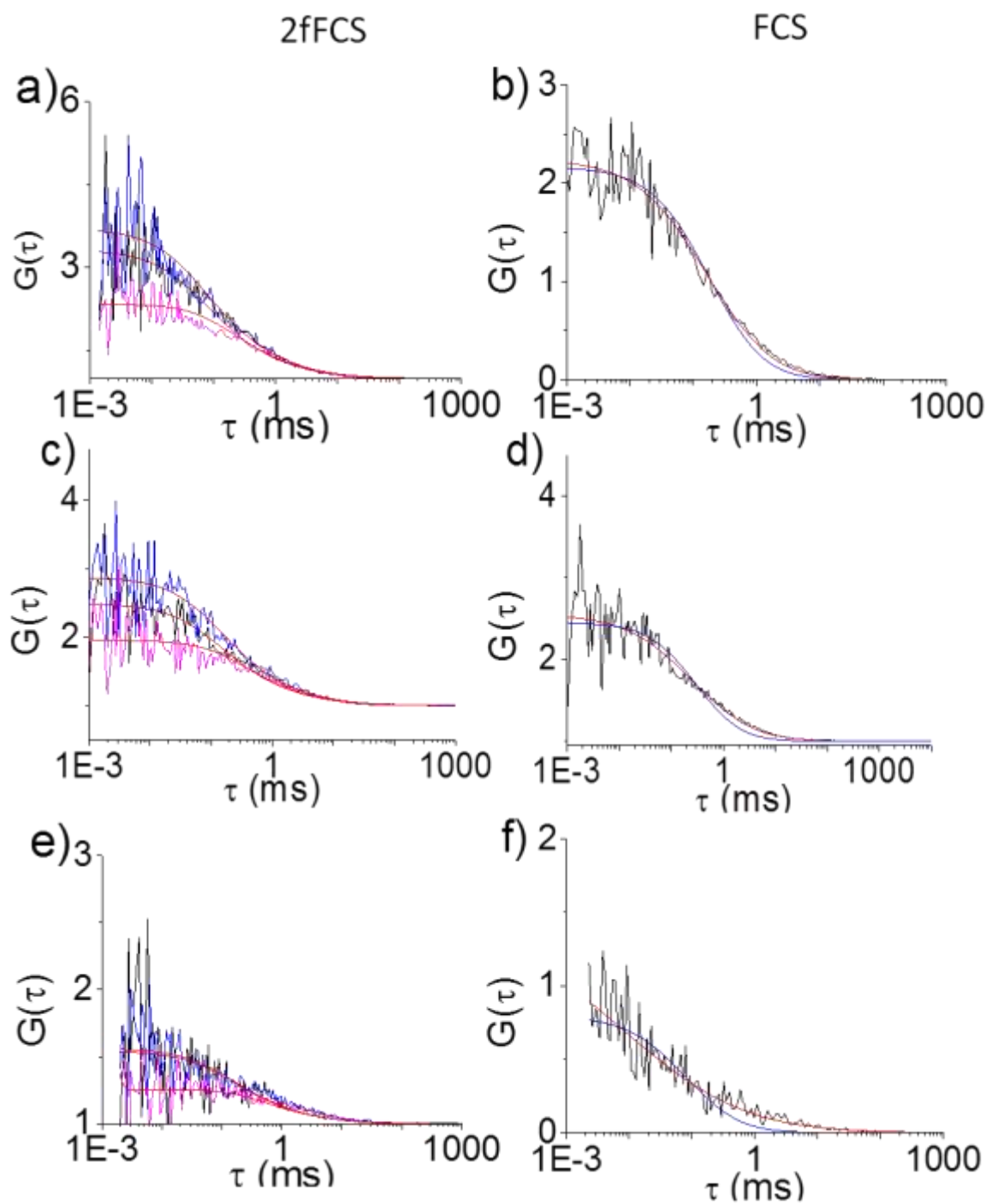


Figure 3.2 Comparison of 2fFCS ((a), (c) (e)) and single-focus FCS ((b), (d), (f)) on 3-kDa tagged dextran tracers that diffuse within semidilute p(AAm-co-DMMIAAm) matrixes. The matrix concentration increases from top to bottom top, covering 28 g L^{-1} ((a),(b)), 56 g L^{-1} ((c), (d)), and 84 g L^{-1} ((e), (f)). The fitting parameter α from Eq. 3.7 decreases in the same order: $\alpha_{28 \text{ g/L}} = 0.83$; $\alpha_{56 \text{ g/L}} = 0.57$; $\alpha_{84 \text{ g/L}} = 0.43$, denoting increasing extent of anomaly of the diffusion. By contrast, no anomalous diffusion is detected in 2fFCS ((a), (c) (e)), which allows for simple data fitting according to Eq. 2 in all cases. The residuals to the fits can be found in the supplemental information, Fig. S.3.3.

In the preceding samples, the refractive index linearly increases with the polymer concentration, as shown in Figure 3.3. This assessment can serve to identify dextran and p(AAm-co-DMMIAAm) polymer matrixes that exhibit the same refractive index, despite being fundamentally different in their chemical composition and nanometer-scale topology. When single-focus FCS results obtained for the 3-kDa dextran tracer in such complimentary pairs of different matrixes are compared, they all show very similar values of the fitting parameter α , as compiled in Table 3.1 and shown in Figure 3.2 and 3.4. In 2fFCS, however, no effect of anomalous diffusion is seen in all these cases, as also shown in Figure 3.2 and 3.4. These results support our hypothesis of optical effects to cause apparent anomalous diffusion in single-focus FCS, whereas 2fFCS is not prone to exhibit these artifacts.

Table 3.1. Best-fit values of α according to Eq. 7 if single-focus FCS is measured on 3-kDa dextran tracers that diffuse in matrixes of either p(AAm-co-DMMIAAm) or 70-kDa dextran, chosen such to exhibit similar refractive indexes (cf. Figure 3.3).

n	$c_{p(\text{AAM-co-DMMIAAm})}$ [g L ⁻¹]	c_{Dextran} [g L ⁻¹]	$\alpha_{p(\text{AAM-co-DMMIAAm})}$	α_{Dextran}
1.337	28	45	0.83	0.81
1.343	56	90	0.57	0.49
1.351	84	130	0.43	0.39

To further strengthen our conclusion, we conduct a last set of experiments with a view to two extreme situations: we compare the diffusion of 3-kDa labeled dextran tracers in either an acrylamide–bisacrylamide monomer solution ($c_{\text{AAM}} = 90 \text{ g L}^{-1}$; $c_{\text{BIS}} = 3.25 \text{ g L}^{-1}$) or in a chemically crosslinked polyacrylamide hydrogel obtained by free-radical crosslinking copolymerization of the latter monomers (Figure 3.5). These samples exhibit the same refractive index, but very different extent of topological constraint on the tracer diffusion, along with different extent of potential matrix–tracer interaction. In

these experiments, single-focus FCS denotes anomalous diffusion in both the monomer solutions and the hydrogels, with best-fit values of $\alpha_{\text{solution}} = 0.49$ and $\alpha_{\text{gel}} = 0.52$. Whereas such anomalous diffusion might be expected in the hydrogel sample, [53, 54] it is unexpected for the simple monomer solution. The finding that even this monomer solution seems to exhibit anomalous diffusion, with a stretching exponent α that closely matches that of the hydrogel, supports our hypothesis of optical artifacts to be the main contributor to apparent anomalous diffusion in single-focus FCS. By contrast, 2fFCS does again not show any indication of anomalous diffusion in both the latter samples.

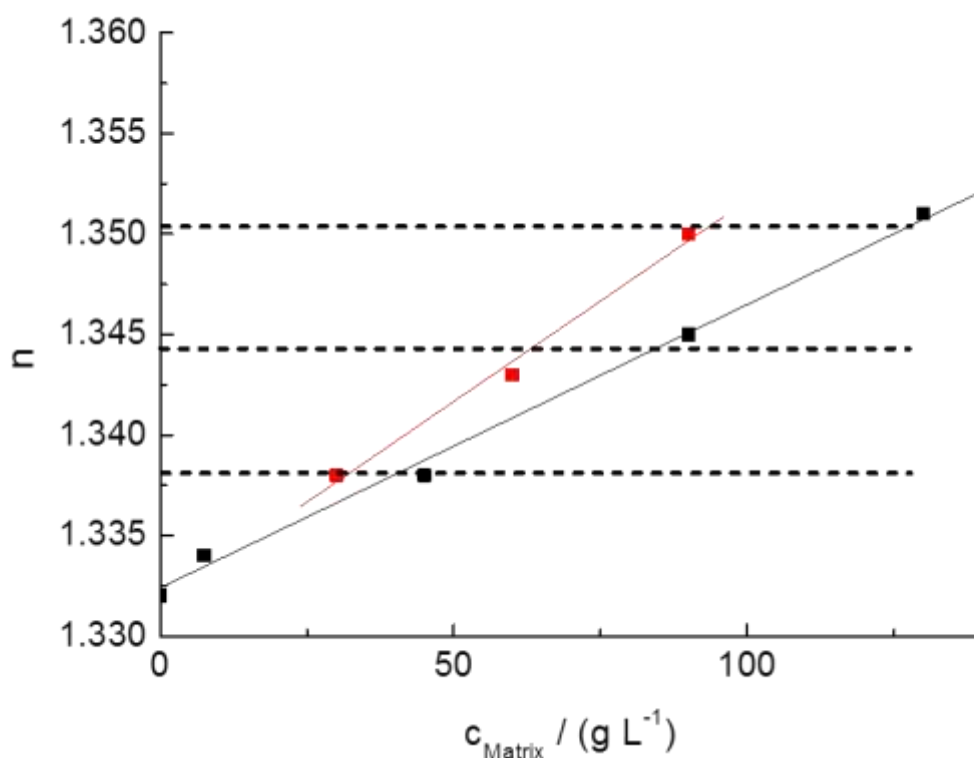


Figure 3.3 Dependence of the refractive index, n , of aqueous solutions of 70-kDa dextran (black) or 687-kDa p(AAm-co-DMMIAAm) (red) on the respective polymer concentration, c . Dashed lines highlight similar values of the refractive indexes that denote complimentary pairs of polymer matrixes, fundamentally different in their composition and polymer topology, but similar in terms of their optical properties.

Some of the present correlation functions have a rather low signal-to-noise ratio of about 1.5 to 1, which we attribute to light scattering of the fluorescence signal in the samples. An evidence for this hypothesis is that the noise in the correlation function increases with the sample refractive index. Nevertheless, the increasing difference of the simple model without anomalous diffusion (Eq.3.6) and the more sophisticated model that includes anomalous diffusion (Eq.3.7) is visible by eye (Figure 3.1, 3.2, 3.4, and 3.5). Therefore, we are convinced that even noisy correlation functions are suitable to demonstrate the effect of the refractive index mismatch on the general shape of the correlation function.

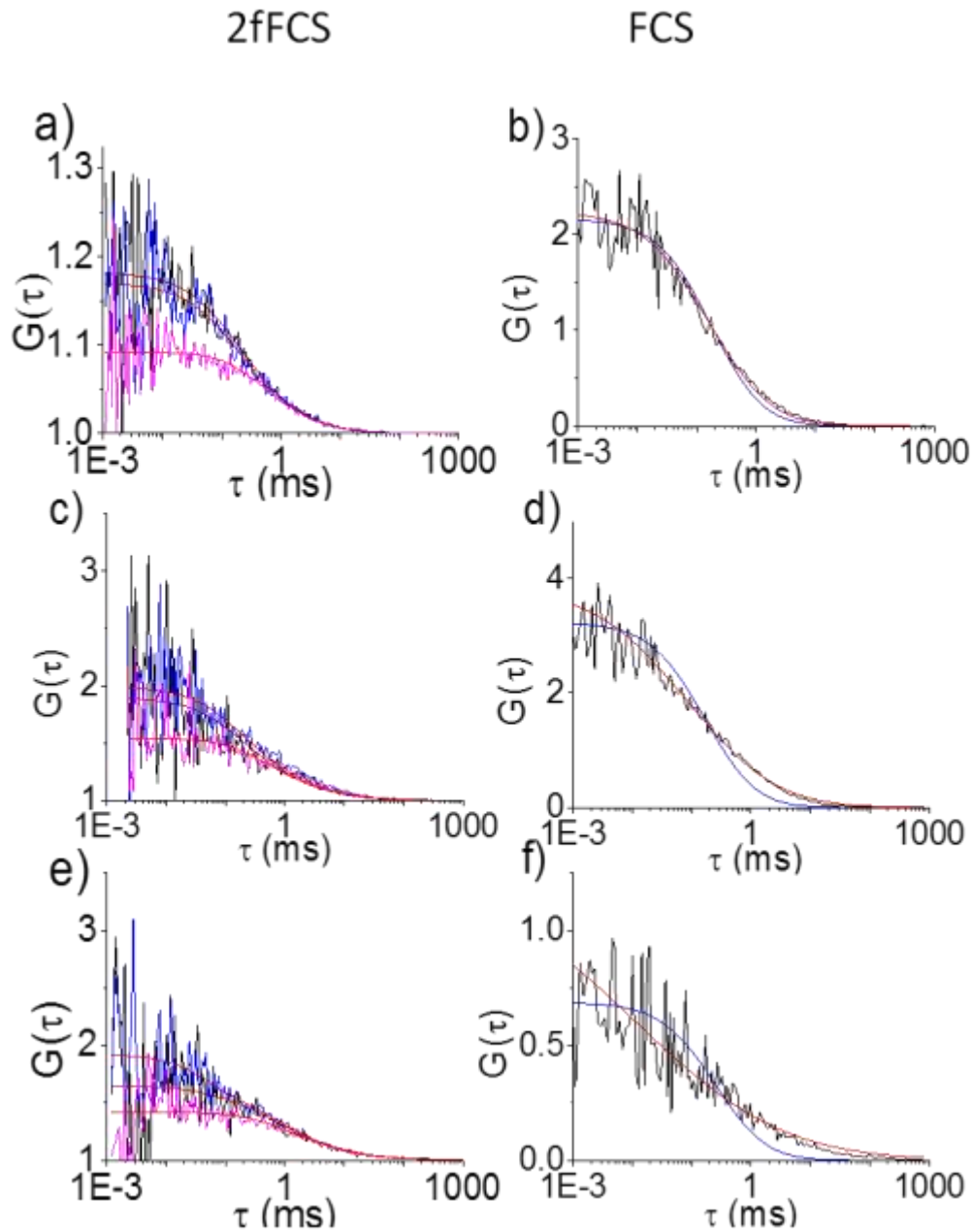


Figure 3.4 Comparison of 2fFCS ((a), (c), (e)) and single-focus FCS ((b), (d), (f)) on 3-kDa tagged dextran tracers that diffuse within 70-kDa dextran matrixes. The matrix concentrations increase from top to bottom. Top: $c_{\text{matrix}} = 45 \text{ g L}^{-1}$; center: $c_{\text{matrix}} = 90 \text{ g L}^{-1}$; bottom: $c_{\text{matrix}} = 130 \text{ g L}^{-1}$. The α value decreases in the same order: $\alpha_{45\text{-g/L}} = 0.81$; $\alpha_{90\text{-g/L}} = 0.49$; $\alpha_{130\text{-g/L}} = 0.39$. By contrast, no anomalous diffusion is detected in 2fFCS ((a), (c), (e)). The refractive indexes of the dextran matrixes match those of the p(AAm-co-DMMIAAm) samples from Figure 3. The values of α are the same for corresponding samples with similar refractive indexes, independent of their chemical composition and polymer topology. The residuals to the fits can be found in the supplemental information, Fig. S.3.4.

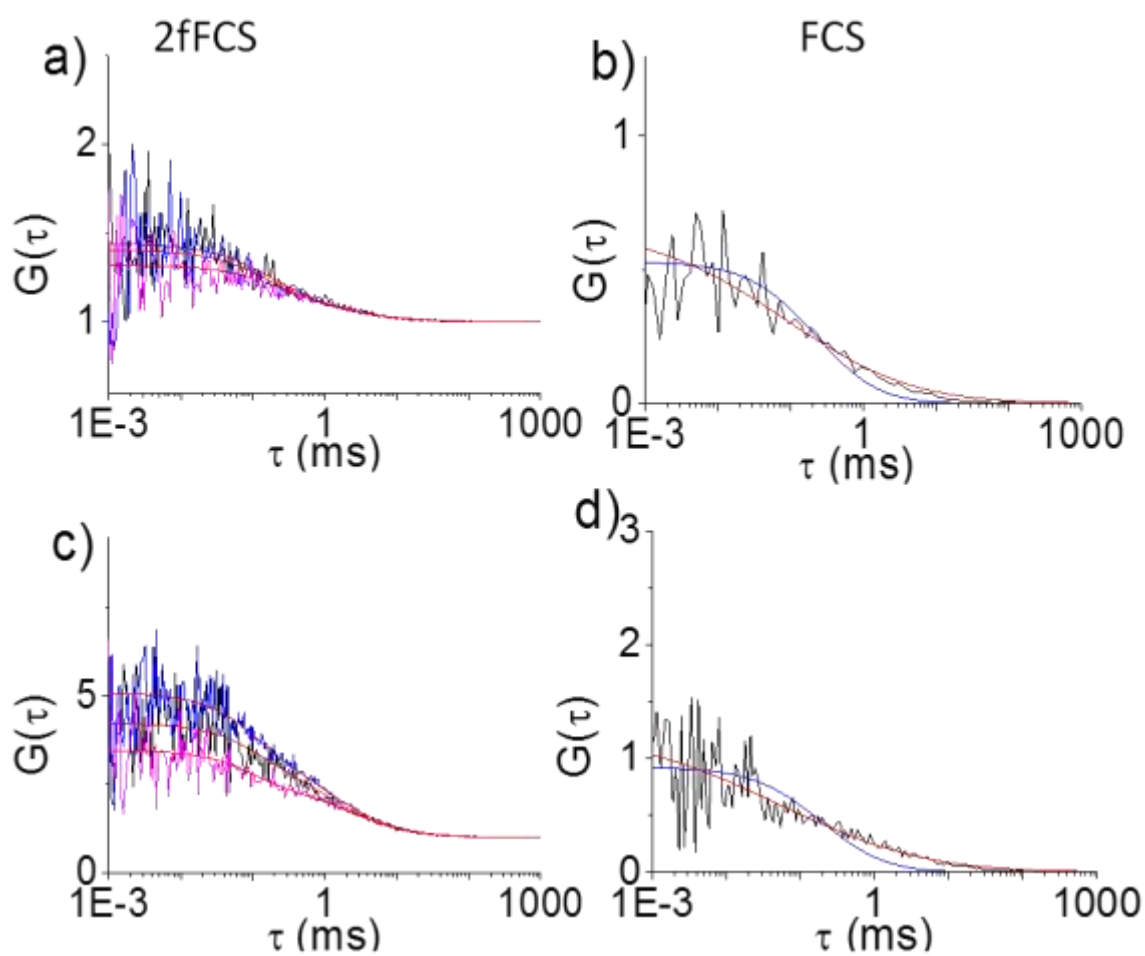


Figure 3.5 Comparison of 2fFCS ((a), (c)) and single-focus FCS ((b), (d)) on 3-kDa tagged dextran tracers that diffuse within a 90-gL^{-1} acrylamide-bisacrylamide solution ((a), (b)) or in a corresponding chemically crosslinked PAAm hydrogel ((c), (d)). Fitting of the single-focus FCS data was performed with the standard model according to Eq. 3.6 (blue lines) and with the model for anomalous diffusion according to Eq. 3.7 (red lines). In both measurements, the standard model does not fit sufficiently, whereas fitting with the anomalous diffusion model is possible with good confidence, yielding $\alpha = 0.49$ for the solution and $\alpha = 0.52$ for the hydrogel. The residuals to the fits can be found in the supplemental information, Fig. S.3.5.

3.4. Conclusions

Comparison of single-focus and two-focus experiments on dextran tracers in different complex environments highlights the relevance of refractive index mismatch in fluorescence correlation spectroscopy. If single-focus FCS must be used in a given experimental situation, refractive index mismatch needs to be taken into account during the data analysis.[21, 35, 37, 44, 56, 57] However, it is not always possible to determine the refractive index, especially for samples with heterogeneous morphology. Such samples are characterized by local variation of their composition and refractive index, preventing correction of single focus FCS data with respect to optical artifacts. In such cases, 2fFCS is a better technique that still provides reliable data.[58, 59] The message of this chapter is to sensitize the reader for the impact of the refractive index mismatch on the single-focus FCS measurements and for the need of taking the refractive index mismatch into account during the data analysis. However, this work does not at all attempt to question the existence of anomalous diffusion.

3.5. Supporting Information

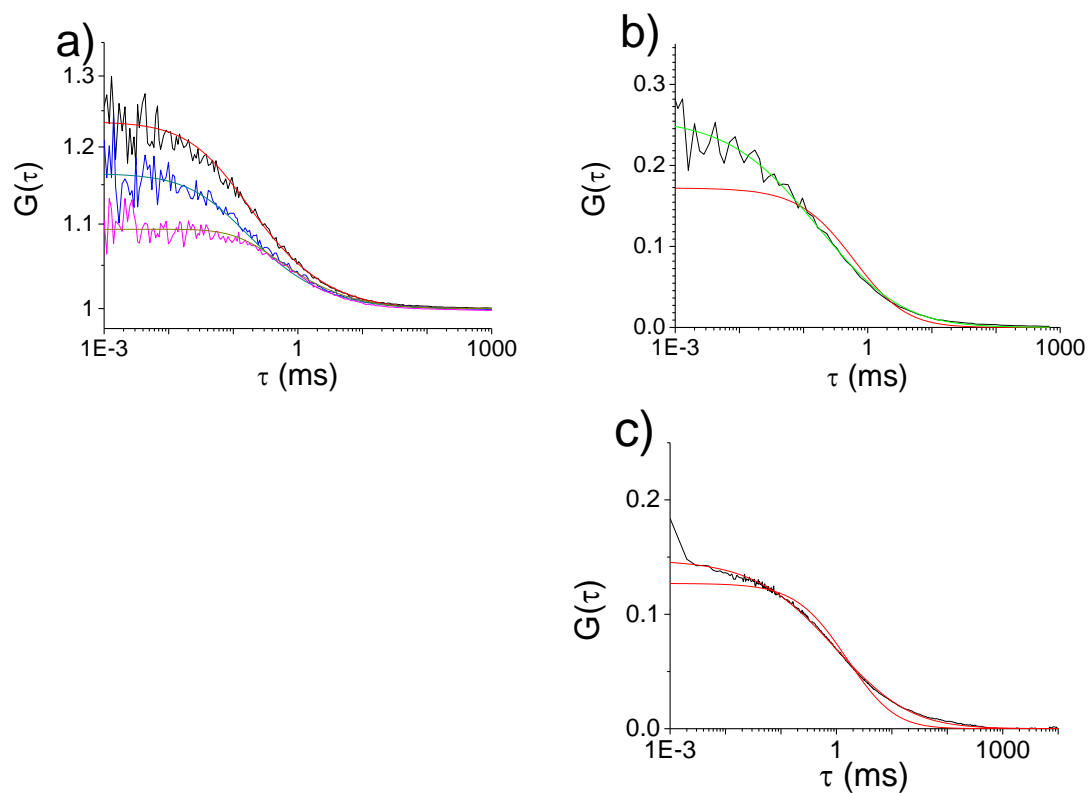


Fig. S.3.1 FCS experiments on 70-kDa dextran tracers that diffuse within 80-gL^{-1} $p(\text{AAm-co-DMMIAAm})$ semidilute polymer matrixes. a) 2fFCS measurement fitted with Eq. 2, not indicating anomalous diffusion. b) Autocorrelation of the first focus of the 2fFCS measurement fitted with Eq. 6 for normal diffusion (red line) and Eq.7 (green line) with $\alpha = 0.665$. c) Related measurement with single-focus FCS instrumentation, fitted with an equation equal to Eq. 6 (red line) and Eq. 7 (green line), again denoting $\alpha = 0.666$.

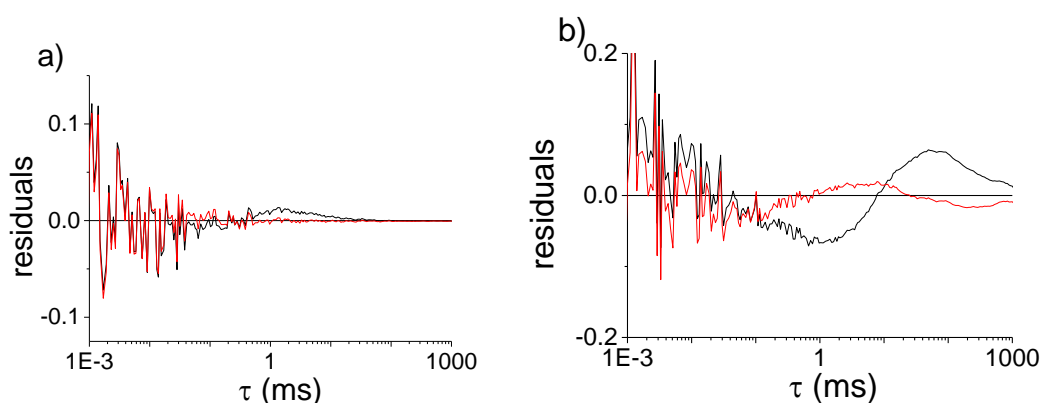


Fig. S.3.2 Residuals to the single focus FCS data in Figure 1. a) Corresponding to Figure 1d; b) corresponding to Figure 1h. Black: fit to Eq.6 without taking anomalous diffusion into account. Red: fit to Eq.7 accounting for anomalous diffusion.

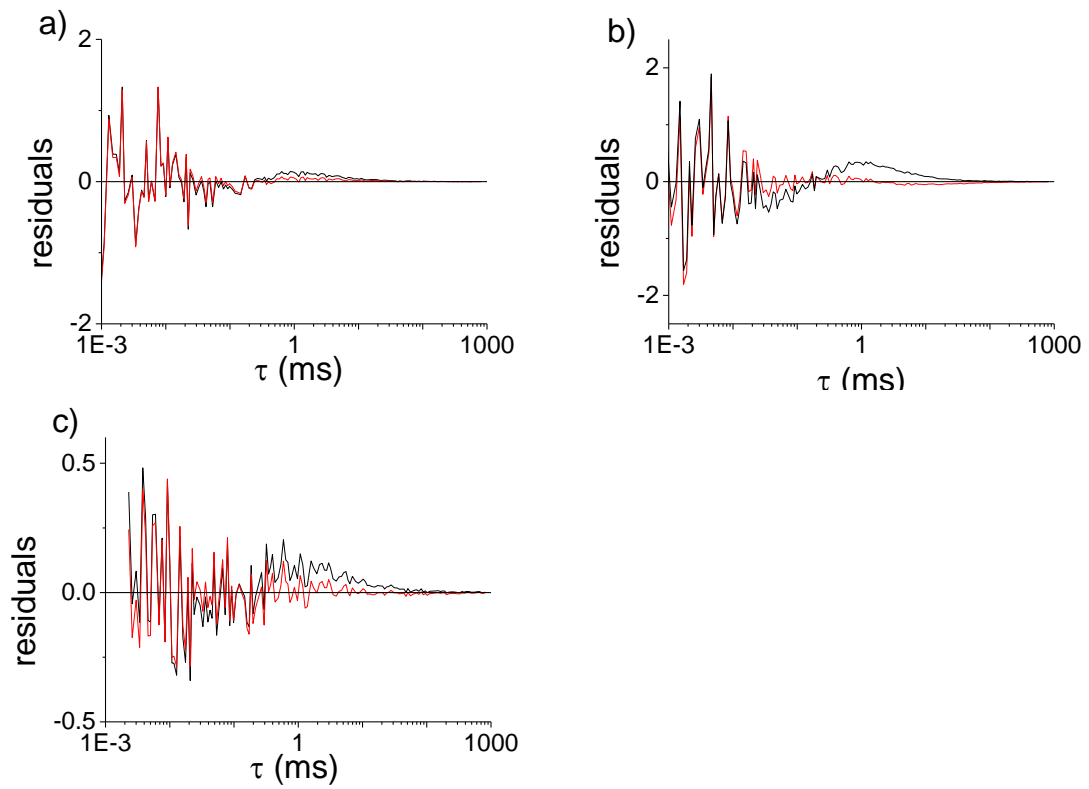


Fig. S.3.3 Residuals to the single focus FCS data in Figure 2. a) Corresponding to Figure 2b; b) corresponding to Figure 2d; c) corresponding to Figure 2f. Black: fit to Eq.6 without taking anomalous diffusion into account. Red: fit to Eq.7 accounting for anomalous diffusion.

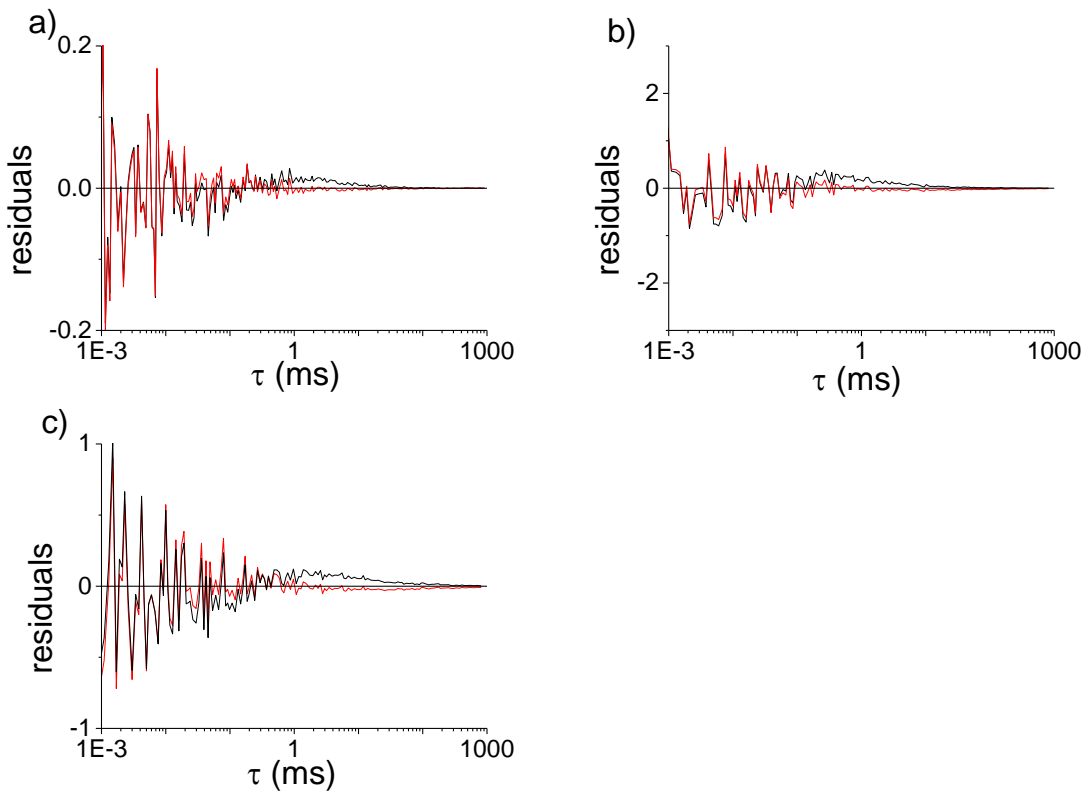


Fig. S.3.4 Residuals to the single focus FCS data in Figure 4. a) Corresponding to Figure 4b; b) corresponding to Figure 4d; c) corresponding to Figure 4f. Black: fit to Eq.6 without taking anomalous diffusion into account. Red: fit to Eq.7 accounting for anomalous diffusion.

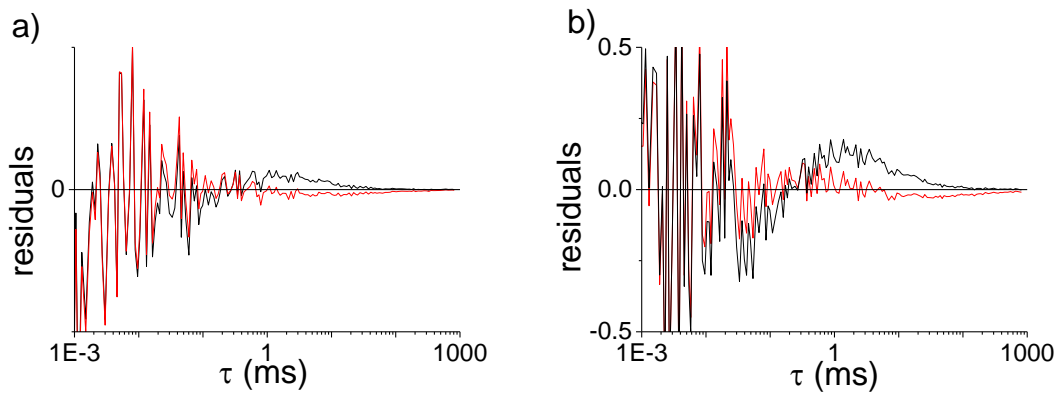


Fig. S.3.5 Residuals to the single focus FCS data in Figure 5. a) Corresponding to Figure 5b; b) corresponding to Figure 5d. Black: fit to Eq.6 without taking anomalous diffusion into account. Red: fit to Eq.7 accounting for anomalous diffusion.

3.6. References

1. Franck, C., et al., *Three-dimensional traction force microscopy: a new tool for quantifying cell-matrix interactions*. PLoS One, 2011. **6**(3): p. e17833.
2. Hannus, S. and R. Brock, *Fluorescence correlation spectroscopy. Analysis of molecular interactions in cell lysates*. BIoSpektrum, 2012. **18**(6): p. 599-601.
3. Malchus, N. and M. Weiss, *Elucidating Anomalous Protein Diffusion in Living Cells with Fluorescence Correlation Spectroscopy-Facts and Pitfalls*. J. Fluoresc., 2010. **20**(1): p. 19-26.
4. Betaneli, V. and P. Schwille, *Fluorescence correlation spectroscopy to examine protein-lipid interactions in membranes*. Methods Mol. Biol., 2013. **974**(Lipid-Protein Interactions): p. 253-278.
5. Weiss, K. and J. Enderlein, *Lipid Diffusion within Black Lipid Membranes Measured with Dual-Focus Fluorescence Correlation Spectroscopy*. ChemPhysChem, 2012. **13**(4): p. 990-1000.
6. Sterling, S.M., et al., *Phospholipid Diffusion Coefficients of Cushioned Model Membranes Determined via Z-Scan Fluorescence Correlation Spectroscopy*. Langmuir, 2013. **29**(25): p. 7966-7974.
7. Muhr, A.H. and J.M.V. Blanshard, *DIFFUSION IN GELS*. Polymer, 1982. **23**(7): p. 1012-1026.
8. Doi, M., *Gel dynamics*. J. Phys. Soc. Jpn., 2009. **78**(5): p. 052001/1-052001/19.
9. Marutani, S., *Method and apparatus for treatment of gel materials deposited in exhaust pipes of CVD apparatus for semiconductor device fabrication*. 2006. p. 13pp.
10. Nishide, T., et al., *Gel-type conductive films and manufacture thereof*. 2012. p. 14pp.
11. Michelman-Ribeiro, A., et al., *Structural changes in polymer gels probed by fluorescence correlation spectroscopy*. Macromolecules, 2004. **37**(26): p. 10212-10214.
12. Zustiak, S.P., H. Boukari, and J.B. Leach, *Solute diffusion and interactions in cross-linked poly(ethylene glycol) hydrogels studied by Fluorescence Correlation Spectroscopy*. Soft Matter, 2010. **6**(15): p. 3609-3618.
13. Chand, D., S.D. Varma, and R.P.S. Kushwaha, *Active transport of glycine by rumen epithelium of betal goats*. J. Dairy Sci., 1968. **51**(9): p. 1420-2.
14. Maines, M.D. and A. Kappas, *Selenium regulation of hepatic heme metabolism: induction of delta-aminolevulinat synthase and heme oxygenase*. Proc Natl Acad Sci U S A, 1976. **73**(12): p. 4428-31.
15. Romero, V., et al., *Frictional and Electrical Effects Involved in the Diffusive Transport through a Nanoporous Alumina Membrane*. Journal of Physical Chemistry C, 2013. **117**(48): p. 25513-25518.
16. Koter, S., et al., *Modeling the transport of sulfuric acid and its sulfates (MgSO₄, ZnSO₄, Na₂SO₄) through an anion-exchange membrane*. Desalination, 2014. **342**: p. 75-84.

17. Vanneste, J., et al., *Novel natural and biomimetic ligands to enhance selectivity of membrane processes for solute-solute separations: beyond nature's logistic legacy*. J. Chem. Technol. Biotechnol., 2014. **89**(3): p. 354-371.
18. Lynch, I., P. de Gregorio, and K.A. Dawson, *Simultaneous release of hydrophobic and cationic solutes from thin-film "plum-pudding" gels: A multifunctional platform for surface drug delivery?* Journal of Physical Chemistry B, 2005. **109**(13): p. 6257-6261.
19. Weiss, M., H. Hashimoto, and T. Nilsson, *Anomalous protein diffusion in living cells as seen by fluorescence correlation spectroscopy*. Biophys. J., 2003. **84**(6): p. 4043-4052.
20. Zustiak, S.P., R. Nossal, and D.L. Sackett, *Hindered Diffusion in Polymeric Solutions Studied by Fluorescence Correlation Spectroscopy*. Biophys. J., 2011. **101**(1): p. 255-264.
21. Zettl, U., et al., *Self-Diffusion and Cooperative Diffusion in Semidilute Polymer Solutions As Measured by Fluorescence Correlation Spectroscopy*. Macromolecules, 2009. **42**(24): p. 9537-9547.
22. Tabatabaei, F., O. Lenz, and C. Holm, *Simulation study of anomalous tracer diffusion in hydrogels*. Colloid Polym. Sci., 2011. **289**(5-6): p. 523-534.
23. Elson, E.L. and D. Magde, *Fluorescence correlation spectroscopy. I. Conceptual basis and theory*. Biopolymers, 1974. **13**(1): p. 1-27.
24. Magde, D., E.L. Elson, and W.W. Webb, *Fluorescence correlation spectroscopy. II. Experimental realization*. Biopolymers, 1974. **13**(1): p. 29-61.
25. Krichevsky, O. and G. Bonnet, *Fluorescence correlation spectroscopy: the technique and its applications*. Rep. Prog. Phys., 2002. **65**(2): p. 251-297.
26. Dertinger, T., et al., *Two-focus fluorescence correlation spectroscopy: A new tool for accurate and absolute diffusion measurements*. Chemphyschem, 2007. **8**(3): p. 433-443.
27. Koynov, K. and H.-J. Butt, *Fluorescence correlation spectroscopy in colloid and interface science*. Curr. Opin. Colloid Interface Sci., 2012. **17**(6): p. 377-387.
28. Woell, D., *Fluorescence correlation spectroscopy in polymer science*. RSC Adv., 2014. **4**(5): p. 2447-2465.
29. Wong, J.E. and W. Richtering, *Layer-by-layer assembly on stimuli-responsive microgels*. Current Opinion in Colloid & Interface Science, 2008. **13**(6): p. 403-412.
30. Wong, J.E., et al., *Study of Layer-by-Layer Films on Thermoresponsive Nanogels Using Temperature-Controlled Dual-Focus Fluorescence Correlation Spectroscopy*. Journal of Physical Chemistry B, 2009. **113**(49): p. 15907-15913.
31. Papadakis, C.M., et al., *Polymers in focus: Fluorescence correlation spectroscopy*. Colloid Polym. Sci., 2014. **292**(10): p. 2399 - 2411.
32. Horton, M.R., et al., *Development of anomalous diffusion among crowding proteins*. Soft Matter, 2010. **6**(12): p. 2648-2656.
33. Sanabria, H. and M.N. Waxham, *Transient Anomalous Subdiffusion: Effects of Specific and Nonspecific Probe Binding with Actin Gels*. J. Phys. Chem. B, 2009. **114**(2): p. 959-972.
34. Enderlein, J., et al., *Performance of fluorescence correlation spectroscopy for measuring diffusion and concentration*. Chemphyschem, 2005. **6**(11): p. 2324-2336.

35. Enderlein, J., et al., *Art and artifacts of fluorescence correlation spectroscopy*. Proc. SPIE-Int. Soc. Opt. Eng., 2005. **5699**(Imaging, Manipulation, and Analysis of Biomolecules and Cells: Fundamentals and Applications III): p. 167-174.
36. Dertinger, T., et al., *The optics and performance of dual-focus fluorescence correlation spectroscopy*. Opt. Express, 2008. **16**(19): p. 1435314368.
37. Muller, C.B., et al., *Dual-focus fluorescence correlation spectroscopy: a robust tool for studying molecular crowding*. Soft Matter, 2009. **5**(7): p. 1358-1366.
38. Ries, J. and P. Schwille, *Fluorescence correlation spectroscopy*. Bioessays, 2012. **34**(5): p. 361-8.
39. Dertinger, T., *Two-Focus Fluorescence Correlation Spectroscopy*, in *Mathematisch - Naturwissenschaftliche Fakultät*. 2007, Universität zu Köln.
40. Aouani, H., et al., *High-efficiency single molecule fluorescence detection and correlation spectroscopy with dielectric microspheres*. Proc. SPIE, 2010. **7571**(Single Molecule Spectroscopy and Imaging III): p. 75710A/1-75710A/12.
41. Harlepp, S., et al., *Subnanometric measurements of evanescent wave penetration depth using total internal reflection microscopy combined with fluorescent correlation spectroscopy*. Appl. Phys. Lett., 2004. **85**(17): p. 3917-3919.
42. Masuda, A., K. Ushida, and T. Okamoto, *Direct observation of spatiotemporal dependence of anomalous diffusion in inhomogeneous fluid by sampling-volume-controlled fluorescence correlation spectroscopy*. Physical Review E, 2005. **72**(6): p. 060101.
43. Masuda, A., K. Ushida, and T.O. Riken, *New fluorescence correlation spectroscopy enabling direct observation of spatiotemporal dependence of diffusion constants as an evidence of anomalous transport in extracellular matrices*. Biophysical Journal, 2005. **88**(5): p. 3584-3591.
44. Enderlein, J., *Polymer Dynamics, Fluorescence Correlation Spectroscopy, and the Limits of Optical Resolution*. Physical Review Letters, 2012. **108**(10): p. 108101/1-108101/4.
45. Armstrong, J.K., et al., *The hydrodynamic radii of macromolecules and their effect on red blood cell aggregation*. Biophys. J., 2004. **87**(6): p. 4259-4270.
46. Ponder, E. and R.V. Ponder, *THE INTERACTION OF DEXTRAN WITH SERUM ALBUMIN, GAMMA-GLOBULIN, AND FIBRINOGEN*. Journal of General Physiology, 1960. **43**(4): p. 753-758.
47. Al-Baradi, A.M., et al., *Magnetic field dependence of the diffusion of single dextran molecules within a hydrogel containing magnetite nanoparticles*. J. Chem. Phys., 2011. **134**(9): p. 094901/1-094901/7.
48. Goins, A.B., H. Sanabria, and M.N. Waxham, *Macromolecular Crowding and Size Effects on Probe Microviscosity*. Biophysical Journal, 2008. **95**(11): p. 5362-5373.
49. Seiffert, S., W. Oppermann, and K. Saalwächter, *Hydrogel formation by photocrosslinking of dimethylmaleimide functionalized polyacrylamide*. Polymer, 2007. **48**(19): p. 5599-5611.
50. Banachowicz, E., et al., *Successful FCS Experiment in Nonstandard Conditions*. Langmuir, 2014. **30**(29): p. 8945-8955.
51. Liu, R.G., et al., *A fluorescence correlation spectroscopy study on the self-diffusion of polystyrene chains in dilute and semidilute solution*. Macromolecules, 2005. **38**(21): p. 8845-8849.

52. Ying, Q.C. and B. Chu, *OVERLAP CONCENTRATION OF MACROMOLECULES IN SOLUTION*. *Macromolecules*, 1987. **20**(2): p. 362-366.
53. Saxton, M.J., *Anomalous diffusion due to obstacles: a Monte Carlo study*. *Biophys J*, 1994. **66**(2 Pt 1): p. 394-401.
54. Netz, P.A. and T. Dorfmueller, *Computer simulation studies of anomalous diffusion in gels: structural properties and probe-size dependence*. *J. Chem. Phys.*, 1995. **103**(20): p. 9074-82.
55. Seiffert, S. and W. Oppermann, *Diffusion of linear macromolecules and spherical particles in semidilute polymer solutions and polymer networks*. *Polymer*, 2008. **49**(19): p. 4115-4126.
56. Tanaka, S., *Fluorescence correlation spectroscopy and Brownian dynamics simulation of protein diffusion under confinement in lipid cubic phases*. *Soft Matter*, 2012. **8**(34): p. 8936-8943.
57. Wang, F., et al., *Conformational Transition of Poly(N-isopropylacrylamide) Single Chains in Its Cononsolvency Process: A Study by Fluorescence Correlation Spectroscopy and Scaling Analysis*. *Macromolecules*, 2012. **45**(22): p. 9196-9204.
58. Lehmann, S., S. Seiffert, and W. Richtering, *Spatially Resolved Tracer Diffusion in Complex Responsive Hydrogels*. *J. Am. Chem. Soc.*, 2012. **134**(38): p. 15963-15969.
59. Lehmann, S., S. Seiffert, and W. Richtering, *Diffusion of guest molecules within sensitive core-shell microgel carriers*. *Journal of Colloid and Interface Science*, 2014. **431**(0): p. 204-208.

4. Diffusion of guest molecules within sensitive core-shell microgel carriers²

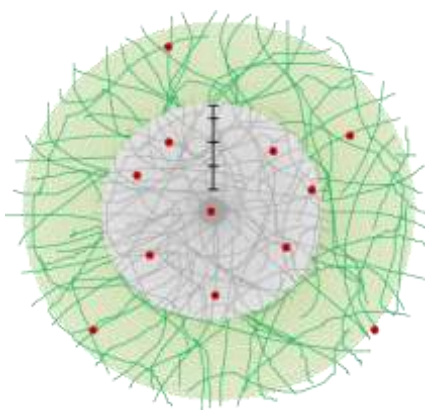
4.1. Introduction

Microgels are small particles with size in the range of 10 nm to 100 μm . [1] They consist of polymer networks swollen by solvent, typically water. These particles have the capability to incorporate guest molecules or colloids within their interior; this makes microgels interesting for a variety of applications [2], including those in catalysis [3], separation procedures [4], and in drug delivery [5-12]. These and other applications are particularly excelled when the microgels exhibit environmentally responsive swelling and deswelling, which is achieved if they consist of environmentally responsive polymer gels. One of the most popular polymers exhibiting such responsivity is poly(*N*-isopropylacrylamide) (PNIPAM) [13]. Water-swollen PNIPAM networks have a lower critical solution temperature (LCST) of 33.6 °C [14-16]. Above this critical temperature, the polymer becomes less soluble in water, and the size of a PNIPAM microgel markedly decreases, entailing volume changes of up to 1000% [17].

There are two different classes of microgel particles: small, colloidal-scale microgels with sizes of a few micrometers to some few micrometers [18, 19], and bigger, non-colloidal microgels with sizes of several tens or hundreds of micrometers [20]. Depending on their targeted application, both these classes of microgels have their specific advantages. For example, whereas colloidal-scale microgels can penetrate cells or

² This chapter was published in Journal of Colloid and Interface Science, 2014. **431**(0): p. 204-208. The article had been accepted. The study was performed in collaboration with the co-authors. My contribution was the synthesis of the final samples. Furthermore, I performed the 2fFCS measurements and did the data analysis.

capillary tubes, above-colloidal microgels cannot, which may both either be desired or undesired in inter- or extracellular drug delivery applications. For both these different classes of microgels, a particularly useful morphology is that of a core–shell particle, because this morphology intrinsically resembles that of a microcapsule [19, 20]. Such core–shell particles allow active compounds to be encapsulated within their core, whereas the shell can be tailored such to allow for triggered, controlled release of the actives [19, 21, 22]. However, to make this truly useful, it must be understood how the shell swelling and deswelling affects the diffusive mobility of the active payload within the microgel core, because it is this mobility that eventually determines the rate of release of the active in an application [23, 24].



Scheme 4.1 Schematic of a core–shell particle as studied in this work. The grey center indicates a temperature insensitive and unlabeled PAAM hydrogel core. The green layer indicates a temperature sensitive, AlexaFluor488-labeled PNIPAM hydrogel shell. The red dots indicate labeled tracer particles. In this work, the diffusive mobility of these tracers is probed by 2fFCS at positions indicated by the black scale.

In this chapter, we study the mobility of different dextran tracer molecules and colloids inside above-colloidal core–shell microgel particles through the use of spatially resolved two-focus fluorescence correlation spectroscopy (2fFCS) [25] as shown in Scheme 4.1.

The microgels consist of a core of polyacrylamide (PAAM) surrounded by a shell of

PNIPAM that slightly interpenetrates the PAAM core at the core–shell interface. Despite this interpenetration, the core shows no change of size and shape upon variation of temperature around 34 °C in aqueous media, whereas the shell does [21]. This mechanism can be used to incorporate guest molecules or colloids inside the core: at elevated temperature, the shell deswells and the guest molecules are trapped within the particle core but still freely diffuse within it, while reswelling the shell by temperature decrease allows the guests to be released [21]. In solvents different than water that are non-solvents or poor solvents for PAAM and PNIPAM, both the core and the shell deswell completely or partially. In both the above scenarios, we find that it is the core degree of swelling or deswelling that determines that of the interpenetrating part of the shell polymer network, independent of the shell degree of swelling or deswelling itself. In neither case, however, we find marked effect of the shell swelling or deswelling on the diffusivity of dextran tracers within the core. This finding assures absence of artifacts such as adsorption of the guests to the amphiphilic shell polymer, supporting the utility of the microgel carriers in encapsulation and controlled release applications.

4.2. Materials and methods

4.2.1. Microgel synthesis

Core–shell particles as sketched in Scheme 4.1 are obtained by two-step droplet-based microfluidic templating [21]. In the first step, 60- μm polyacrylamide (PAAM) hydrogel core particles are prepared. In the second step, these particles are wrapped into 30- μm hydrogel shells of poly(*N*-isopropylacrylamide) (PNIPAM) labeled with AlexaFluor488. To

allow for rapid shell gelation at room temperature, a photochemical polymer-analogous approach is employed: instead of using monomer polymerization, the shell hydrogel is prepared from pre-polymerized PNIPAM chains that carry small percentages of photoreactive moieties, dimethylmaleimide. These moieties can be rapidly dimerized by UV-induced [2+2] addition without marked heat of reaction, thereby ensuring a homogeneous, non-porous polymer gel layer to be formed at high reaction rate [26].

4.2.2. Tracer entrapment

We probe two kinds of labeled dextran tracers that diffuse within the core-shell microgels: a 3000 g mol⁻¹ dextran labeled with AlexaFluor647 (Invitrogen) with a hydrodynamic radius of $R_h = 1$ nm and a 70,000 g mol⁻¹ dextran labeled with Rhodamine (Invitrogen) with a hydrodynamic radius of $R_h = 6.5$ nm. Whereas the first tracer resembles a typical molecular active compound, the second tracer resembles a typical colloidal active. The hydrodynamic radii of both these tracers are calculated via the Stokes-Einstein equation from their diffusion coefficients determined at infinite dilution. To load these tracers into the microgels, an aqueous (LiChroSolv water, Merck) solution of both dextrans is mixed with an aqueous microgel suspension and then left to equilibrate for 24 h, allowing the tracers to penetrate the microgels by diffusion. The samples are then transferred into a temperature controlled sample cell [27] that allows the sample temperature to be varied between 5 and 60 °C. At low temperature, both the PAAM core and the PNIPAM shell are swollen in aqueous medium, whereas the shell deswells at elevated temperature.

To supplement contrary experiments with particles with deswollen core and partially swollen shell, methanol (MeOH) is added to the water to serve as a precipitation agent for PAAM. When this is done, the co-nonsolvency effect of water/MeOH on PNIPAM [28-32] allows the shell degree of swelling to be determined by the water/MeOH mixing ratio [33]. To quantify this, we measure the swelling ratio of a PAAM gel with the same composition as the core of the core-shell particles, along with the swelling ratio of plain PNIPAM microgels with the same composition as the shell of the core-shell particles in different water/MeOH mixtures, as shown in Figure 4.1. To realize the PAAM-gel control experiment, a macroscopic PAAM gel with a radius of 50 mm and a height of 7 mm is prepared by photo-crosslinking similar to the procedure of the core microgel gelation. This gel is stored for 24 hours and then cut into discs of equal size each (radius 10 mm). The gel discs are dried at room temperature for 16 days until no further mass changes are measurable. The dried discs are then immersed in water/MeOH mixtures with compositions as detailed in Figure 4.1 (left) and stored in these media for 7 days to reach equilibrium-swollen states. The mass-swelling ratios are calculated from the masses of the discs before and after swelling.

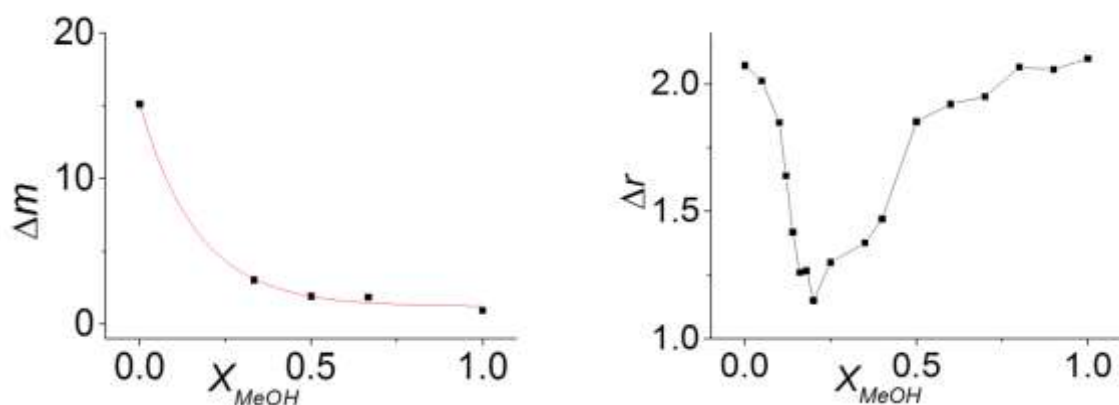


Figure 4.1 Comparison of the deswelling of a PAAM hydrogel (left) and the co-nonsolvency of a PNIPAM microgel [30] (right) in mixtures of water and methanol (MeOH) at 20 °C. The red line in the left diagram indicates a single exponential fit. Δm is the mass ratio of the PAAM hydrogels with respect to the mass in dry state (before dissolving in the water/MeOH mixtures). Δr is the ratio of the PNIPAM microgel radii in swollen and deswollen states, referenced to the particle size in water at 40 °C. x_{MeOH} is the mol fraction of MeOH in the solvent mixture.

4.2.3. 2fFCS

To probe the diffusivities of fluorescently labeled dextran tracers within the microgels in a spatially resolved fashion, we use two-focus fluorescence correlation spectroscopy (2fFCS). The simpler one-focus variant of this technique (FCS) is often used to determine tracer diffusion in hydrogels [34-37], and the two-focus extension allows us to conduct these experiments in complex environments, solving potential problems due to refractive-index mismatch between the immersion medium and the microgel sample specimen. This is achieved by introduction of an external length scale δ , which is the shift distance between two overlapping laser foci that is adjustable by a Nomarski prism [38]. To evaluate the diffusion coefficient from the 2fFCS experiments, the following equation is used:

$$g(\tau, \delta, \nu) = \frac{c}{4} \sqrt{\frac{\pi}{D \tau}} \int dz_1 \int dz_2 \left(\begin{array}{c} \frac{\kappa(z_1)\kappa(z_2)}{8 D \tau + w^2(z_1) + w^2(z_2)} \\ - \frac{(z_2 - z_1 - \nu_z \tau)^2}{4 D \tau} \\ - 2 \frac{(\delta - \nu_x \tau)^2 + \nu_y^2 \tau^2}{8 D \tau + w^2(z_1) + w^2(z_2)} \end{array} \right) \quad (4.1)$$

In eq. (4.1), D is the translational diffusion coefficient, τ the lag time of the cross-correlation, c the concentration of the fluorescent dextran tracers, δ is the shift distance (determined independently) and x , y , and z are Cartesian coordinates with z along the optical axis. Further functions are:

$$w(z) = w_0 \left[1 + \left(\frac{\lambda_{ex} z}{\pi w_0^2 n} \right)^2 \right]^{1/2} \quad (4.2)$$

$$\kappa(z) = 2 \int_0^a \frac{d\rho \rho}{R^2(z)} \exp\left(-\frac{2\rho^2}{R^2(z)}\right) = 1 - \exp\left(-\frac{2\rho^2}{R^2(z)}\right) \quad (4.3)$$

$$R(z) = R_0 \left[1 + \left(\frac{\lambda_{ex} z}{\pi R_0^2 n} \right)^2 \right]^{1/2} \quad (4.4)$$

In these latter equations, λ_{ex} is the excitation wavelength, λ_{em} is the emission wavelength, n is the refractive index, and R_0 is the confocal pinhole radius. The correlation function can be calculated numerically, and w_0 and R_0 are fit parameters [39]. A great benefit of the 2f-FCS data evaluation is that three correlation functions are fitted simultaneously with the same three fitting parameters D , w_0 , and R_0 ; this makes the fitting very accurate. Even in the case of poor statistics in the measurement, the simultaneous fitting of the three correlation functions leads to an accurate result [40].

The high accuracy of 2fFCS in crowded environments has been demonstrated previously [41, 42]. To achieve high spatial resolution for tracer-diffusion experiments, we employ a confocal microscope equipped with a 3D piezo table with a range of 100 μm in all three dimensions that serves to locate the regions of interest. With this setup, we measure the diffusion coefficient at several defined points in the sample, as indicated in Scheme 4.1.

4.3. Results and discussion

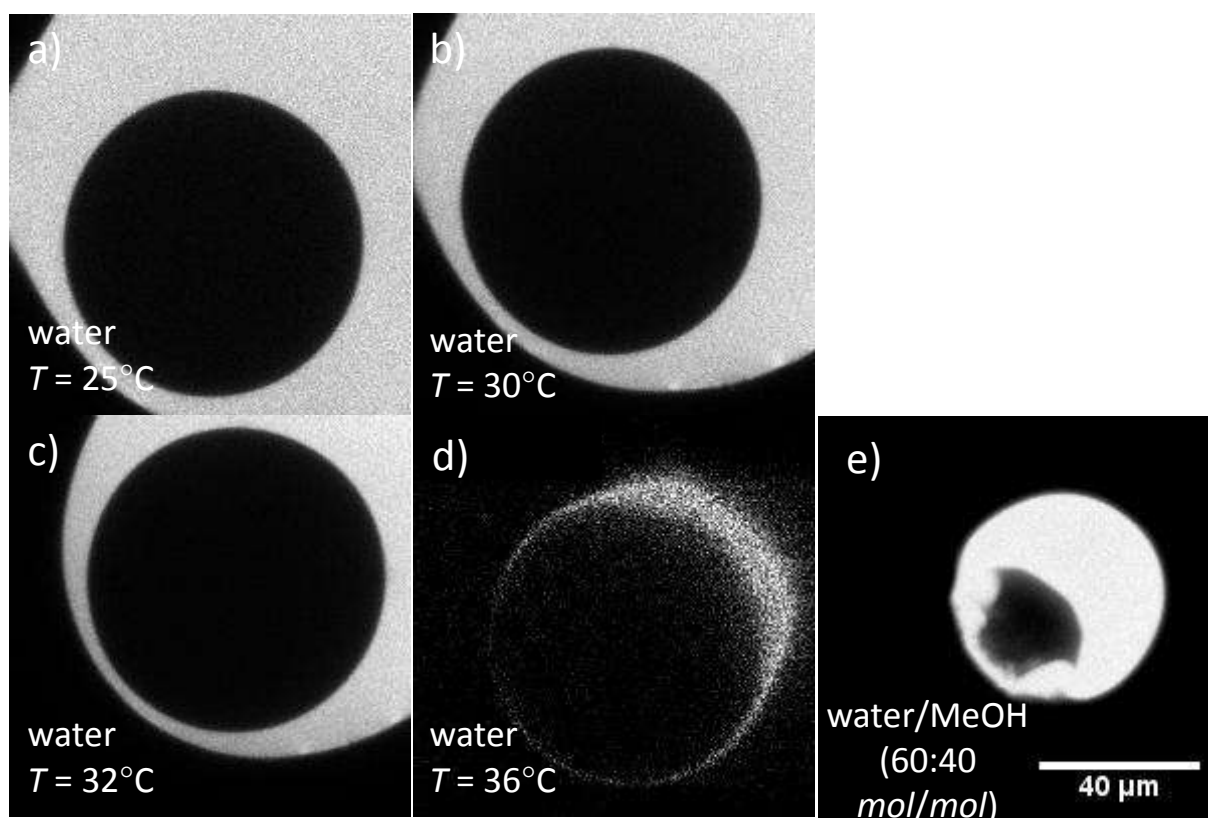


Figure 4.2 Confocal fluorescence microscopy images of a core-shell microgel particle as sketched in Scheme 1. The images are taken at the equator plan of the core of a core-shell particle lying on the lower cover slide of the sample cell. a) – d): particle in pure water at different temperatures; the core diameter of about 60 μm is retained upon heating and cooling. e): particle in water/MeOH mixture with 40 mol% of MeOH. Adding MeOH lead to deswelling of the core and the shell, but the shell is more swollen than the core. The shell thickness influences the deswelling of the core and leads to a deformation of the core in regions where the shell is thin (lower-left part of the particle); vice versa, this deformation also deforms the shell in these regions. No effect of adhesion between particle and cover slide on the deswelling of the core is visible. The scale bar in Panel e) equally applies to all panels.

Our study is based on composite microgels with core–shell architecture that consist of different core and shell polymer networks, PAAM (core) and PNIPAM (shell). These different networks exhibit different swelling in different media: whereas the shell gradually deswells in water if the temperature increases from 25 to 36 °C, the core remains swollen and has the same size and shape at all these temperatures, as shown in Figure 4.2 a) – d). By contrast, the shell is partially swollen in a water/MeOH mixture (60:40, mol/mol), but the core completely deswells in this medium, as shown in Figure 4.2 e). At these conditions, the core is deformed from its originally spherical shape dependent on the shell thickness: in a region with high shell thickness (upper right of the microgel in Figure 4.2e), the spherical shape is retained, whereas in regions with low shell thickness (lower left of the microgel in Figure 4.2e), the core is deformed, and so is the shell. This observation is made because the shell is mechanically connected to the core. During the core–shell microgel preparation, the shell precursor polymer can penetrate into the rim region of the pre-fabricated core microgel before crosslinking of the shell occurs. This leads to an interpenetrating core and shell network in the outer rim of the core. The polymer density profile at the core–shell interface is therefore gradual rather than sharp, such that the shell follows the deformation of the core in regions of low shell thickness. The asymmetric position of the core in the core–shell particle is caused by the microfluidic synthesis procedure: in this procedure, the densities of the pre-fabricated microgel core and the pre-microgel shell polymer solution are not matched, thereby entailing sedimentation or floatation of the core particles inside the shell pre-microgel droplet. Depending on how rapidly these transient structures are fixed by droplet gelation, the resulting core–shell particles exhibit more or less pronounced anisotropic architectures [21]. For all confocal microscopy images,

samples were equilibrated for 2 h before micrographs were recorded. During this time, adhesion of the PNIPAM microgel shells on the microscopy glass slide leads to small deformation of the microgel particles, but this has no visible effect on their deswelling [25]. To further ensure consistency, all samples were checked again after the diffusion measurements with respect to the shape of the particles, indicating no changes in either case.

The latter interpenetration and interaction of the core and shell polymer gel networks poses a potential challenge to the use of the core–shell microgels in encapsulation and release applications. To check for such potential complexity, we probe the tracer diffusion of molecular and colloidal probes at different regions of the core–shell carrier microgels. We use 3000 g mol^{-1} and $70,000 \text{ g mol}^{-1}$ dextrans as tracers and probe them by spatially resolved two-focus fluorescence correlation spectroscopy (2fFCS). In all these experiments, we do not observe complex sub diffusive behavior, as shown exemplarily in Figure 4.3, indicating that the tracers do not bind to the gel network.

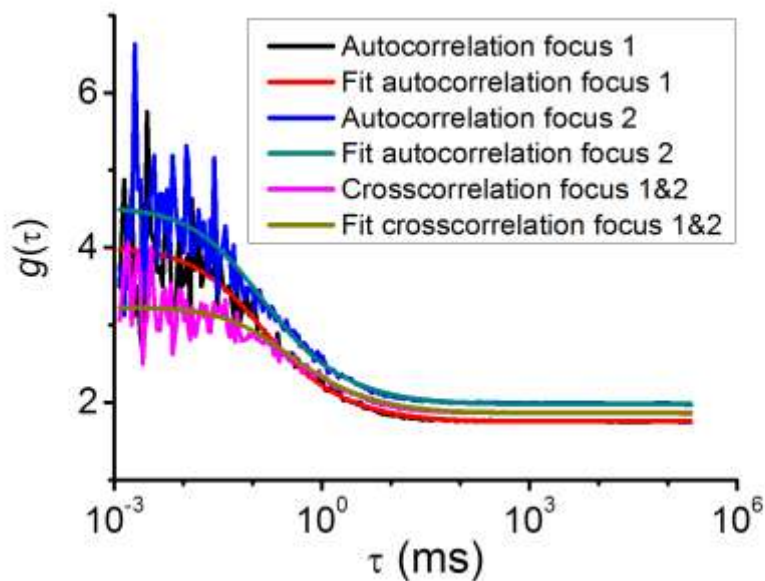


Figure 4.3 2fFCS measurement on 3000 g mol^{-1} dextran labelled with AlexaFluor 647 in the PAAM core of the microgel shown in Figure 4.2 in water at $25 \text{ }^\circ\text{C}$. A single-exponential model function is used to fit the data (smooth lines). Fluorescence excitation is achieved with $\lambda_{\text{ex}} = 637 \text{ nm}$ at an excitation power of $2 \text{ } \mu\text{W}$. The detection signal is filtered by a HC 687/70 (AHF) band pass filter.

When 2fFCS experiments are conducted in aqueous medium at different regions of the core–shell microgel, as indicated in Scheme 4.1, the diffusion coefficients of the two different tracers vary similarly as a function of the location of the probing, as seen in Figure 4.4. For better comparison, we focus on diffusion coefficients in a form normalized to the temperature and the viscosity of the outer medium to blank the direct impact of the temperature change on the diffusion coefficient. In the bulk interior of the core, close to its center, the diffusion coefficient exhibits no perceptible spatial variation. In addition, no effect of the shell degree of swelling on the diffusion of the tracers is visible. By contrast, at about $5 \text{ } \mu\text{m}$ distance to the core–shell interface inside the core, the diffusion of the tracers slightly decreases as the measuring position is moved outbound at both swollen and deswollen shell. This is again because this region of the microgel consists of an interpenetrating network of core and shell polymer with a

higher polymer segment density. As a result, the obstruction on the tracer diffusion increases. Nevertheless, we do not observe any marked effect of temperature, as shown in Figure 4.5. In particular, the tracer diffusivity inside the core is the same for both swollen and partially deswollen PNIPAM shell; only at the complete shell deswelling, at 36 °C, a slight decrease of the tracer diffusivity is detected, as also shown in Figure 4.5. This finding indicates that the PAAM core polymer, which remains swollen at all temperatures, prevents the interpenetrating part of the PNIPAM shell polymer network from deswelling thereby entailing no change of the polymer segment density and its effect on the tracer diffusion up to this point.

In the water/MeOH mixture, diffusion of the 70,000 g mol⁻¹ dextran is not measurable. While we still detect perceptible fluorescence intensity in FCS, which assures that the tracer has not been squeezed out of the microgel upon deswelling the core, correlation of fluctuations of this intensity is impossible. This finding indicates that the 70,000 g mol⁻¹ dextran tracer is immobilized within the deswollen core polymer network. In contrast to this, diffusion of the 3000 g mol⁻¹ dextran is still measurable in the deswollen core. We detect it to be much slower than inside the preceding set of experiments with swollen cores, as also seen in Figure 4.4, which is expected because the polymer segment density is much higher within a deswollen core, thereby more effectively obstructing the tracer diffusion. This decrease of mobility also entails greater data scattering, because the inflection points of the semi-log fluorescence correlation curves are shifted to longer correlation times that require longer sampling and that are therefore more sensitive to noise. In these latter experiments, no radial decrease of the diffusion coefficient is observed if the measuring position approaches the core–shell interface (Figure 4.4, open inverted triangles, open diamonds, and open pentagons).

This indicates that the shell cannot prevent the deswelling of the core. This is in contrast to the opposite scenario discussed above, where the swollen core could prevent shell-polymer deswelling in the region of core-shell interpenetration. It is therefore the core polymer network alone that dictates the extent of tracer-diffusion obstruction: if the core is swollen, the tracer diffusion is not markedly hindered, nearly independent of the degree of shell swelling or deswelling, but if the core is deswollen, the tracer diffusion is greatly obstructed, and the degree of swelling of the shell has no influence.

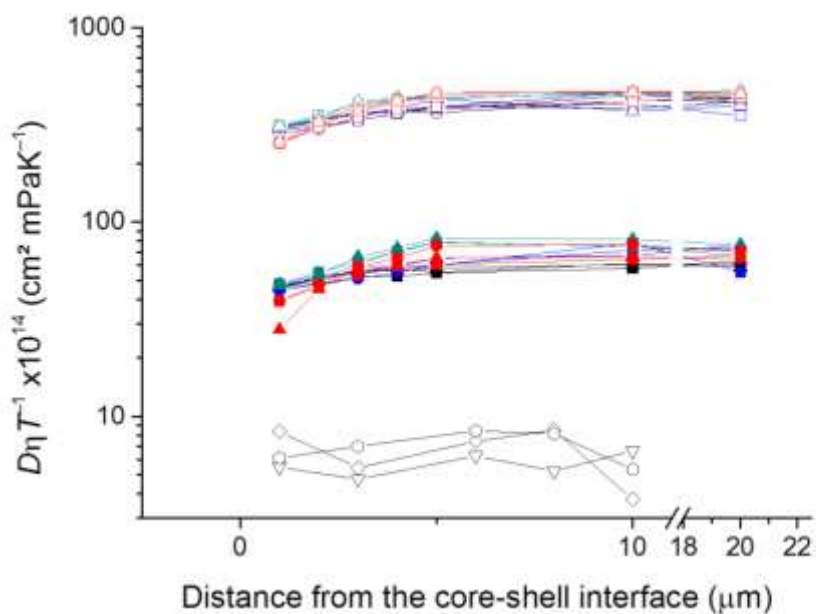


Figure 4.4 Normalized dextran-tracer diffusion coefficients at different positions within core-shell microgel particles, as sketched in Scheme 4.1. Filled symbols correspond to $70,000 \text{ g mol}^{-1}$ dextran, whereas open symbols correspond to 3000 g mol^{-1} dextran. Different colors indicate different measurement temperatures: black $25 \text{ }^\circ\text{C}$, blue $30 \text{ }^\circ\text{C}$, dark cyan $32 \text{ }^\circ\text{C}$, and red $36 \text{ }^\circ\text{C}$. The different symbol types (square, triangle, and circle) indicate experiments conducted on three different core-shell particles. The inverted triangles, diamonds, and pentagons in the lowermost dataset indicate measurements on a deswollen core in a water/MeOH mixture (60:40, mol/mol). Error bars are smaller than the symbols for the data points; therefore no error bars are shown.

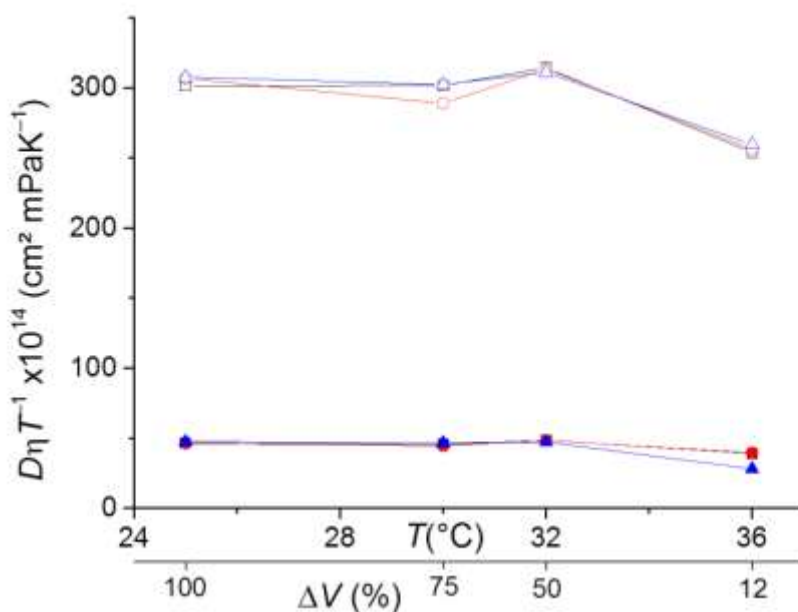


Figure 4.5 Normalized diffusion coefficient at the core–shell interface in aqueous medium as a function of temperature, which corresponds to different degrees of microgel-shell deswelling. Filled symbols indicate the diffusion coefficients of 70,000 g mol⁻¹ dextran; open symbols indicate the diffusion coefficients of 3000 g mol⁻¹ dextran. Different colors indicate measurements performed on different microgel particles. A decrease of the diffusion coefficients is only visible for the measurements at 36 °C. This indicates that the deswelling of the shell hardly influences the density of the core, in good agreement with the results shown in Figure 4.2. The second abscissa indicates the degree of swelling of the shell with respect to the swelling degree at 25 °C. The swelling degree was calculated from the fluorescence microscopy images in Figure 4.2. Error bars are smaller than the symbols for the data points; therefore no error bars are shown.

4.4. Conclusions

Sub-millimeter-sized hydrogel particles consisting of a thermoresponsive shell that surrounds a non-thermoresponsive core can be used as microcarriers that allow molecular and small colloidal additives to be encapsulated and released by selective shell deswelling or swelling [6, 21]. In this work, 2fFCS is used to probe the mobility of oligomeric guest molecules with spatial resolution. The data demonstrate that 2fFCS is

indeed able to provide information on how the local network structure affects tracer mobility [25]. This will allow for exploiting recent developments of gel synthesis to control the structure of complex gels for a rational control of mobility of actives inside gels [43-45]. Determining the local mobility will be important in the development for tissue engineering scaffolds containing colloidal particles [46] and also for sensors [47] and microgel-modified membranes [48].

In this chapter, a small deceleration of the tracer diffusion is observed very close to the core-shell interface, indicating that an interpenetrating network is present in that region. Changing the degree of swelling in the shell has no marked effect on the mobility of the additives within the microgel core. Thus, the release properties of such core-shell particles can be changed by controlling the degree of swelling of the shell without affecting the mobility of the non-binding dextran additives inside the core. This is in agreement with earlier findings by Seiffert et al. [21], where the retaining core size of the core-shell-particle was demonstrated by fluorescence microscopy. In addition, this finding shows that the guest oligomers are entrapped within the microgel carrier by topological constraints only, without binding to the network. This greatly facilitates rational design of such carriers for biomedical applications [46-48].

4.5. References

1. Seiffert, S., *Sensitive microgels as model colloids and microcapsules*. Journal of Polymer Science Part A: Polymer Chemistry, 2014. **52**(4): p. 435-449.
2. Thorne, J.B., G.J. Vine, and M.J. Snowden, *Microgel applications and commercial considerations*. Colloid and Polymer Science, 2011. **289**(5-6): p. 625-646.
3. Bergbreiter, D.E., et al., *Poly(N-isopropylacrylamide) Soluble Polymer Supports in Catalysis and Synthesis*. Macromolecules, 1998. **31**(18): p. 6053-6062.
4. Tanaka, T., et al., *Polymer gels that can recognize and recover molecules*. Faraday Discuss., 1995. **101**(Gels): p. 201-206.
5. Saunders, B.R., et al., *Microgels: From responsive polymer colloids to biomaterials*. Advances in Colloid and Interface Science, 2009. **147-48**: p. 251-262.
6. Bysell, H., et al., *Microgels and microcapsules in peptide and protein drug delivery*. Advanced Drug Delivery Reviews, 2011. **63**(13): p. 1172-1185.
7. Sivakumaran, D., D. Maitland, and T. Hoare, *Injectable Microgel-Hydrogel Composites for Prolonged Small-Molecule Drug Delivery*. Biomacromolecules, 2011. **12**(11): p. 4112-4120.
8. Smith, M.H. and L.A. Lyon, *Tunable Encapsulation of Proteins within Charged Microgels*. Macromolecules, 2011. **44**(20): p. 8154-8160.
9. Bai, Y., et al., *Thermo- and pH-responsive microgels for controlled release of insulin*. Polym. Int., 2012. **61**(7): p. 1151-1157.
10. Kang, M.K., S.K. Hong, and J.-C. Kim, *Release property of microgels formed by electrostatic interaction between poly(N-isopropylacrylamide-co-methacrylic acid) and poly(N-isopropylacrylamide-co-dimethylaminoethylmethacrylate)*. J. Appl. Polym. Sci., 2012. **125**(3): p. 1993-1999.
11. Nuhn, L., et al., *Cationic Nanohydrogel Particles as Potential siRNA Carriers for Cellular Delivery*. Acs Nano, 2012. **6**(3): p. 2198-2214.
12. Smith, M.H. and L.A. Lyon, *Multifunctional Nanogels for siRNA Delivery*. Accounts of Chemical Research, 2012. **45**(7): p. 985-993.
13. Schild, H.G., *Poly(N-isopropylacrylamide): experiment, theory and application*. Progress in Polymer Science, 1992. **17**(2): p. 163-249.
14. Heskins, M. and J.E. Guillet, *Solution properties of poly(N-isopropylacrylamide)*. J. Macromol. Sci., Chem., 1968. **2**(8): p. 1441-55.
15. Sato Matsuo, E. and T. Tanaka, *Kinetics of discontinuous volume-phase transition of gels*. The Journal of Chemical Physics, 1988. **89**(3): p. 1695-1703.
16. Li, Y. and T. Tanaka, *Study of the universality class of the gel network system*. The Journal of Chemical Physics, 1989. **90**(9): p. 5161-5166.
17. Schild, H.G., *Super-absorbency and phase transition of gels in physiological salt solutions*. Macromol. Chem., 1992. **3**(6): p. 393-395.
18. Das, M., H. Zhang, and E. Kumacheva, *Microgels: Old materials with new applications*, in *Annual Review of Materials Research*. 2006, Annual Reviews: Palo Alto. p. 117-142.
19. Berndt, I., J.S. Pedersen, and W. Richtering, *Temperature-sensitive core-shell microgel particles with dense shell*. Angewandte Chemie-International Edition, 2006. **45**(11): p. 1737-1741.

20. Kim, J.W., et al., *Fabrication of monodisperse gel shells and functional microgels in microfluidic devices*. *Angewandte Chemie-International Edition*, 2007. **46**(11): p. 1819-1822.
21. Seiffert, S., et al., *Smart Microgel Capsules from Macromolecular Precursors*. *J. Am. Chem. Soc.*, 2010. **132**(18): p. 6606-6609.
22. Keerl, M., et al., *Copolymer Microgels from Mono- and Disubstituted Acrylamides: Phase Behavior and Hydrogen Bonds*. *Macromolecules* (Washington, DC, U. S.), 2008. **41**(18): p. 6830-6836.
23. Bysell, H., P. Hansson, and M. Malmsten, *Transport of poly-L-lysine into oppositely charged poly(acrylic acid) microgels and its effect on gel deswelling*. *J. Colloid Interface Sci.*, 2008. **323**(1): p. 60-69.
24. Hansson, P., et al., *Peptide-Microgel Interactions in the Strong Coupling Regime*. *Journal of Physical Chemistry B*, 2012. **116**(35): p. 10964-10975.
25. Lehmann, S., S. Seiffert, and W. Richtering, *Spatially Resolved Tracer Diffusion in Complex Responsive Hydrogels*. *J. Am. Chem. Soc.*, 2012. **134**(38): p. 15963-15969.
26. Seiffert, S. and D.A. Weitz, *Controlled fabrication of polymer microgels by polymer-analogous gelation in droplet microfluidics*. *Soft Matter*, 2010. **6**(14): p. 3184-3190.
27. Muller, C.B. and W. Richtering, *Sealed and temperature-controlled sample cell for inverted and confocal microscopes and fluorescence correlation spectroscopy*. *Colloid and Polymer Science*, 2008. **286**(11): p. 1215-1222.
28. Winnik, F.M., H. Ringsdorf, and J. Venzmer, *Methanol-water as a co-nonsolvent system for poly(N-isopropylacrylamide)*. *Macromolecules*, 1990. **23**(8): p. 2415-16.
29. Crowther, H.M. and B. Vincent, *Swelling behavior of poly(N-isopropylacrylamide) microgel particles in alcoholic solutions*. *Colloid Polym. Sci.*, 1998. **276**(1): p. 46-51.
30. Kojima, H., et al., *Temperature dependent phase behavior of PNIPAM microgels in mixed water/methanol solvents*. *Journal of Polymer Science Part B: Polymer Physics*, 2013. **51**(14): p. 1100-1111.
31. Heppner, I.N., M.R. Islam, and M.J. Serpe, *Unexpected Cononsolvency Behavior of Poly (N-isopropylacrylamide)-Based Microgels*. *Macromol. Rapid Commun.*, 2013.
32. Hofmann, C.H., et al., *Cononsolvency Revisited: Solvent Entrapment by N-Isopropylacrylamide and N,N-Diethylacrylamide Microgels in Different Water/Methanol Mixtures*. *Macromolecules* (Washington, DC, U. S.), 2013. **46**(2): p. 523-532.
33. Scherzinger, C., et al., *Cononsolvency of poly-N-isopropyl acryl amide (PNIPAM): Microgels versus linear chains and macrogels*. *Current Opinion in Colloid & Interface Science*, 2014(0).
34. Modesti, G., et al., *Diffusion in Model Networks as Studied by NMR and Fluorescence Correlation Spectroscopy*. *Macromolecules*, 2009. **42**(13): p. 4681-4689.
35. Raccis, R., et al., *Probing mobility and structural inhomogeneities in grafted hydrogel films by fluorescence correlation spectroscopy*. *Soft Matter*, 2011. **7**(15): p. 7042-7053.

36. Koynov, K. and H.-J. Butt, *Fluorescence correlation spectroscopy in colloid and interface science*. Curr. Opin. Colloid Interface Sci., 2012. **17**(6): p. 377-387.
37. Woell, D., *Fluorescence correlation spectroscopy in polymer science*. RSC Adv., 2014. **4**(5): p. 2447-2465.
38. Dertinger, T., et al., *Two-focus fluorescence correlation spectroscopy: A new tool for accurate and absolute diffusion measurements*. Chemphyschem, 2007. **8**(3): p. 433-443.
39. Muller, C.B., et al., *Precise measurement of diffusion by multi-color dual-focus fluorescence correlation spectroscopy*. Epl, 2008. **83**(4): p. 5.
40. Dertinger, T., et al., *The optics and performance of dual-focus fluorescence correlation spectroscopy*. Opt. Express, 2008. **16**(19): p. 1435314368.
41. Muller, C.B., et al., *Dual-focus fluorescence correlation spectroscopy: a robust tool for studying molecular crowding*. Soft Matter, 2009. **5**(7): p. 1358-1366.
42. Enderlein, J., *Polymer Dynamics, Fluorescence Correlation Spectroscopy, and the Limits of Optical Resolution*. Physical Review Letters, 2012. **108**(10): p. 108101/1-108101/4.
43. Wong, J.E. and W. Richtering, *Layer-by-layer assembly on stimuli-responsive microgels*. Current Opinion in Colloid & Interface Science, 2008. **13**(6): p. 403-412.
44. Richtering, W. and B.R. Saunders, *Gel architectures and their complexity*. Soft Matter, 2014. **10**(21): p. 3695-3702.
45. Peak, C.W., J.J. Wilker, and G. Schmidt, *A review on tough and sticky hydrogels*. Colloid Polym. Sci., 2013. **291**(9): p. 2031-2047.
46. Clarke, K.C., et al., *Colloid-matrix assemblies in regenerative medicine*. Curr. Opin. Colloid Interface Sci., 2013. **18**(5): p. 393-405.
47. Islam, M.R., et al., *Responsive polymers for analytical applications: A review*. Anal. Chim. Acta, 2013. **789**: p. 17-32.
48. Menne, D., et al., *Temperature-Modulated Water Filtration Using Microgel-Functionalized Hollow-Fiber Membranes*. Angew. Chem., Int. Ed., 2014. **53**(22): p. 5706-5710.

5. Spatially Resolved Tracer Diffusion in Complex Responsive Hydrogels³

5.1. Introduction

Hydrogels are highly hydrated, cross-linked polymer networks that are valuable for many biological applications,[1, 2] including those in drug delivery,[3-5] biosensing,[6] and tissue engineering.[7-11] In one class of applications, hydrogels serve as scaffolds for the encapsulation of living cells.[12] Such systems provide a versatile platform to study the interaction of cells with confining environments that exhibit mechanical characteristics similar to that of the cells. A particularly important technique to be used in this context is traction force microscopy.[13] In this approach, cells are imbedded into a hydrogel along with colloidal tracer particles. Tracking the displacements of these particles serves to measure the traction forces that the encapsulated cells exert on their environment in response to external stimuli. These studies provide a basis to understanding the complex relationship between cells and physiological environments, which is a crucial step towards understanding physiological processes such as cell migration, tissue morphogenesis, and signaling pathways.[13]

The use of cell-laden hydrogels in traction force experiments requires sound knowledge on the micro- and nanostructural complexity of the gel environment close to the encapsulated cells. In addition, it is necessary to understand the dynamics of additives

³ This chapter was published in *J. Am. Chem. Soc.*, 2012. 134(38): p. 15963-15969. The study was performed in collaboration with the co-authors. My contribution was the synthesis of the final samples. Furthermore, I performed the 2fFCS measurements and did the data analysis.

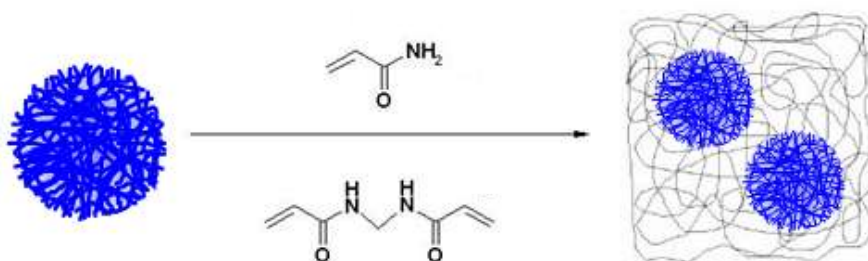
such as cell nutrition and signaling compounds inside these systems, because this affects the viability and ability of the encapsulated cells to communicate and to be stimulated.

To acquire such knowledge, it is helpful to perform investigations on model systems that are less complex and provide more flexibility for custom variation of experimental parameters than real cell-laden gels. For this purpose, composite gels that consist of micrometer-sized hydrogel particles embedded into a surrounding independent hydrogel matrix are of particular value.[14-16] If the embedded microgel particles are built from environmentally-sensitive polymers[17] that can react to changes in their surrounding by pronounced swelling and deswelling, they provide a perfect model for cells that contract or relax upon stimulation.[18]

To ascertain the utility of microgel-laden, composite gel systems as models for more complex cell-laden gels, it must be known to what extent the presence of the external scaffolding gel matrix affects the ability of the embedded microgels to swell and deswell. Conversely, it must also be known how the swelling and deswelling of the embedded microgels affects and distorts the surrounding scaffolding gel. Previous work by our group has shown that the incorporation of environmentally responsive microgels into a scaffolding gel matrix retains the sensitivity the embedded microgels. For example, the size of poly(*N*-isopropylacrylamide) (PNIPAM) microgel particles embedded into a scaffolding poly(acrylamide) (PAAM) gel matrix has the same temperature dependence as in plain aqueous environment.[15], [19] Moreover, when these particles undergo their volume-phase transition, the size and shape of the entire composite system remains unaffected; this is because the gel matrix takes up the water that is released by the embedded microgels.[20]

These observations suggest that the sensitive microgels are embedded freely into the scaffolding gel matrix, without formation of an interpenetrating network. However, large microgel beads might behave differently due to their different internal structure as compared to small microgels.[21] Thus, knowledge about the presence or absence of interpenetrating network domains in composite gel matrixes filled with large microgel beads is crucial to appraise their utility as model systems for more complex, cell-laden gels. In addition, no previous work has yet focused on using composite gels to investigate the influence of heterogeneous structures on the local, spatially resolved dynamics of nano- and mesoscopic probe molecules that move through the hydrogel. The derivation of a sound knowledge on the tracer mobility in these complex environments is another precondition to ascertain the utility of composite gels as models for cell-laden gels. This knowledge is also of direct relevance to understand the viability and reactivity of cells that are immobilized in hydrogel matrixes.[12],[22]

In this chapter, we use composite hydrogels that consist of micrometer-sized, thermosensitive microgel particles (labeled with a fluorescent dye) embedded into a soft hydrogel matrix (see Scheme 5.1) to study the diffusive mobility of nanometer-sized tracers (labeled with a different fluorescent dye); this is achieved by two-focus fluorescence correlation spectroscopy.[23] In addition, we use these composites to study the interplay of the embedded microgel particles with the surrounding scaffolding gel matrix to unravel the presence or absence of interpenetrating polymer network structures within the microgel beads. This is achieved by observing the swelling and deswelling of the thermosensitive microgel beads within the scaffolding hydrogel matrixes through the use of confocal laser scanning microscopy.



Scheme 5.1 Illustration of the formation of composite hydrogels that consist of micrometer-sized, thermoresponsive microgel beads embedded into a soft hydrogel matrix. [24]

5.2. Experimental Part

5.2.1. Sample Preparation

Fluorescently labeled PNIPAM microgel beads were prepared from *N*-isopropylacrylamide (NIPAM, Acros Organics), BIS, and methacryloxyethyl thiocarbonyl rhodamine B (Polysciences Inc.) in two different ways: type-A beads (cross-linker to monomer ratio 1:70, PNIPAM concentration 100 gL^{-1}) were fabricated by droplet-based microfluidic templating,[25] whereas type-B beads (cross-linker to monomer ratio 1:13, PNIPAM concentration 143 gL^{-1}) were synthesized by inverse suspension polymerization.[26]

Dextran labeled with Alexa Fluor 647 (10 kDa and 3 kDa, Invitrogen) or Alexa Fluor 488 (70 kDa, Invitrogen) were dissolved in water (LiChroSolv, Merk). 3-kDa dextran has a hydrodynamic radius of $R_h = 1 \text{ nm}$, 10-kDa dextran has $R_h = 2.3 \text{ nm}$, and 70-kDa dextran has $R_h = 6.5 \text{ nm}$. All hydrodynamic radii were calculated via the Stokes–Einstein equation from the diffusion coefficient measured at infinite dilution.

Composite hydrogel samples were prepared with a final bead volume fraction of 0.05 at $25 \text{ }^\circ\text{C}$. Less than 1 mg of the UV-cleavable initiator VA-086 (2,2'-azobis[2-methyl-*N*-2-

hydroxyethyl)propionamide], Wako) was added, and the solutions were filled into a temperature-controlled sample cell.[27] The polymerization was performed under UV exposure with an intensity of 1.5 Wcm^{-2} at $\lambda = 254 \text{ nm}$ for 30 min at $25 \text{ }^\circ\text{C}$ after mixing the stock solutions.

All bead particles, the hydrogels and the composite gels were synthesized at 25°C . In this state, monomers and cross-linkers are homogeneously distributed in the pre-gel reaction mixtures, which lead to a rather uniform distribution of cross-linker in the hydrogel. Thus, we assume that gel matrix and gel beads exhibit similar spatial distribution of cross-links.

Table 5.1 Compositions of composite hydrogel samples that consist of PNIPAM microgel beads embedded within PAAM hydrogel matrixes

Sample name	c_{PAAM} (gL^{-1})	c_{PNIPAM} (gL^{-1})	$n_{\text{BIS}} / n_{\text{PAAM}}$	$n_{\text{BIS}} / n_{\text{PNIPAM}}$
HG-25-A	25	100	1:60	1:70
HG-50-A	50	100	1:60	1:70
HG-25-B	25	143	1:60	1:13
HG-50-B	50	143	1:60	1:13

HG in the sample name indicates the existence of a PAAM hydrogel; 25 or 50 indicates the PAAM concentration in the hydrogel; A and B denote the bead type; c_{PAAM} is the matrix concentration; c_{PNIPAM} the PNIPAM concentration during bead preparation; $n_{\text{BIS}} : n_{\text{PAAM}}$ is the molar ratio of cross-linker to monomer in the matrix; $n_{\text{BIS}} : n_{\text{PNIPAM}}$ is the molar ratio of cross-linker to monomer in the beads.

Note that the type-A beads are less cross-linked and contain less polymer than the type-B beads. Hence, the type-A beads are referred to as soft beads, whereas the type-B beads are referred to as dense beads.

5.2.2. Dynamic Light Scattering

Dynamic light scattering (DLS) experiments are performed to determine the mesh size of the gels. We use an ALV DLS with a 7004 correlator (ALV-Laser Vertriebsgesellschaft m.b.H., Langen, Germany), equipped with a 473-nm 40-mW DPSS laser (Cobold AB, Sweden). As gels are non-ergodic, we used the Pusey–van Megen method to determine the mesh size of our gel samples.[28] To determine the mesh size of the PNIPAM beads, we synthesize macroscopic hydrogels with same composition at comparable reaction conditions.

The mesh size of a PAAM hydrogel with a composition of 50 gL^{-1} of PAAM and $n_{\text{BIS}} : n_{\text{PAAM}}$ of 1:60 at 25°C is in the order of 15 nm, whereas the mesh size of a PNIPAM hydrogel with a composition of 100 gL^{-1} of PNIPAM and $n_{\text{BIS}} : n_{\text{PNIPAM}}$ of 1:70 at 25°C is in the order of 19 nm.

5.2.3. Spatially Resolved 2fFCS

Fluorescence correlation spectroscopy (FCS) is well suited to measure the diffusion coefficient of tracer particles in gels.[29, 30] In this context, the correct treatment of potential changes in the confocal volume, which can occur due to changes in the sample refractive index, is of major importance.[31] This is particularly relevant for the present study, because the local polymer density varies with the position in composite gels, leading to different refractive indexes and thus different sizes and shapes of the confocal volume.

To account for these complications, we use 2fFCS.[23] In 2fFCS, two laterally shifted but overlapping laser foci are used to determine correlation functions of each focus and of the cross-section of the two foci. The lateral shift is obtained by the use of a Nomarski prism, which leads to the shift distance δ that is not affected by refractive index mismatch and optical saturation.

The correlation function in 2fFCS is given by:

$$g(\tau, \delta, \nu) = \frac{c}{4} \sqrt{\frac{\pi}{D \tau}} \int dz_1 \int dz_2 \left(\begin{array}{c} \frac{\kappa(z_1)\kappa(z_2)}{8 D \tau + w^2(z_1) + w^2(z_2)} \\ - \frac{(z_2 - z_1 - \nu_z \tau)^2}{4 D \tau} \\ - 2 \frac{(\delta - \nu_x \tau)^2 + \nu_y^2 \tau^2}{8 D \tau + w^2(z_1) + w^2(z_2)} \end{array} \right) \quad (5.1)$$

In eq. (5.1), D is the translational diffusion coefficient, t the lag time of the correlation, c the concentration of the fluorescent particles, δ is the shift distance (determined independently) and x , y , and z are Cartesian coordinates with z along the optical axis. ν_i are optical fit parameters including the fluorescence excitation efficiency and quantum yield.

$$w(z) = w_0 \left[1 + \left(\frac{\lambda_{ex} z}{\pi w_0^2 n} \right)^2 \right]^{1/2} \quad (5.2)$$

$$\kappa(z) = 2 \int_0^a \frac{d\rho \rho}{R^2(z)} \exp\left(-\frac{2\rho^2}{R^2(z)}\right) = 1 - \exp\left(-\frac{2\rho^2}{R^2(z)}\right) \quad (5.3)$$

$$R(z) = R_0 \left[1 + \left(\frac{\lambda_{ex} z}{\pi R_0^2 n} \right)^2 \right]^{1/2} \quad (5.4)$$

λ_{ex} is the excitation wavelength, λ_{em} is the emission wavelength, n the refractive index, and a is the confocal pinhole radius. The correlation function can be calculated numerically, and w_0 and R_0 are fit parameters.[32] The high accuracy of 2fFCS in crowded environments has been demonstrated previously.[33]

Tracer diffusion measurements in pure PAAM hydrogels are performed at 9 different positions, each yielding the same diffusion coefficient. This shows that 2fFCS probes diffusion processes on length scales larger than spatial heterogeneities within the hydrogels.[34, 35]

To achieve high spatial resolution for tracer diffusion experiments in 2fFCS, we employ a confocal microscope. A 3D piezo table with a range of 100 μm in all three directions serves to locate the regions of interest. With this setup, we measure the diffusion coefficient at several defined points in the sample. Measurements inside microgel beads at 36 °C are precluded due to the high scattering intensity caused by the collapsed particles. Similar effects were reported by Raccis et al. for the diffusion of dyes in collapsed PNIPAM hydrogels.[30]

A typical measurement time is 1 hour. The error bars for the diffusion coefficients obtained in spatially resolved measurements are obtained from fits of the correlation function.

5.3. Results and Discussion

PNIPAM microgels show pronounced swelling and deswelling upon changes in temperature; this transition is accompanied by microgel volume changes of up to 1000%.[36] The swellability of these and other microgel particles depends on the cross-link density of their constituent polymer network. The swellability of the PNIPAM microgel beads to be used in this work is characterized by their temperature-dependent sizes prior to their incorporation into a hydrogel matrix; this is determined by fluorescence microscopy. Fluorescence micrographs recorded at 25 °C and 36 °C show that soft, loosely cross-linked microgel beads, hereinafter referred to as “type-A beads”, deswell with $\Delta V = V_c / V_s = (R_c / R_s)^3 = 0.09 \pm 0.01$, whereas stiff, densely cross-linked beads, hereinafter referred to as “type-B beads”, deswell with $\Delta V = 0.42 \pm 0.15$, (Supporting information Fig. S.5.1). Here, ΔV is the ratio of the microgel volume in the collapsed state, V_c , and the microgel volume in swollen state, V_s . R_c and R_s are the corresponding microgel particle radii.

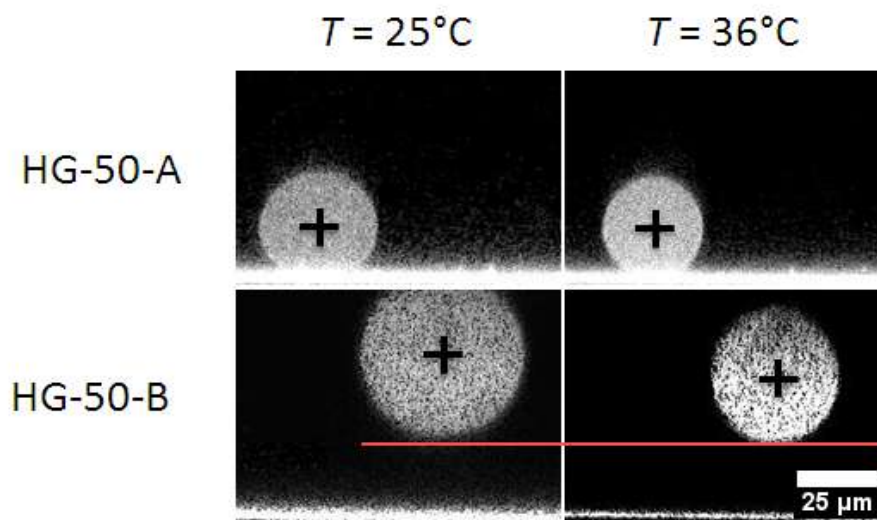


Figure 5.1 Side view of PNIPAM beads embedded in a PAAM hydrogel with an AAM concentration of 50 gL^{-1} . The white line at the bottom of the pictures is the glass cover slide. The beads are scanned in the center plane of the particle along the x - z -directions (Supporting Information Fig. S.5.2). Top: PNIPAM bead of type A at 25°C (left) and at 36°C (right). The bead collapse is much less pronounced than in water. Bottom: PNIPAM bead of type B at 25°C (left) and at 36°C (right). The bead collapses as in water, and the center of the bead moves down until the bottom of the collapsed bead reaches the level of the bottom of the swollen bead. Black crosses indicate the center of the beads. The scale bar denotes 25 micrometers and applies to all panels.

If these microgels are embedded into surrounding 50-gL^{-1} PAAM hydrogel matrixes, the less cross-linked, soft type-A beads (HG-50-A) collapse ($\Delta V = 0.61$) much less upon heating as compared to their behavior in water ($\Delta V = 0.09$), as shown in Figure 5.1. This can be explained by the formation of a PAAM gel inside the beads that interpenetrates the gel-bead PNIPAM gel network, thereby obstructing the thermo-induced collapse of the beads. By contrast, the dense type-B beads (sample HG-50-B) collapse just as they do in water, as also shown in Figure 5.1. This indicates that their dense structure prevents the formation of an interpenetrating gel network.

Figure 5.1 also shows that the center of mass of the type-B beads moves downwards when these beads collapse. Again, this indicates that there is hardly any coupling between the type-B beads to the surrounding hydrogel matrix.

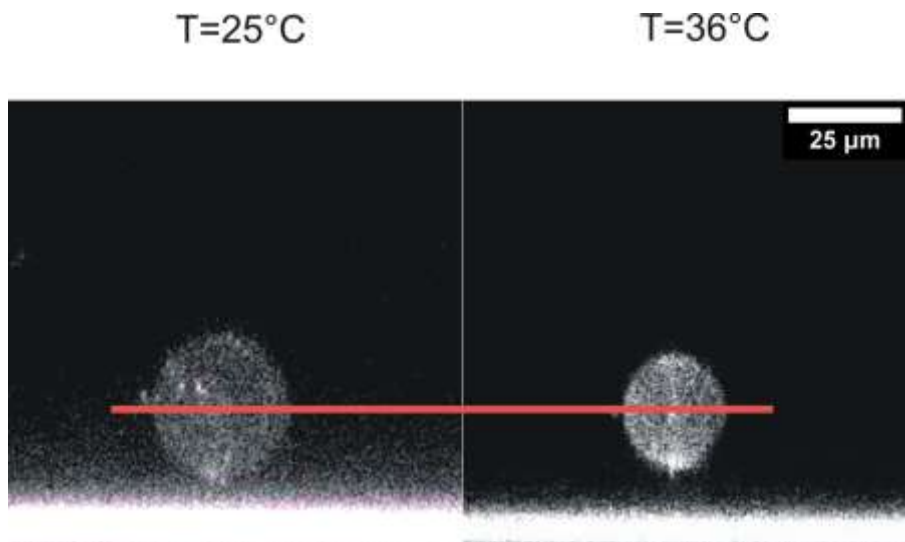


Figure 5.2 Side view of type-A PNIPAM bead embedded in a PAAM hydrogel with an AAM concentration of 25 gL^{-1} . The bead collapses almost to the same extent as in water, and the bead center does not move. The scale bar denotes 25 micrometers and applies to both panels.

When the segmental density of the PAAM matrix is lowered to only 25 gL^{-1} (sample HG-25-A), a different result is obtained: in this case, the soft type-A beads *do* collapse inside the PAAM matrix just as they do in water, as shown in Figure 5.2. In this sample, however, the center of the bead does *not* move when the bead collapses, different from the behavior of the highly cross-linked beads in sample HG-50-B, which collapse and move downwards upon heating. This marked difference is an indication for the formation of an interpenetrating network that is not strong enough to prevent bead collapse, but still strong enough to keep the bead at its position upon heating.

The previous experiments demonstrate how the coupling with a surrounding gel matrix influences the temperature sensitive swelling of hydrogel-embedded microgel beads. To supplement a nanometer-scale picture, we now turn to the molecular scale and discuss the influence of this coupling on the mobility of molecules that diffuse through these gels. In particular we investigate how the heterogeneous local environment affects the mobility of these probe molecules. We use fluorescently labeled dextrans as tracer

particles; these tracers hardly interact with other molecules[37] and have therefore been employed in related previous investigations.[38-41] We quantify the dextran diffusivity inside the microgel beads and outside of them in the surrounding hydrogel matrix by 2fFCS.

The diffusion of 10-kDa dextran is slower inside the water-swollen type-A PNIPAM beads than it is in pure water, as illustrated in Figure 5.3 (open symbols). The diffusivities inside the beads agree well with those in macroscopic PNIPAM hydrogels of the same composition. This finding suggests that the gel architecture inside the type-A microgels resembles that inside a bulk macroscopic gel. This appears justified, because these beads were templated in emulsion droplets that solely act as micrometer-sized reaction vessels without any impact on the course of the free-radical polymer network formation.

The tracer diffusion inside the water-swollen beads depends slightly on the position of measurement. The tracer diffusion coefficient determined in the center of the bead is lower than that determined near to the bead surface. This is surprising, as it is expected that beads prepared in the swollen state have a homogenous cross-link density. We address this finding to the circumstance that the beads, when dissolved in water, swell a little compared to the size during their polymerization. Our spatially resolved tracer diffusion experiments indicate that this swelling is not fully affine.

Corresponding investigations on a composite gel with a matrix concentration of 25 gL^{-1} that is loaded with the same type-A microgel beads show that the tracer diffusion inside the embedded beads is slower as compared to both the diffusion in beads dissolved in water and to the diffusion in the surrounding PAAM hydrogel matrix (Supporting Information Fig. S.5.3), as shown in Figure 5.3 (filled symbols). This finding indicates that an interpenetrating network has formed inside the beads.

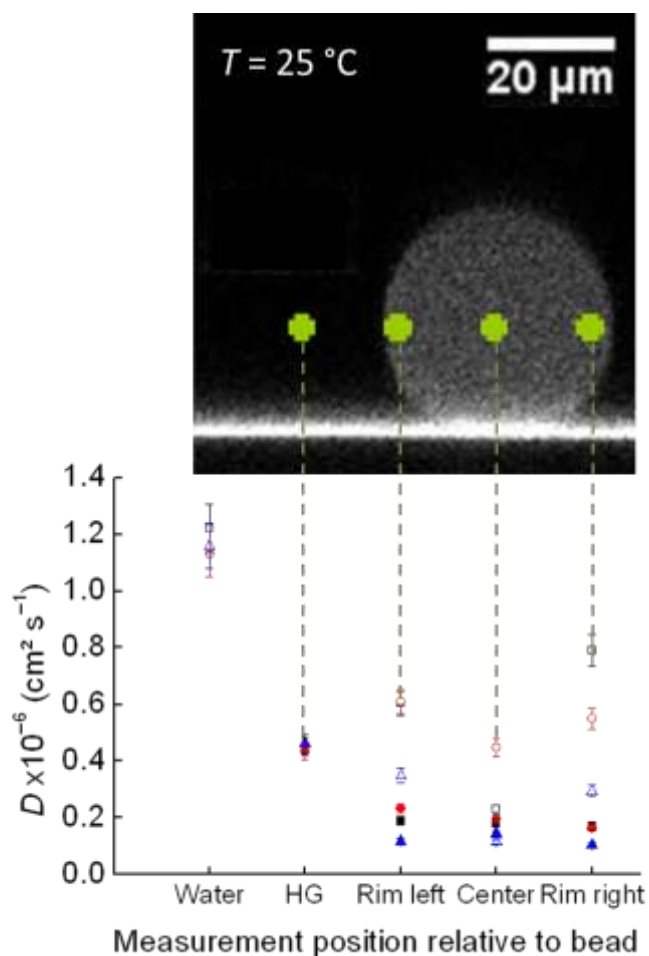


Figure 5.3 Diffusion coefficient of 10-kDa dextran out- and inside of type-A PNIPAM microgel beads, either embedded into a 25-gL⁻¹ PAAM hydrogel matrix (filled symbols) or suspended in water (open symbols). The upper picture is a confocal micrograph showing the different positions of measurement. $T = 25 \text{ }^\circ\text{C}$. Different symbols (triangles, squares, and circles) indicate measurements performed on different beads. For 3-kDa dextran see Supporting Information Fig.S.5.4.

Increase of the concentration of PAAM in the surrounding hydrogel matrix pronounces the effect of tracer deceleration inside the microgel beads: if the same experiments are repeated at a PAAM concentration of 50 gL⁻¹, the dextran tracer diffusion coefficient inside the embedded bead is reduced further; it is also again lower as compared to the hydrogel matrix and the free bead in pure water, as shown in Figure 5.4.

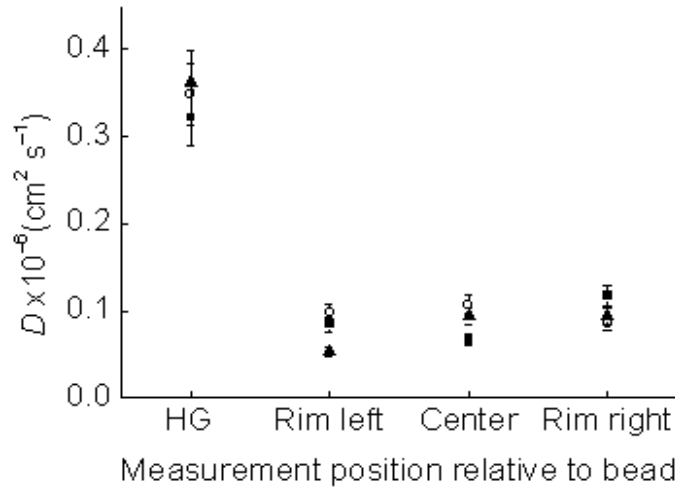


Figure 5.4 Diffusion coefficient of 10-kDa dextran out- and inside of type-A PNIPAM microgel beads embedded into a 50-gL⁻¹ PAAM hydrogel matrix. $T = 25 \text{ }^\circ\text{C}$. Different symbols (triangles, squares, and circles) indicate measurements on different beads.

The diffusion of tracers through a gel depends on the mesh size of the constituent polymer network relative to the size of the tracer.[42] The mesh size of PAAM gels at 50 gL⁻¹ and different cross-linker ratios can be determined by dynamic light scattering. We follow this approach and determine it to be in the order of 15 nm, in good agreement with literature data.[43] The hydrodynamic diameter of 10-kDa dextran in water is 4.6 nm; this is rather small compared to the polymer network mesh size. We describe the diffusion coefficient of the tracer as

$$D = \frac{kT}{f_{eff}} \quad (5.5)$$

with kT the thermal energy and f_{eff} an effective friction coefficient. In this approach, the hydrogel is considered as a continuous environment providing an effective friction for the random motion of the tracer on the length scale probed by FCS.[44]

Hydrogels are known to exhibit heterogeneities on length scales of 10 to 100 nm.[34, 35] This is smaller than the optical resolution of our 2fFCS measurements, which probes the mobility of labeled molecules on length scales that are limited by the optical resolution. The shift distance between the two foci in our 2fFCS setup is of the order >300 nm. Thus, the mobility of tracer molecules probed by 2fFCS is averaged over both, mesh size fluctuations and heterogeneities.

The two-foci cross-correlation data acquired in this study can all be fitted to eq. 5.1 (Supporting Information Fig. S.5.5). Thus, we do not observe anomalous diffusion.

Table 5.2 summarizes the diffusion coefficients of the 10-kDa tracer in different environments. Dividing the diffusion coefficient in water (D_w) by the diffusion coefficient in a complex environment (PNIPAM bead or PAAM matrix plus embedded bead, respectively) yields the effective friction coefficient of the tracer inside this environment relative to that in water.

The data in Table 5.2 show that the increased friction encountered by the 10-kDa dextran tracers inside the embedded microgel beads in sample HG-25-A ($f_{\text{eff}} = 7$) can be approximated by a sum of the friction coefficients of the beads ($f_{\text{eff}} = 2.6$) and the gel matrix ($f_{\text{eff}} = 2.6$). However, in the case of sample HG-50-A, the experimental friction coefficient ($f_{\text{eff}} = 13$) is much higher and cannot be modeled by simple addition of the bead ($f_{\text{eff}} = 2.6$) and gel ($f_{\text{eff}} = 3.4$) friction contributions. This indicates that the effective mesh size of the interpenetrating network inside the beads in sample HG-50-A is no longer large compared to the size of the tracer; thus, the topological restrictions of the network affect the tracer diffusion in this case.

Table 5.2 Diffusivities and relative friction coefficients of 10-kDa dextran tracers that diffuse through PNIPAM-PAAM composite gel matrixes at 25°C.

Medium	D ($10^{-6} \text{ cm}^2 \text{ s}^{-1}$)	f_{eff}
Water	1.17	-----
Bead A	0.443	2.6
HG-25	0.449	2.6
HG-50	0.344	3.4
HG-25-A	0.167	7
HG-50-A	0.089	13

Finally, we address the question whether the formation of interpenetrating networks and potential bead collapse also affect the tracer diffusion within the surrounding hydrogel matrix *outside* the beads. For this purpose, we probe the diffusion coefficients of 3-kDa and 70-kDa dextrans in the hydrogel matrixes at 25 °C and 36 °C with sample HG-25-A and HG-25-B. At 25 °C, which corresponds to the preparation temperature of the pure PAAM gel and the two composite gels HG-25-A and HG-25-B, we find identical tracer diffusion coefficients in the matrix. This is expected and demonstrates that the incorporation of the microgel beads does not affect the formation of the PAAM gel.

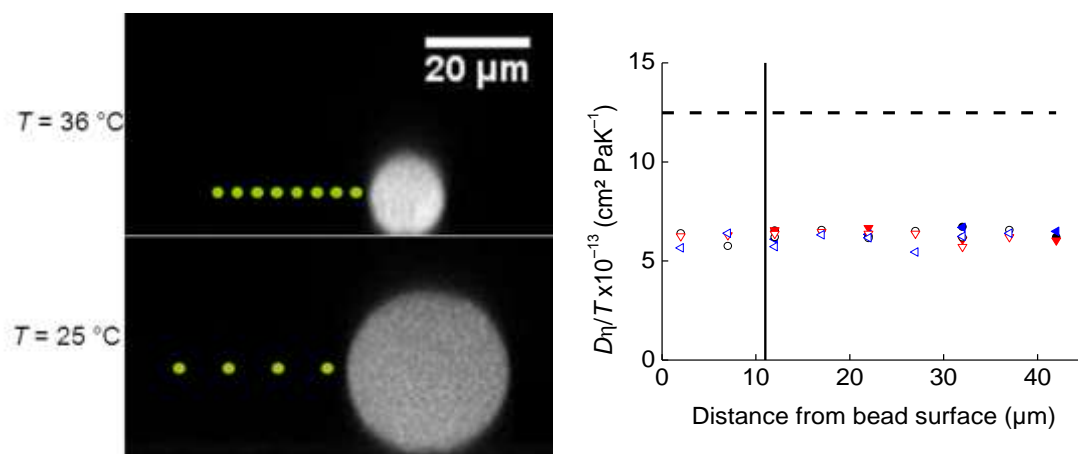


Figure 5.5 Normalized diffusion coefficients of 70-kDa dextran in the hydrogel matrix close to the bead surface in sample HG-25-A. Full symbols denote $T = 25\text{ }^{\circ}\text{C}$, whereas open symbols denote $T = 36\text{ }^{\circ}\text{C}$. Measurements were conducted on three different beads, as represented by different symbols (circles, upright triangles, and inverted triangles). The dashed line indicates the normalized diffusion coefficients of 70-kDa dextran in water. The vertical solid line indicates the position of the bead surface at $T = 25\text{ }^{\circ}\text{C}$.

Figure 5.5 displays the diffusion coefficient of 70-kDa dextran in the hydrogel matrix of sample HG-25-A. In this plot, the diffusion coefficient is normalized by the solvent viscosity, η , and by the temperature, T , to account for the trivial temperature dependence of diffusion. The normalized diffusion coefficients do not change when the sample is heated from $25\text{ }^{\circ}\text{C}$ to $36\text{ }^{\circ}\text{C}$, and there is no dependence on the distance to the bead surface. For this sample, we have shown that an interpenetrating network is formed. However, the collapse of the bead does not affect the tracer diffusion in the surrounding matrix. The same result is found for 3-kDa dextran in this sample (Supporting Information Fig. S.5.6).

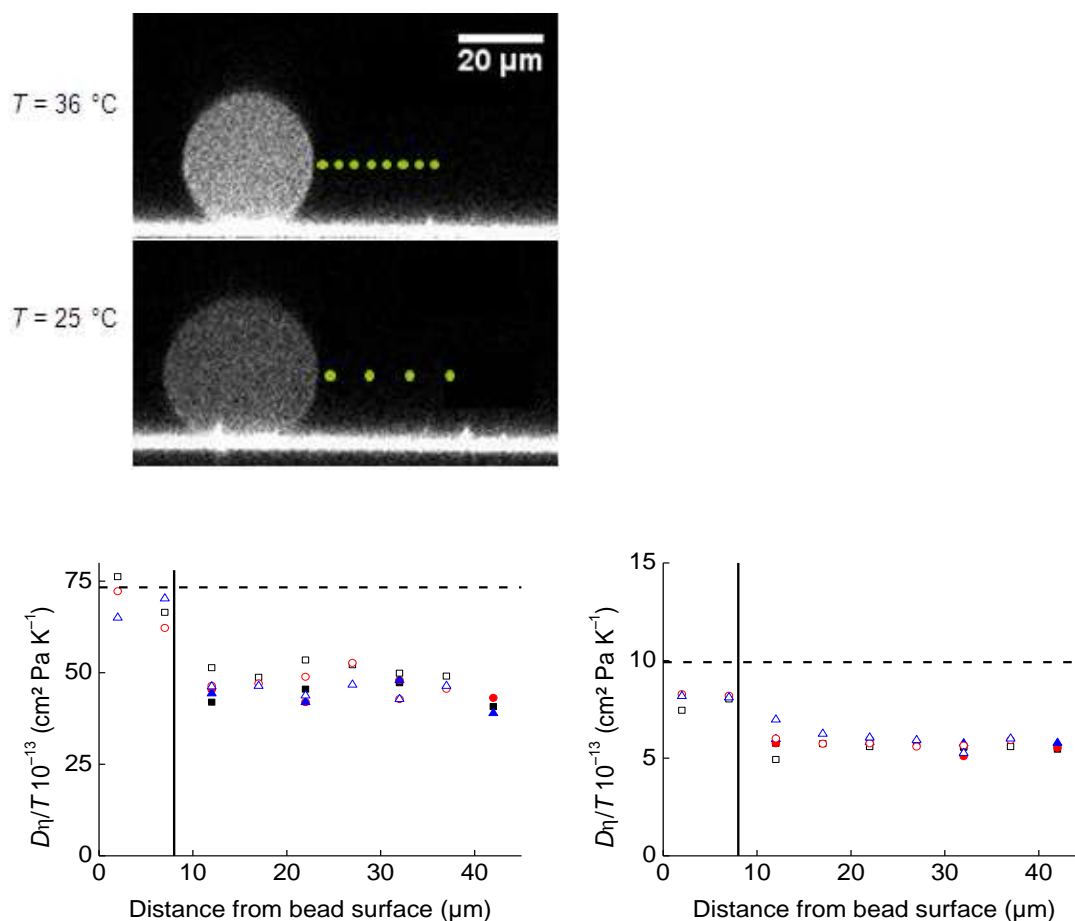


Figure 5.6 Normalized diffusion coefficients of 3-kDa dextran (center) and 70-kDa dextran (bottom) in the hydrogel matrix close to the bead surface in sample HG-25-B. Full symbols denote $T = 25\text{ }^{\circ}\text{C}$, whereas open symbols denote $T = 36\text{ }^{\circ}\text{C}$. Measurements were conducted on three different beads, as represented by different symbols (squares, circles, and triangles). The dashed lines indicate the normalized diffusion coefficients of the dextrans in water. The vertical solid line indicates the position of the bead surface at $T = 25\text{ }^{\circ}\text{C}$. The scale bar denotes 20 micrometers and applies to both panels.

In contrast to the presence of an interpenetrating network in sample HG-25-A, there are no indications for an interpenetrating network in sample HG-25-B. The normalized tracer diffusion coefficients in the gel matrix of this sample are enhanced near the particle surface upon heating, as shown in Figure 5.6. We address this finding to the following rationale:

The data at $25\text{ }^{\circ}\text{C}$ are taken at positions outside the beads, and when these positions are studied at $36\text{ }^{\circ}\text{C}$, the diffusion coefficient, normalized by the change of η and T , is not

affected. Due to the strong collapse of the beads, however, it is possible to measure tracer diffusivities at positions that were occupied by the bead at 25 °C but are no longer occupied at 36 °C, as represented by the 36 °C data left of vertical line in Figure 5.6. These tests show that the tracer diffusivity *increases* in the volume formerly occupied by the bead when the bead is deswollen at 36 °C (Measurements near the bead surface were performed after annealing times of 7 hours to ensure that the hydrogel matrix has enough time to reach equilibrium swelling.). The value of the increased normalized diffusion coefficient of 3-kDa dextran is the same as in water at 36 °C (Figure 5.6, lower left). This suggests that the PAAM hydrogel is locally swollen so much by the water released from the collapsed bead that the small 3-kDa dextran is no longer restricted in its diffusion. The 70-kDa dextran also shows accelerated diffusion inside the volume previously occupied by the beads (Figure 5.6, lower right). The normalized diffusion is, however, always smaller than in water.

These results show that the PAAM hydrogel matrix has swollen into the volume that was formerly occupied by the bead at 25 °C. The local segmental density of the PAAM hydrogel in these regions is lower than that in the bulk gel away from the bead, indicating that the gel matrix swells heterogeneously. The segmental density is still sufficiently high to hinder the diffusion of 70-kDa dextran compared to its diffusion in pure water, but the gel does no longer obstruct the diffusion of 3-kDa dextran. As the swelling of the matrix is localized to the volume close to the beads, it might be possible to form channels across the composite hydrogel when the bead concentration is so high that the beads are close together in the swollen state but apart from each other at higher temperatures when they are deswollen.

5.4. Conclusions

Interpenetrating polymer networks can be formed in composite hydrogels that consist of microgel particles embedded in a surrounding macroscopic gel matrix. This, however, depends on the density of the embedded microgel beads. No interpenetrating networks are formed inside the incorporated beads when the beads are highly cross-linked. In this limit, spatially resolved tracer diffusion measurements reveal that the hydrogel matrix swells heterogeneously when the beads collapse, indicating the formation of pores near their surface.

By contrast, interpenetrating networks are found with less cross-linked beads; this entails slower diffusion of tracers inside the beads. In this scenario, the temperature dependent swelling of the PNIPAM beads depends on the polymer concentration of the hydrogel matrix.

These results show that the properties of thermo-sensitive composite hydrogels as well as the mobility of guest species can be tailored by the composition of the embedded particles and the surrounding gel matrix. Tuning these parameters can therefore serve to control the movement of active species through such composite hydrogels. This foreshadows the utility of these systems as membranes with tunable permeability in separation techniques and analytical sciences. In addition, our experiments demonstrate the utility of 2fFCS for the determination of spatially resolved tracer diffusion in complex gels or biomaterials.

5.5. Supporting Information

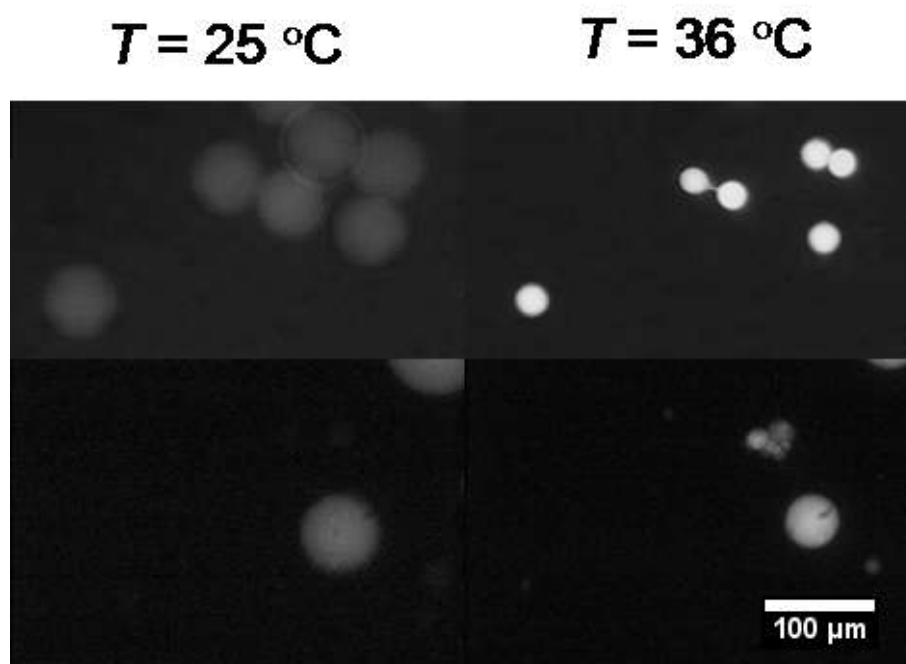


Fig. S.5.1 PNIPAM beads in water, imaged by fluorescence microscopy. Top: PNIPAM beads of type A at $25\text{ }^{\circ}\text{C}$ (left) and at $36\text{ }^{\circ}\text{C}$ (right). Bottom: PNIPAM beads of type B at $25\text{ }^{\circ}\text{C}$ (left) and at $36\text{ }^{\circ}\text{C}$ (right). The scale bar denotes 100 micrometers and applies to all panels.

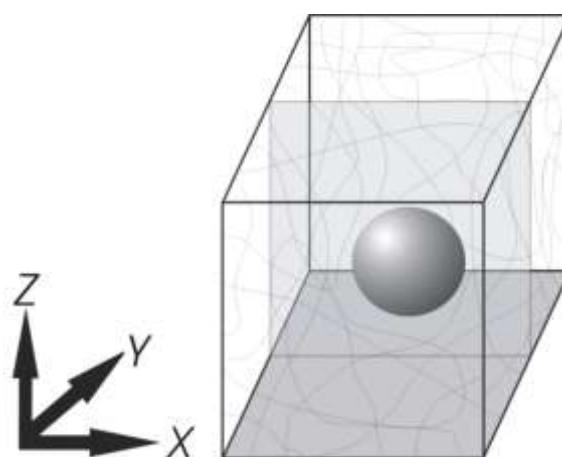


Fig. S.5.2 3D schematic of the filled hydrogels. The sphere represents a microgel bead, the lower grey plane indicates the lower glass cover slide; the light grey plane indicates the vertical confocal scanning plane.

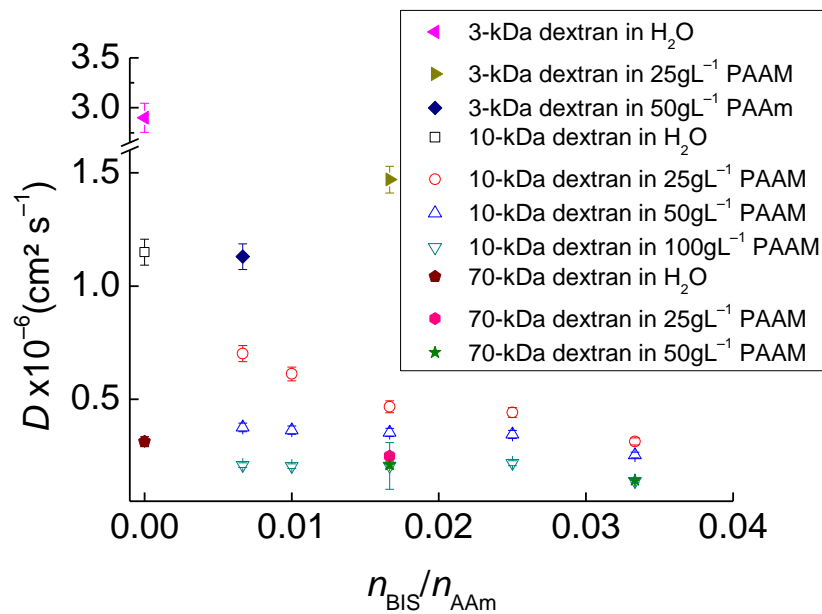


Fig. S.5.3 Diffusion coefficients of different dextran in PAAM hydrogels of different compositions and in water.

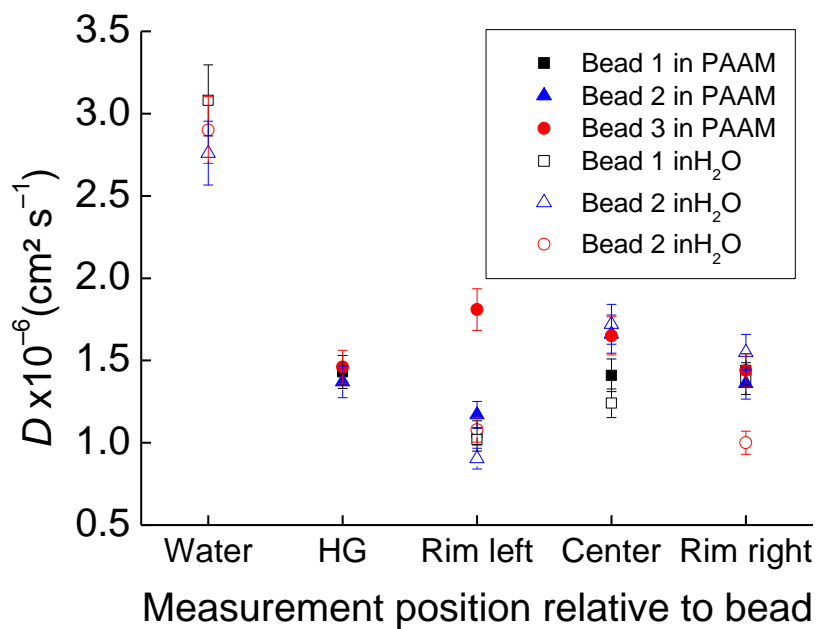


Fig. S.5.4 Diffusion of 3-kDa dextran in microgel beads of type A suspended in water (open symbols) or embedded into polymer matrixes HG-25-A (filled symbols). $T = 25 \text{ }^\circ\text{C}$.

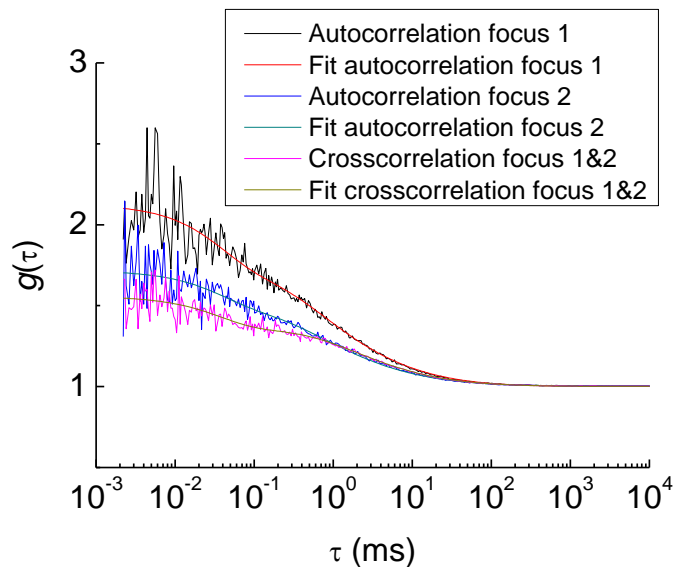


Fig. S.5.5 2fFCS measurement on 10-kDa dextran labeled with Alexa Fluor 647 in a PAAM hydrogel matrix with cross-linker to monomer ratio of 1:60 and a PAAM concentration of 50 gL^{-1} at $25 \text{ }^\circ\text{C}$. A single particle model including triplet state relaxation is used to fit the data (smooth lines). Fluorescence excitation was achieved with $\lambda_{\text{ex}} = 470 \text{ nm}$ at an excitation power of $2 \text{ } \mu\text{W}$. The detection signal was filtered by a HC 687/70 (AHF) band pass filter.

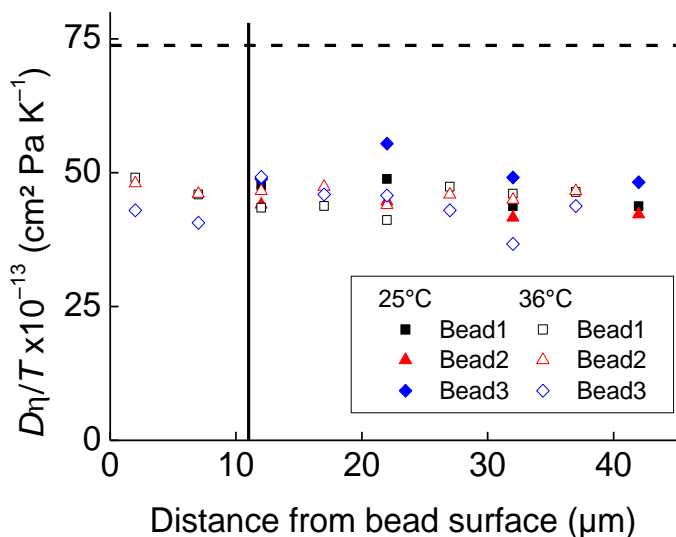


Fig. S.5.6 Normalized diffusion coefficients of 3k-Da dextran in the hydrogel matrix close to the bead surface in sample HG-25-A. Full symbols denote $T = 25 \text{ }^\circ\text{C}$, whereas open symbols denote $T = 36 \text{ }^\circ\text{C}$. Measurements at three different beads are shown and represented by different symbols (squares, triangles, and diamonds). The dashed line indicates the normalized diffusion coefficient of the same dextran tracer in water. The vertical solid line indicates the position of the bead surface at $T = 25 \text{ }^\circ\text{C}$.

5.6. References

1. Xu, X., et al., *Hyaluronic acid-based hydrogels: from a natural polysaccharide to complex networks*. *Soft Matter*, 2012. **8**(12): p. 3280-3294.
2. Kuckling, D., *Responsive hydrogel layers-from synthesis to applications*. *Colloid Polym. Sci.*, 2009. **287**(8): p. 881-891.
3. Sivakumaran, D., D. Maitland, and T. Hoare, *Injectable Microgel-Hydrogel Composites for Prolonged Small-Molecule Drug Delivery*. *Biomacromolecules*, 2011. **12**(11): p. 4112-4120.
4. Gurski, L.A., et al., *Hyaluronic acid-based hydrogels as 3D matrices for in vitro evaluation of chemotherapeutic drugs using poorly adherent prostate cancer cells*. *Biomaterials*, 2009. **30**(30): p. 6076-6085.
5. McGillicuddy, F.C., et al., *Novel "plum pudding" gels as potential drug-eluting stent coatings: Controlled release of fluvastatin*. *J. Biomed. Mater. Res., Part A*, 2006. **79A**(4): p. 923-933.
6. Jonas, U. and A. Mateescu, *Novel hydrogel thin film materials from photocrosslinkable polymers*. *Polym. Prepr. (Am. Chem. Soc., Div. Polym. Chem.)*, 2012. **53**(1): p. 297-298.
7. Tumarkin, E., et al., *High-throughput combinatorial cell co-culture using microfluidics*. *Integr. Biol.*, 2011. **3**(6): p. 653-662.
8. Cohen Stuart, M.A., et al., *Emerging applications of stimuli-responsive polymer materials*. *Nat. Mater.*, 2010. **9**(2): p. 101-113.
9. Langer, R. and J.P. Vacanti, *TISSUE ENGINEERING*. *Science*, 1993. **260**(5110): p. 920-926.
10. Dong, Y.X., et al., *Thermoresponsive hyperbranched copolymer with multi acrylate functionality for in situ cross-linkable hyaluronic acid composite semi-IPN hydrogel*. *Journal of Materials Science-Materials in Medicine*, 2012. **23**(1): p. 25-35.
11. Nakajima, T., et al., *SUPER TOUGH GELS WITH A DOUBLE NETWORK STRUCTURE*. *Chinese Journal of Polymer Science*, 2009. **27**(1): p. 1-9.
12. Velasco, D., E. Tumarkin, and E. Kumacheva, *Microfluidic Encapsulation of Cells in Polymer Microgels*. *Small*, 2012. **8**(11): p. 1633-1642.
13. Legant, W.R., et al., *Measurement of mechanical tractions exerted by cells in three-dimensional matrices*. *Nat. Methods*, 2010. **7**(12): p. 969-971.
14. Salvati, A., O. Soderman, and I. Lynch, *Plum-pudding gels as a platform for drug delivery: Understanding the effects of the different components on the diffusion behavior of solutes*. *Journal of Physical Chemistry B*, 2007. **111**(25): p. 7367-7376.
15. Musch, J., et al., *Unperturbed volume transition of thermosensitive poly-(N-isopropylacrylamide) microgel particles embedded in a hydrogel matrix*. *Journal of Physical Chemistry B*, 2008. **112**(20): p. 6309-6314.
16. Lynch, I. and K.A. Dawson, *Synthesis and characterization of an extremely versatile structural motif called the "plum-pudding" gel*. *Journal of Physical Chemistry B*, 2003. **107**(36): p. 9629-9637.
17. Pelton, R., *Temperature-sensitive aqueous microgels*. *Adv. Colloid Interface Sci.*, 2000. **85**(1): p. 1-33.
18. Raz, N., et al., *Microgels with an Interpenetrating Network Structure as a Model System for Cell Studies*. *Macromolecules*, 2010. **43**(17): p. 7277-7281.

19. Meid, J., et al., *Composite hydrogels with temperature sensitive heterogeneities: influence of gel matrix on the volume phase transition of embedded poly-(N-isopropylacrylamide) microgels*. *Physical Chemistry Chemical Physics*, 2011. **13**(8): p. 3039-3047.
20. Meid, J., et al., *Mechanical properties of temperature sensitive microgel/polyacrylamide composite hydrogels-from soft to hard fillers*. *Soft Matter*, 2012. **8**(15): p. 4354-4263.
21. Pich, A. and W. Richtering, *Microgels by precipitation polymerization: synthesis, characterization, and functionalization*. *Adv. Polym. Sci.*, 2010. **234**(Chemical Design of Responsive Microgels): p. 1-37.
22. Rossow, T., et al., *Controlled Synthesis of Cell-Laden Microgels by Radical-Free Gelation in Droplet Microfluidics*. *J. Am. Chem. Soc.*, 2012. **134**(10): p. 4983-4989.
23. Dertinger, T., et al., *Two-focus fluorescence correlation spectroscopy: A new tool for accurate and absolute diffusion measurements*. *Chemphyschem*, 2007. **8**(3): p. 433-443.
24. Soddemann, M., *Lichtstreuung und Rheologie an gefüllten, vernetzten und verzweigten Polymersystemen*. PhD. Thesis, 2002.
25. Seiffert, S., *Functional Microgels Tailored by Droplet-Based Microfluidics*. *Macromolecular Rapid Communications*, 2011. **32**(20): p. 1600-1609.
26. Annaka, M., et al., *Preparation of Comb-Type N-Isopropylacrylamide Hydrogel Beads and Their Application for Size-Selective Separation Media*. *Biomacromolecules*, 2003. **4**(2): p. 395-403.
27. Muller, C.B. and W. Richtering, *Sealed and temperature-controlled sample cell for inverted and confocal microscopes and fluorescence correlation spectroscopy*. *Colloid and Polymer Science*, 2008. **286**(11): p. 1215-1222.
28. Pusey, P.N. and W. van Megen, *Dynamic light scattering by non-ergodic media*. *Physica A (Amsterdam)*, 1989. **157**(2): p. 705-41.
29. Modesti, G., et al., *Diffusion in Model Networks as Studied by NMR and Fluorescence Correlation Spectroscopy*. *Macromolecules*, 2009. **42**(13): p. 4681-4689.
30. Raccis, R., et al., *Probing mobility and structural inhomogeneities in grafted hydrogel films by fluorescence correlation spectroscopy*. *Soft Matter*, 2011. **7**(15): p. 7042-7053.
31. Enderlein, J., et al., *Performance of fluorescence correlation spectroscopy for measuring diffusion and concentration*. *Chemphyschem*, 2005. **6**(11): p. 2324-2336.
32. Muller, C.B., et al., *Precise measurement of diffusion by multi-color dual-focus fluorescence correlation spectroscopy*. *Epl*, 2008. **83**(4): p. 5.
33. Muller, C.B., et al., *Dual-focus fluorescence correlation spectroscopy: a robust tool for studying molecular crowding*. *Soft Matter*, 2009. **5**(7): p. 1358-1366.
34. Nie, J., B. Du, and W. Oppermann, *Influence of formation conditions on spatial inhomogeneities in poly(N-isopropylacrylamide) hydrogels*. *Macromolecules*, 2004. **37**(17): p. 6558-6564.
35. Shibayama, M., *Spatial inhomogeneity and dynamic fluctuations of polymer gels*. *Macromolecular Chemistry and Physics*, 1998. **199**(1): p. 1-30.
36. Schild, H.G., *Super-absorbency and phase transition of gels in physiological salt solutions*. *Macromol. Chem.*, 1992. **3**(6): p. 393-395.

37. Ponder, E. and R.V. Ponder, *THE INTERACTION OF DEXTRAN WITH SERUM ALBUMIN, GAMMA-GLOBULIN, AND FIBRINOGEN*. Journal of General Physiology, 1960. **43**(4): p. 753-758.
38. Vermonden, T., et al., *Macromolecular Diffusion in Self-Assembling Biodegradable Thermosensitive Hydrogels*. Macromolecules, 2010. **43**(2): p. 782-789.
39. Branco, M.C., et al., *Macromolecular diffusion and release from self-assembled beta-hairpin peptide hydrogels*. Biomaterials, 2009. **30**(7): p. 1339-1347.
40. Al-Baradi, A.M., et al., *Magnetic field dependence of the diffusion of single dextran molecules within a hydrogel containing magnetite nanoparticles*. Journal of Chemical Physics, 2010. **134**(9).
41. Seiffert, S. and W. Oppermann, *Diffusion of linear macromolecules and spherical particles in semidilute polymer solutions and polymer networks*. Polymer, 2008. **49**(19): p. 4115-4126.
42. Cheng, Y., R.K. Prud'homme, and J.L. Thomas, *Diffusion of Mesoscopic Probes in Aqueous Polymer Solutions Measured by Fluorescence Recovery after Photobleaching*. Macromolecules, 2002. **35**(21): p. 8111-8121.
43. Lindemann, B., U.P. Schroder, and W. Oppermann, *Influence of the cross-linker reactivity on the formation of inhomogeneities in hydrogels*. Macromolecules, 1997. **30**(14): p. 4073-4077.
44. Enderlein, J., *Polymer Dynamics, Fluorescence Correlation Spectroscopy, and the Limits of Optical Resolution*. Physical Review Letters, 2012. **108**(10): p. 108101/1-108101/4.

6. Summary and Outlook

Hydrogels and hydrogel particles have a great potential in a huge numbers of applications. One of the most important parameters for applications such as drug delivery, catalysis and membranes is the diffusion coefficient. The macroscopic diffusion coefficient through a hydrogel or a hydrogel particle is rather easy to address. A located diffusion coefficient at defined positions inside a hydrogel or a hydrogel particle is much more difficult even if the hydrogel is of high complexity.

The capability of reliable measurements of the diffusion coefficient inside complex stimulus-responsive hydrogels and hydrogel particles lead to very important information about the structure and possible applications, especially if the measurements can be done spatially resolved. One target for spatial resolution is the complex structure of the refractive index inside these samples. The single focus FCS suffers from this. We were able to show that an insufficient consideration of the refractive index in the data evaluation of single focus FCS can lead to a misinterpretation of anomalous diffusion. The highly complex structure inside complex stimulus responsive hydrogels makes it very hard to calculate the correct refractive index distribution for one measurement point inside the sample. This makes reliable single focus FCS measurements in such samples very hard.

The spatial resolution is even harder to be realized. Therefore, a huge number of refractive index distributions inside the sample must be calculated, at least for each measurement point. The number is even multiplied by the number of variations of stimulus-responsive parameters.

The 2fFCS is introduced in the spatial resolved mode. The changes of the refractive index upon changing the position or stimulus relevant parameters do not influence the measurement results. This makes the 2fFCS the method of choice for spatial resolved diffusion measurements inside complex gel structures.

The comparison of single-focus and two-focus experiments on dextran tracers in different complex environments with same refractive indexes demonstrates the impact of the refractive index mismatch in single-focus FCS data evaluation. The refractive index of the sample must be taken into account to avoid artifacts which can be misinterpreted as anomalous diffusion. If the refractive index can't be determined, especially in hydrogels with heterogeneous morphologies, 2fFCS is the better technique to determine the diffusion coefficient. Anomalous diffusion itself is a relevant and interesting phenomenon and has to be investigated, but the refractive index mismatch always has to be considered in such investigations.

A system where the complex refractive index is of high importance is, a sub-millimeter-sized hydrogel particles consisting of a thermo-responsive shell that surrounds a non-thermo-responsive core. Such particles can be used as microcarriers that allow molecular and small colloidal additives to be encapsulated and released by selective shell deswelling or swelling.[1, 2] The used 2fFCS probes the mobility of oligomeric guest molecules with spatial resolution. The data demonstrate that 2fFCS is indeed able to provide information on how the local network structure affects tracer mobility [3]. We were able to show that core and shell affect each other only at the interface. Therefore we have demonstrated a carrier with a controlled entrapment of guest molecules and a defined diffusion of those inside the core of the particle. The defined

diffusion inside the core can be used to control the release of the guest molecule if the shell is swollen and permeable for the guest molecules. This will allow for exploiting recent developments of gel synthesis to control the structure of complex gels for a rational control of mobility of actives inside gels [4-6]. Determining the local mobility will be important in the development for tissue engineering scaffolds containing colloidal particles [7] and also for sensors [8] and microgel-modified membranes [9].

Modifying membranes or, more generally speaking, hydrogels with microgels is a simple way to combine the fast responds of responsive microgels with macroscopic scale applications. The microgels are immobilized and located in the macroscopic gel matrix and retain their fast respond. The concentration of the microgel particles inside the hydrogel matrix can be easily defined with respect to the requirements of the application. One big question in such systems is the formation of interpenetrating networks. In the discussed composite hydrogels, interpenetrating networks can be formed.

This, however, depends on the density of the embedded microgel beads. No interpenetrating networks are formed inside the incorporated beads when the beads are highly cross-linked. In this limit, spatially resolved tracer diffusion measurements reveal that the hydrogel matrix swells heterogeneously when the beads collapse, indicating the formation of pores near their surface.

By contrast, interpenetrating networks are found with less cross-linked beads; this entails slower diffusion of tracers inside the beads. In this scenario, the temperature dependent swelling of the PNIPAM beads depends on the polymer concentration of the hydrogel matrix.

These results show that the properties of thermo-sensitive composite hydrogels as well as the mobility of guest species can be tailored by the composition of the embedded particles and the surrounding gel matrix. Tuning these parameters can therefore serve to control the movement of active species through such composite hydrogels. This foreshadows the utility of these systems as membranes with tunable permeability in separation techniques and analytical sciences. In addition, our experiments demonstrate the utility of 2fFCS for the determination of spatially resolved tracer diffusion in complex gels or biomaterials.

6.1. Outlook

6.1.1. Anomalous diffusion

6.1.1.1. Detection of anomalous diffusion via 2fFCS

Tackling the field of anomalous diffusion, it would be nice to test whether the 2fFCS is able to measure the anomalous diffusion in systems, where anomalous diffusion is predicted. I would suggest measuring the diffusion of proteins inside a functionalized hydrogel which offers specific none covalent binding sites for the protein. In such systems the prediction of Enderlein et al.[10] about the optical resolution of the 2fFCS can be proofed. If anomalous diffusion can be seen in 2fFCS measurements, an improved data evaluation for 2fFCS can be introduced. Or, if no anomalous diffusion is visible in the experiments, the approach of Masuda et al. [11, 12], using different sizes of the detection volume to determine anomalous diffusion, can be applied to the 2fFCS.

6.1.2. Diffusion inside core-shell particles

6.1.2.1. Core-shell particle composition

We demonstrated that the core-shell structure of microgel particles is a very promising architecture for controlled release and uptake of small molecules. In this field it would be interesting to change the core and the shell polymer. Introducing different responsibilities to the core and shell and even the polymer density in the core and the shell may lead to very powerful properties for application. If core and shell respond completely independent on specific stimuli, measurement series with respect for both stimuli are interesting to determine whether the collapse of the core squeezes out the incorporated guest molecule or immobilizes the guest molecule upon shrinking.

6.1.2.2. Core-shell particle architecture

Another interesting question is the solidity of the collapsed shell with respect to the diffusion of the incorporated guest oligomers. This can be tested by incorporating the guest molecules into the core-shell particle, than completely collapsing the shell of the particle. Afterwards cleaning the particles by simultaneously cleaning the shell completely collapsed at any time and finally disperses the particles with collapsed shell in clear solvent. The diffusion of the guest molecule has to be measured before swelling the shell in a series with several time steps for equilibration, up to about some weeks and after swelling the shell, again with an equilibration time determined by the diffusion coefficients of the guest oligomers in the swollen particle.

If the solidity of the shell is not sufficient, a core-shell-shell architecture may lead to a sufficient solidity. A particle with two responsive shells with independent triggers is

more difficult to handle but, using micro fluidic devices, almost as simple to synthesize as a particle with only one shell. The different triggers for the core and the shells have to be chosen very carefully for applications but the variety of potentially useful polymers is that high that it should be possible.

6.1.3. Hydrogels with switchable inhomogenities

Until now we studied the diffusion in PAAM hydrogels filled with PNIPAM microgel beads. The beads were incorporated in swollen state into the hydrogel. An interesting sample would be if the beads are incorporated into the hydrogel at collapsed state. In agreement with our results we would expect to see no interpenetrating polymer networks. But how do the beads swell? Is there a limitation in swelling, due to the surrounding hydrogel? If the beads swell how this does effect the diffusion close to the surface of the beads and in the hydrogel bulk. Is the effect of the bead swelling again local close to the beads, as we had shown in chapter 5 for the effect on the diffusion inside the hydrogel due to collapsing the beads?

Further on, it would be interesting to modify the architecture of the composite hydrogel. Preparing vertical channels with a high concentration of microgel beads, which are almost in contact to each other but do not aggregate, in a microgel free hydrogel film may lead to a membrane with defined diffusion which can be controlled by switching the beads from swollen to collapsed state.

6.1.3.1. Combining core-shell particles with hydrogels

Another interesting approach is to combine the core-shell particles with the composite hydrogels. A great benefit of such systems is the well defined location for the core-shell particles. The resulting hydrogel or hydrogel film has a high potential to be a novel pad for skin injuries. The hydrogel would cover the injury and can be filled with additives that supports the healing if the injury and at the same time the core-shell particles are carrying drugs that are released in the case of an infection of the injury to cure the infection. Such pads would be very interesting in the therapy of burns of the skin.

6.2. References

1. Bysell, H., et al., *Microgels and microcapsules in peptide and protein drug delivery*. Advanced Drug Delivery Reviews, 2011. **63**(13): p. 1172-1185.
2. Seiffert, S., et al., *Smart Microgel Capsules from Macromolecular Precursors*. J. Am. Chem. Soc., 2010. **132**(18): p. 6606-6609.
3. Lehmann, S., S. Seiffert, and W. Richtering, *Spatially Resolved Tracer Diffusion in Complex Responsive Hydrogels*. J. Am. Chem. Soc., 2012. **134**(38): p. 15963-15969.
4. Wong, J.E. and W. Richtering, *Layer-by-layer assembly on stimuli-responsive microgels*. Current Opinion in Colloid & Interface Science, 2008. **13**(6): p. 403-412.
5. Richtering, W. and B.R. Saunders, *Gel architectures and their complexity*. Soft Matter, 2014. **10**(21): p. 3695-3702.
6. Peak, C.W., J.J. Wilker, and G. Schmidt, *A review on tough and sticky hydrogels*. Colloid Polym. Sci., 2013. **291**(9): p. 2031-2047.
7. Clarke, K.C., et al., *Colloid-matrix assemblies in regenerative medicine*. Curr. Opin. Colloid Interface Sci., 2013. **18**(5): p. 393-405.
8. Islam, M.R., et al., *Responsive polymers for analytical applications: A review*. Anal. Chim. Acta, 2013. **789**: p. 17-32.
9. Menne, D., et al., *Temperature-Modulated Water Filtration Using Microgel-Functionalized Hollow-Fiber Membranes*. Angew. Chem., Int. Ed., 2014. **53**(22): p. 5706-5710.
10. Enderlein, J., *Polymer Dynamics, Fluorescence Correlation Spectroscopy, and the Limits of Optical Resolution*. Physical Review Letters, 2012. **108**(10): p. 108101/1-108101/4.
11. Masuda, A., K. Ushida, and T. Okamoto, *Direct observation of spatiotemporal dependence of anomalous diffusion in inhomogeneous fluid by sampling-volume-controlled fluorescence correlation spectroscopy*. Physical Review E, 2005. **72**(6): p. 060101.

12. Masuda, A., K. Ushida, and T.O. Riken, *New fluorescence correlation spectroscopy enabling direct observation of spatiotemporal dependence of diffusion constants as an evidence of anomalous transport in extracellular matrices*. *Biophysical Journal*, 2005. **88**(5): p. 3584-3591.

7. Appendix

7.1. Quantum dots as tracer particles

Quantum dots (QD) are photoactive nano-crystals that emit light upon excitation with light of short wave-lengths like UV-light[1]. The emission of light is quite similar to fluorescence. In contrast to classical fluorescence the excitation is not done by increasing the energy level of single electrons but by electron hole interactions[1]. This means that the electrons near the conduction band of the crystal absorb the energy of the excitation light and not a single electron alone. This leads to a very broad absorbance band for QDs. The emission of light is again much defined and has a small width[1]. The wave-length of the emitted light is strongly correlated to the size of the QDs[1]. The broad absorption band and the small emission band makes the QDs very interesting for labeling cells, polymers or proteins.

One big disadvantage of the “simple” QDs is that they perform blinking [1-3]. This means the QDs have dark states during the excitation. This is due to plasmon reactions with the crystal. To overcome this problem core-shell structures of the QDs are introduced [2, 3]. The core of such particles is again the photoactive QD surrounded by a shell which minimizes side effects of the plasmon interactions with the crystal. A scheme of the architecture of QDs is shown in Figure 7.1.

Another big disadvantage is that the QDs are built out of metals and therefore are not water soluble. This is unlikely for applications in biological systems and all other systems built on water. To overcome this problem a second shell is added using water soluble polymers with a water insoluble anchor group. The anchor group attaches to the QDs and the water soluble rest dissolves in water and makes the whole QD water soluble. A

second effect of the polymer shell is that they prevent the QDs from aggregation[2]. The aggregation leads to a shift to higher wave-lengths in the emission of the QD aggregates.

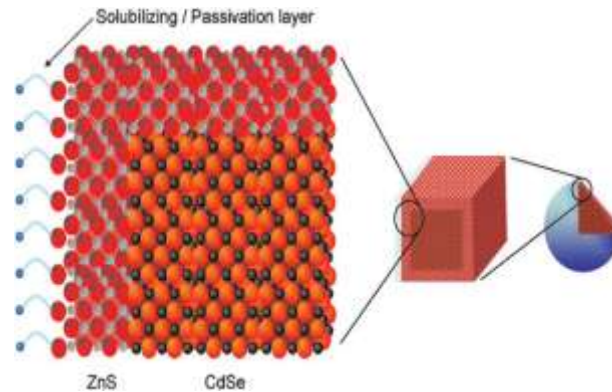


Figure 7.1 Schematic draw of the core-shell structure of the QDs. [2]

QDs are very interesting to be used as tracers in FCS measurements. Therefore we tested two different QD sorts: The commercially available Qtracer 705 (Invitrogen) and the handmade QDs from Dr. Marc Thiry (University of Hamburg).

The QDs from Hamburg are PEO covered CdSe/CdS/ZnS nano particles with a particle diameter of 7 nm and a Quantum yield of 36%. The emission maximum of the fluorescence of the particles is at 590 nm.

We performed SAXS and DLS measurements on these particles to verify the particle structure and to check whether the redispersed particles are aggregated or not.

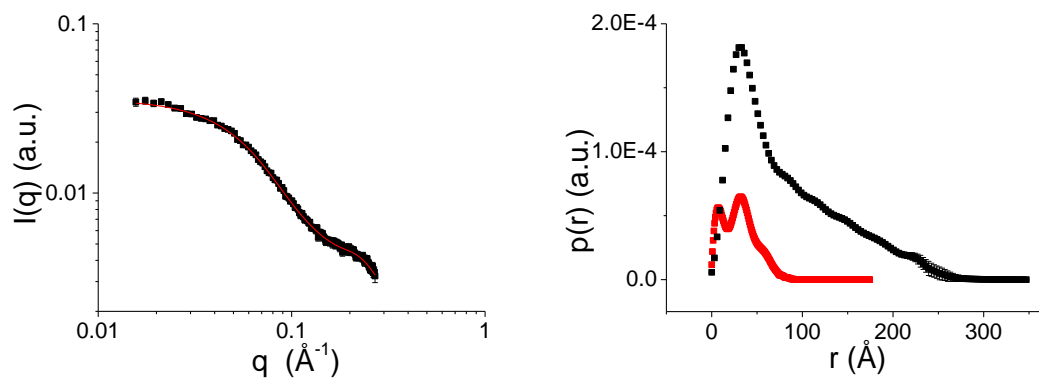


Figure 7.2 Measurement results of the SAXS experiment. left: scattering intensity; black: measurement data; red: corresponding fit. right: The pair correlation function from the SAXS measurements of the QD solutions with concentrations of 1 gL^{-1} (red) and 3 gL^{-1} (black). For the lower concentration (red) the core-shell architecture of the particle is retained. The radius of gyration is found to be 25.1 \AA ; the resulting particle diameter is 64.9 \AA . For the higher concentration (black) the information of the core-shell structure is lost. The resulting radius diameter of the particle is 72.24 \AA .

We performed SAXS experiments to check the architecture and size of the single QDs (Figure 7.2). SAXS measurements can only address small particles therefore we do not get information about aggregates. For the experiment with a concentration of 1 gL^{-1} (Figure 7.2, red) we were able to show the core-shell structure of the QDs. The resulting particle diameter of 64.9 \AA is in good agreement with the given 7 nm diameter from the specifications from Hamburg.

The information about the core-shell structure is lost for higher concentrations. The size of the particle is calculated to be 72.24 \AA . This is in good agreement with the former results.

Then we performed DLS measurements to get information about aggregation in our samples. We made an angle dependent measurement with a scattering angle from 30° to 150° .

In these measurements (Figure 7.3) we found that there are single particles in our samples as well as big aggregates.

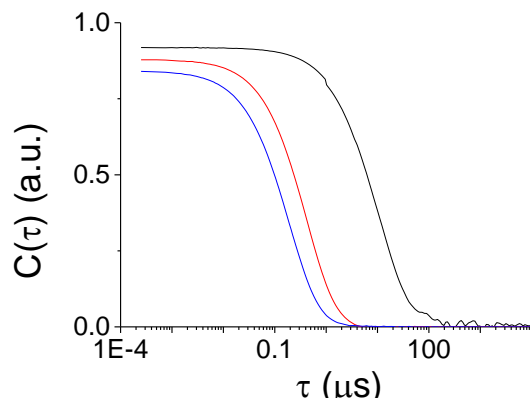


Figure 7.3 Autocorrelation functions of the measurement of the QD's from Hamburg. Black: measurement angle 30°; red: 90°; blue 150°.

Due to the fact that bigger particles have a higher scattering intensity, we recalculated the intensity weighted distribution (Figure 7.4, left) into a mass weighted distribution (Figure 7.4, right). In the recalculated distribution, it is shown, that aggregates with a size of about two times of the diameter of a single particle are dominating. The origin of these particles can be the single QDs with a PEO shell of 5 nm, or if the shell does not scatter high enough, these particles are aggregates of 2 to 4 QDs. This would lead to major problems for FCS measurements. We will discuss this later.

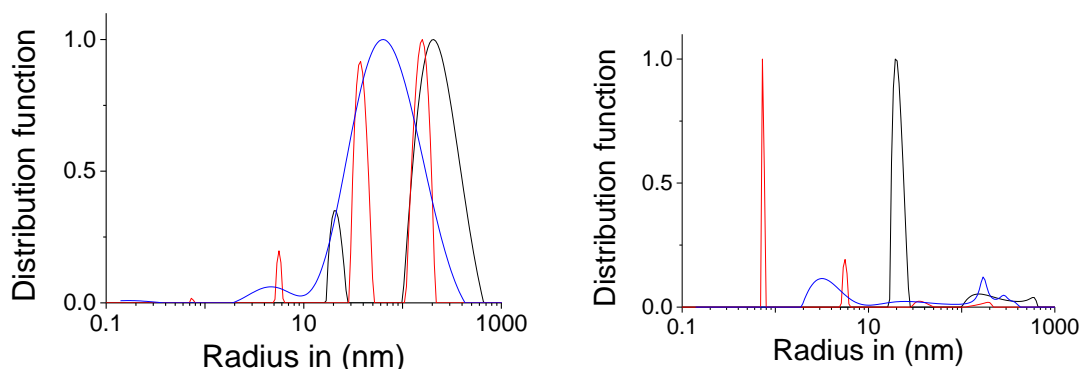


Figure 7.4 DLS measurements of the QDs. left: intensity weighted size distribution; right: mass weighted size distribution. The black lines indicate measurements at an angle of 30°, red at 90° and blue at 150°. The peaks below 1 nm are artifacts due to bad statistics for short times. The measurements duration was 120 s.

At the moment we think that the particles with a size of about 11 nm are the single QDs with a shell of 5 nm. On the other hand bigger aggregates are visible in the measurements.

To measure the QDs in the 2f-FCS, we diluted the QD solution to a concentration of $c = 0.001 \text{ gL}^{-1}$. This is equal to a particle concentration of about 2.4 nM. We performed a series of independent measurements with this solution, each with duration of 6h.

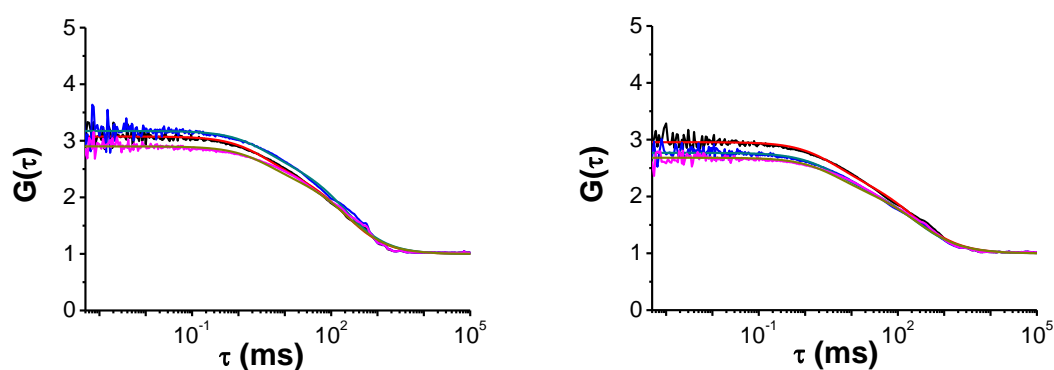


Figure 7.5 2f-FCS measurements of the QDs. Two independent measurements are shown to demonstrate reproducibility. Both measurements show the auto correlation functions of the two foci (black and blue) and the cross correlation of the two foci (red). All correlation functions had to be fitted with a two particle model. The resulting diffusion coefficients and radii are for the bigger particles: left: $D = 1.41 \mu\text{m}^2\text{s}^{-1}$; $R = 173.54 \text{ nm}$; right: $D = 1.33 \mu\text{m}^2\text{s}^{-1}$; $R = 183.97 \text{ nm}$; and for the smaller particles: left: $D = 73.7 \mu\text{m}^2\text{s}^{-1}$; $R = 3.32 \text{ nm}$; right: $D = 73.3 \mu\text{m}^2\text{s}^{-1}$; $R = 3.34 \text{ nm}$.

Two of the measurement results are shown in Figure 7.5. The fitting of the resulting correlation functions had to be done using a two particle model. The resulting hydrodynamic radii of the smaller particles are in good agreement with the SAXS and DLS experiment. The bigger particles in the 2f-FCS measurement are much bigger than the dominating species in the DLS measurement. On the other hand, a dominating species with a radius double of the radius of a single QD are not visible in the 2f-FCS measurements. This is a strong indication that this particle species does not fluoresce.

The species dominating in the DLS measurements therefore can be explained by clusters of free PEO.

The PEO is only adsorbed on the surface of the QDs. Diluting the QDs lead to desorption of PEO. The no longer attached PEO forms clusters to prevent the hydrophobic anchor group from water. The QDs on the other hand are no longer sufficiently covered by PEO and aggregate. Dialysis and centrifugation are no options to get rid of the aggregates. One solution would be to dilute the sample using a PEO solution or chemically bind the PEO to the surface of the QDs to avoid desorption.

The Qtracer 705 from Invitrogen is covered by PEG and has its emission maximum at 705 nm. We used the specifications given by Invitrogen.

As for the QDs from Hamburg, we performed angle-dependent measurements with a scattering angle ranging from 30° to 150° (Figure 7.6).

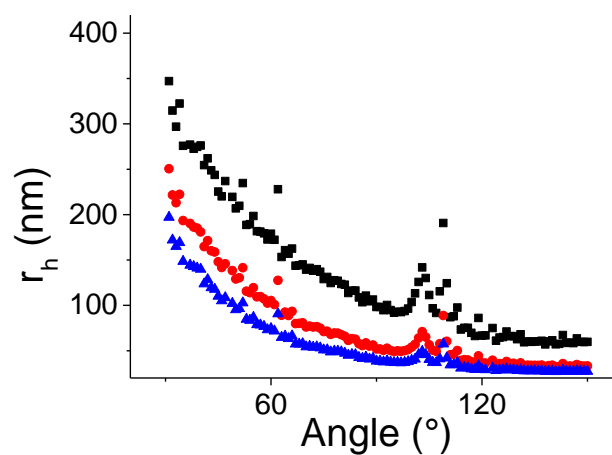


Figure 7.6 Angle-dependent DLS measurement. Shown are the resulting hydrodynamic radii for each measured angle. Black: hydrodynamic radii from the first order cumulant fit; red: second order cumulant fit; Blue: third order cumulant fit.

Comparing the results of the cumulant fits for the hydrodynamic radii (Figure 7.6) shows that the Qtracer 705 sample is polydisperse. Furthermore, the minimum hydrodynamic

radius is about 55 nm. This is about six times higher than the pure QDs are. The Qtracers therefore have a very thick shell of about 18 nm. The thickness of the shell may lead to the polydispersity. This makes the Qtracer 705 difficult to handle in 2f-FCS measurements. The polydispersity of the QDs result in different results compared to the DLS measurements.

In Figure 7.7 a measurement results of the Qtracer 705 are shown. The resulting diffusion coefficient and hydrodynamic radii for the smaller particles is strange. The diffusion coefficient indicates that the particles are smaller than the QDs from Hamburg, which cannot be. The emission wave-length of the Qtracers is higher than the emission wavelength of the QDs from Hamburg. This can only be if the Qtracer is larger than the QDs from Hamburg. This is in contradiction to the 2f-FCS results. The diffusion coefficient of the bigger particle species ($D = 1.78 \mu\text{m}^2\text{s}^{-1}$) is in the same order as the diffusion coefficient of the QDs from Hamburg ($D = 1.33 \mu\text{m}^2\text{s}^{-1}$). The polydispersity in the Qtracer 705 sample is too high to measure the QDs in the 2f-FCS.

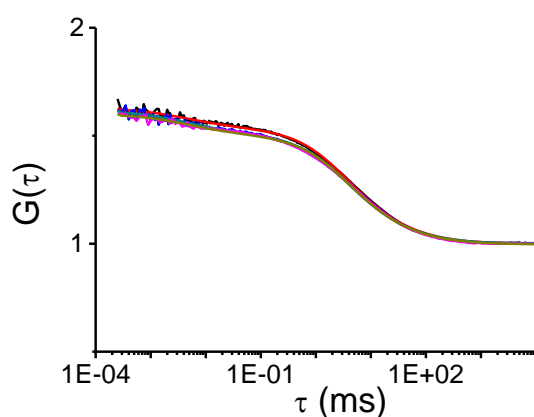


Figure 7.7 2f-FCS measurement of the Qtracer 705. The measurement shows the auto correlation functions of the two foci (black and blue) and the cross correlation of the two foci (red). All correlation functions had to be fitted with a two particle model. The resulting Diffusion coefficients and radii are for the bigger particles: $D = 1.78 \mu\text{m}^2\text{s}^{-1}$, $R = 137.5 \text{ nm}$ and for the smaller particles: $D = 116.6 \mu\text{m}^2\text{s}^{-1}$ and $R = 2.1 \text{ nm}$.

Comparing the commercially available Qtracer 705 and the QDs, made by Dr. Marc Thiry from Hamburg, shows us that the Qtracers are very polydispers. It was not possible to measure the correct hydrodynamic radius in the 2f-FCS whereas this is possible for the QDs from Hamburg. Both samples suffer from the polydispersity and aggregation. This makes the QDs still interesting as a tracer for 2f-FCS but improvements have to be made for both samples to get better results in the 2f-FCS measurements. For the Qtracer 705 from Invitrogen, the different species of particle sizes has to be separated. This would lead to high cost for a sufficient number of QDs and this makes it unlikely to use the Qtracer. On the other hand, other commercially available QDs should be tested.

The QDs from Hamburg are custom made and therefore they are very nice in mono-dispersity. On the other hand the PEO shell is not chemically bond to the QDs this has to be solved to have accurate tracer particles with a very high signal to noise ratio and therefore can be used in samples with a high background.

7.1.1 References

1. Gomez, D.E., M. Califano, and P. Mulvaney, *Optical properties of single semiconductor nanocrystals*. Physical Chemistry Chemical Physics, 2006. **8**(43): p. 4989-5011.
2. Heuff, R.F., J.L. Swift, and D.T. Cramb, *Fluorescence correlation spectroscopy using quantum dots: advances, challenges and opportunities*. Phys. Chem. Chem. Phys., 2007. **9**(16): p. 1870-1880.
3. Dong, C., et al., *Controllable Blinking-to-Nonblinking Behavior of Aqueous CdTeS Alloyed Quantum Dots*. Chem. - Eur. J., 2014. **20**(7): p. 1940-1946.

7.2. Dimerization of STAT3 protein and measurement in living cells⁴

In cooperation with Prof. Dr. Müller-Neven and Tamas Domszalai we investigated the protein- protein interactions of STAT3 (Signal Transducers and Activators of Transcription 3) proteins. A schematic draw of the STAT proteins is shown in Figure 7.8.

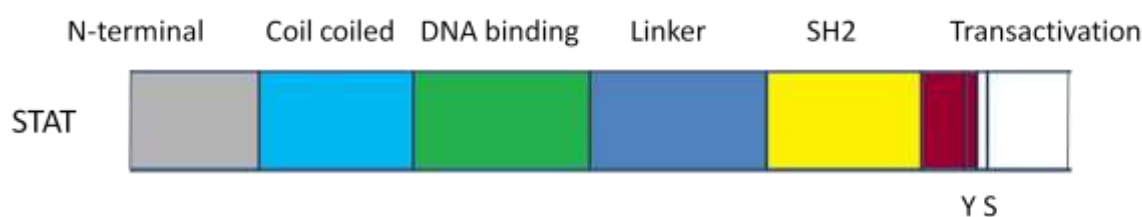


Figure 7.8 Schematic draw of the STAT protein. The N-terminal (grey) is assumed to be the functional group for dimerization of the protein.

For our research the important group is the N-terminal (Figure 7.8, grey). To this group the dimerization of the STAT proteins is dedicated. We used the natural STAT3 protein and an artificial Δ N-STAT3 protein mutant. The Δ N-STAT3 protein is identical with the natural STAT3 protein except the N-terminal which is missing in the Δ N-STAT3 mutant. Comparing both should give us information about the role of the N-terminal in dimerization of the protein.

The STAT3 proteins are labeled by eGFP (enhanced green fluorescent protein). To test if the eGFP signal leads to a sufficient signal to noise ratio on our 2fFCS we measured the diffusion coefficient of the protein in aqueous solution (Figure 7.9).

⁴ This chapter was published in Journal of Cell Science, 2011. 124(6): p. 900-909. The study was performed in collaboration with the co-authors. My contribution was the performance of the 2fFCS measurements and I supported the data analysis.

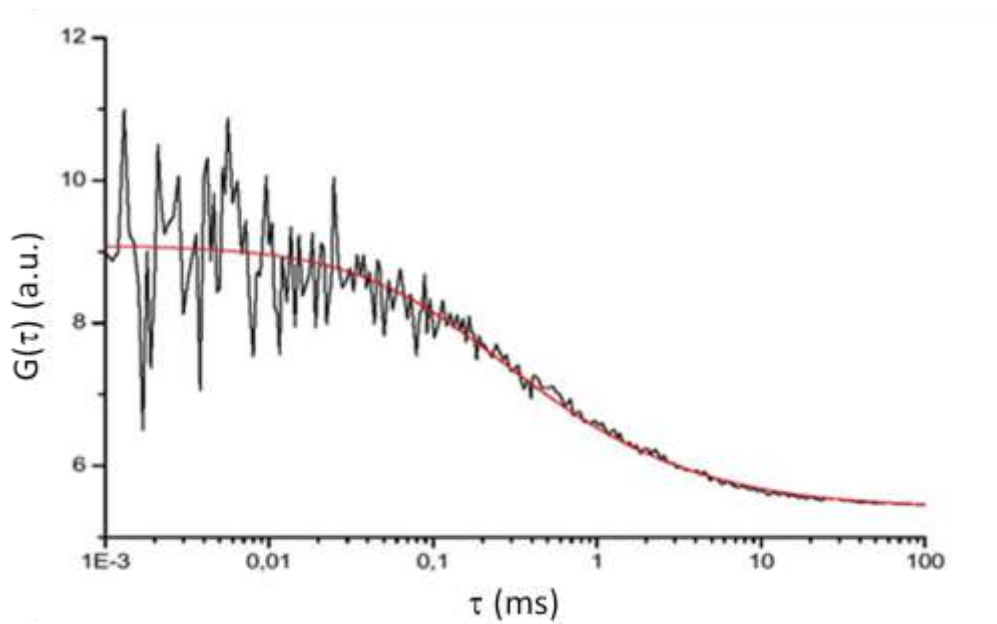


Figure 7.9 2fFCS measurement of the eGFP. Only the cross correlation function (black) and the corresponding fit (red) is shown. The measurement temperature was 25°C, the duration was 2h. As fit model we used a single particle model including triplet state.

Figure 7.9 shows non-normalized measurement results. The rather low background in figure 7.9 demonstrates the low signal background during the measurement. This indicates that eGFP is a sufficient label for the investigation of the STAT3 dimerization.

We measured the diffusion coefficient three times. The results of the measurements are shown in table 7.2.

Table 7.2 Summary of the measurements of eGFP in aqueous solution. D denotes the diffusion coefficient; Average is the average of the diffusion coefficients; SD denotes the standard deviation of the diffusion coefficient and R_h denotes the hydrodynamic radius calculated from the average diffusion coefficient calculated from the Stokes-Einstein equation (Eq. 2.13).

Measurement	D / x 10 ⁻⁶ cm ² s ⁻¹		
1	1.02	Average	1.03
2	1.08	SD	0.04
3	0.98	R_h / nm	2.4

The standard deviation of 0.04 is equal to the systematic error of the 2fFCS instrument. The resulting hydrodynamic radius of $R_h = 2.4$ nm is in good agreement with literature [1, 2].

The next step was to measure the Δ N-STAT3 mutant. We measured the protein in the cell lysate from the cells which produced the protein previously. The information about the diffusion coefficient of the mutant gives us an upper boundary for the diffusion coefficient of the natural STAT3 protein.

Table 7.3 Summary of the measurements of the Δ N-STAT3 mutant in aqueous solution. D denotes the diffusion coefficient; Average is the average of the diffusion coefficients; SD denotes the standard deviation of the diffusion coefficient and R_h denotes the hydrodynamic radius calculated from the average diffusion coefficient calculated from the Stokes-Einstein equation (Eq. 2.13).

Measurement Series	D / $\times 10^{-6} \text{ cm}^2 \text{ s}^{-1}$		
1	0.67		
1	0.71		
1	0.65		
1	0.75		
1	0.72		
2	0.64		
2	0.69		
2	0.75	Average	0.7
2	0.7	SD	0.04
3	0.7	R_h / nm	3.5

Table 7.3 shows the result of several measurement series. One series was measured in one sample in a time series. Each measurement had a duration of 2h and a measurement temperature of 25°C.

Measuring the natural STAT3 protein, under the same conditions as the Δ N-STAT3 mutant in cell lysate, lead to interesting results, which are summarized in table 7.4.

We fitted all results using a single particle model including triplet state. The results can be divided in to two groups of diffusion coefficients, the results with a slower diffusion coefficient (Table 7.4, left) can be dedicated to the dimmers of the protein, whereas the faster diffusion coefficients (Table 7.4, right) are almost equal to the diffusion coefficients of the Δ N-STAT3 mutant. This clearly indicates that this species is the monomer of the STAT3 protein. The resulting hydrodynamic radii of both species support the conclusion that the slower species is the species of the dimmers. The hydrodynamic radius of this species is almost twice of the radius of the monomer species.

Table 7.4 Summary of the measurements of the STAT3 protein in aqueous solution. D denotes the diffusion coefficient; Average is the average of the diffusion coefficients; SD denotes the standard deviation of the diffusion coefficient and R_h denotes the hydrodynamic radius calculated from the average diffusion coefficient calculated from the Stokes-Einstein equation (Eq. 2.13). left: results corresponding to the dimmers; right: results corresponding to the monomers.

dimers		monomers	
Measurement series	D / $\times 10^{-6} \text{ cm}^2 \text{ s}^{-1}$	Measurement series	D / $\times 10^{-6} \text{ cm}^2 \text{ s}^{-1}$
1	0.45	1	0.73
1	0.57	1	0.68
1	0.54	2	0.64
2	0.48		
3	0.42		
3	0.52		
4	0.54		
5	0.42		
Average	0.49	Average	0.68
SD	0.05	SD	0.03
R_h / nm	5	R_h / nm	3.6

A complete description of the role of the N-terminal of the STAT3 protein in dimerization can be found elsewhere [3].

In a second approach we tried to measure the diffusion coefficient of the STAT3-eGFP protein inside a living cell. A picture of the living cell before and after the test measurement is shown in figure 7.10.

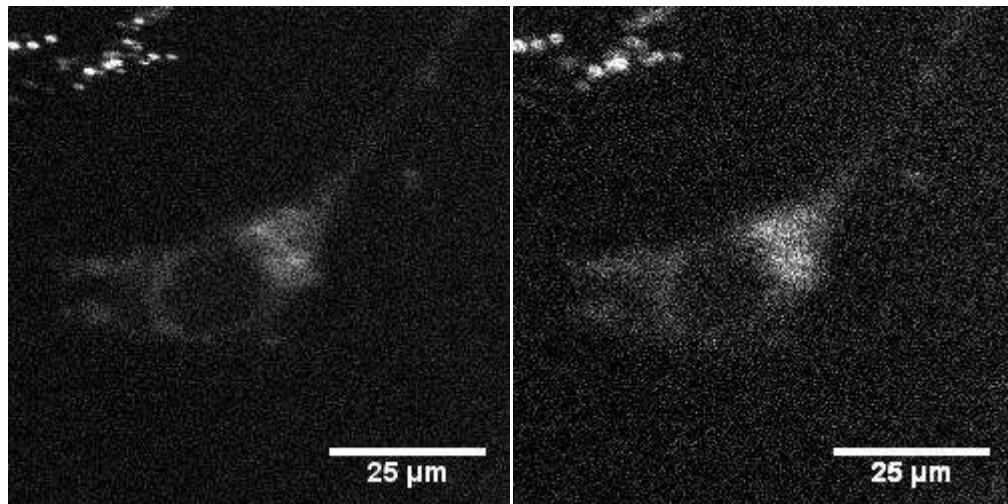


Figure 7.10 Confocal fluorescence microscopy images of a living cell. The labeling was done by STAT3-eGFP which was produced by the cell previously. left: the cell before the diffusion measurement; right: the same cell after the diffusion measurement (2h). In the top left corner of both images are dead cells visible.

The cell survived inside the sample cell the duration of the measurement and therefore is sufficient for the 2fFCS to measure inside the cell. Nevertheless the protein concentration in the cell was too high for the diffusion measurement. No useful results could be obtained. This makes further investigations and the control of the protein concentration inside the cell necessary or the detection volume had to be decreased, by lowering the pinhole radius, until a sufficient concentration inside the detection volume is reached.

7.2.1. References

1. Liarzi, O. and B.L. Epel, *Development of a quantitative tool for measuring changes in the coefficient of conductivity of plasmodesmata induced by developmental, biotic, and abiotic signals*. Protoplasma, 2005. **225**(1-2): p. 67-76.
2. Terry, B.R. and A.W. Robards, *Hydrodynamic radius alone governs the mobility of molecules through plasmodesmata*. Planta, 1987. **171**(2): p. 145-157.
3. Vogt, M., et al., *The role of the N-terminal domain in dimerization and nucleocytoplasmic shuttling of latent STAT3*. Journal of Cell Science, 2011. **124**(6): p. 900-909.

7.3. DNA-functionalized gold nano particles (Au-NP)

In cooperation with Katrina Witten from the Institute of inorganic chemistry we investigated ssDNA functionalized Au-NP diffusion in buffer solution. The ssDNA molecules are built out of two parts. One part is labeled using the fluorescence dye Cy5 and is called DNA-Cy5. The other one carries the linker group (DNA-linker) and is able to form double helixes with the DNA-Cy5. As linker groups of the ssDNA molecules we used thymine instead of adenine. Thymine adsorbs less to the Au-NP than adenine. This leads to a larger distance between Au-NP and the Cy5 dye and to a higher stabilization of the Au-NP in water based buffer solutions, due to higher surface coverage[1]. The linker group had a repetition number of 10 repeating units per DNA molecule. The DNA-linker has got the following structure:

TTT TTT TTT T **CCC AAA GGA GTT TCC AAA ACG GGG**-5`

and the DNA-Cy5 has got this structure:

5'-**GGG TTT CCT CAA AGG TTT TGC CCC**-3`-Cy5

The overall length of the ssDNA is calculated from the number of base pairs of 24 times the length of one base of 0.34 nm. This leads to a total length of 8.2 nm.

As buffer solution we used phosphate buffered saline (PBS) and PBS/sodium dodecyl sulfate (SDS) solutions.

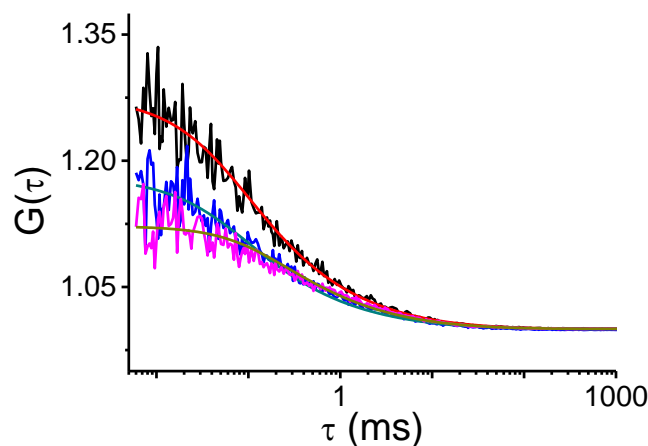


Figure 7.11 2fFCS measurement result of DNA-Cy5 in PBS buffer solution. Shown are the two auto correlation functions (black and blue), the cross correlation function (magenta) and the corresponding fits (red). The resulting diffusion coefficient is $D = 335 \mu\text{m}^2\text{s}^{-1}$.

In Figure 7.11 is shown the measurement of the diffusion coefficient of DNA-Cy5. The high diffusion coefficient of $D = 335 \mu\text{m}^2\text{s}^{-1}$ shows that the DNA-Cy5 diffuses free through the PBS buffer solution.

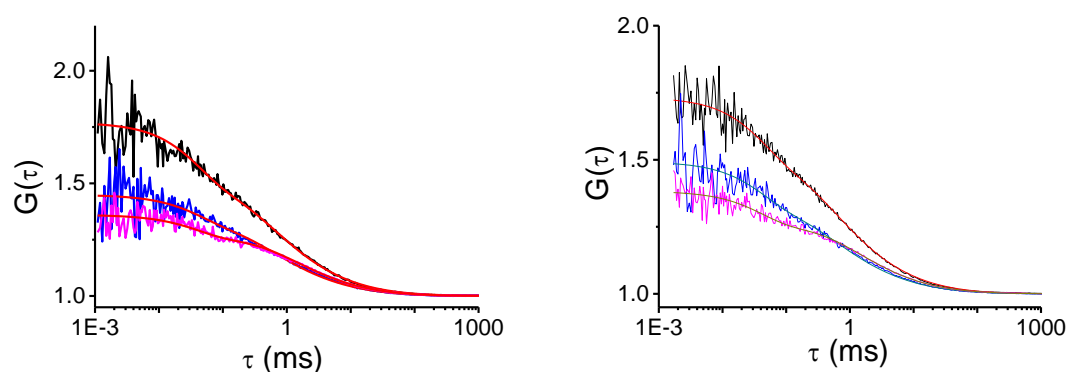


Figure 7.12 2fFCS measurement results of ssDNA labeled with Cy5 in PBS-SDS buffer solution. Two independent measurements are shown (left and right). The two auto correlation functions (black and blue), the cross correlation function (magenta) and the corresponding fits (red) are shown for each measurement. The resulting diffusion coefficients are $D = 73,8 \mu\text{m}^2\text{s}^{-1}$ (left) and $D = 73,6 \mu\text{m}^2\text{s}^{-1}$ (right).

Adding SDS to the PBS buffer decreases the diffusion coefficient of the DNA-Cy5 to $73.7 \mu\text{m}^2\text{s}^{-1}$ (Figure 7.12). This is a factor of 4.5. Origin of the strong decrease of the diffusion coefficient is the adsorption of SDS on the DNA-Cy5 molecule.

The two independent measurements of two equal samples demonstrate the high reproducibility of the measurements.

In the next step we measured two different sizes of Au-NPs. The smaller one (Au-NP-s) has got a hydrodynamic radius of $R_h = 17 \text{ nm}$ and the larger one (Au-NP-l) has got a hydrodynamic radius of $R_h = 29 \text{ nm}$. Both Au-NPs were stabilized and labeled using the same DNA-Cy5 solution.

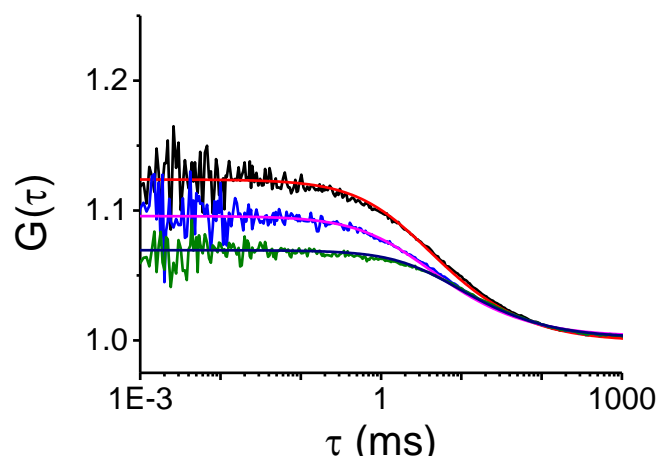


Figure 7.13 2fFCS measurement of Au-NP-s. Shown are the two auto correlation functions (black and blue), the cross correlation function (magenta) and the corresponding fits (red). The resulting diffusion coefficient is $D = 9.91 \mu\text{m}^2\text{s}^{-1}$. This leads to a hydrodynamic radius of $R_h = 24.7 \text{ nm}$.

Figure 7.13 shows the results of the measurement of the Au-NP-s sample. The resulting hydrodynamic radius of the Au-NP-s/ssDNA-Cy5 complex (24 nm) is in very good agreement with the sum of the known radius of the Au-NP (17 nm) and the size of the ssDNA (8.2 nm).

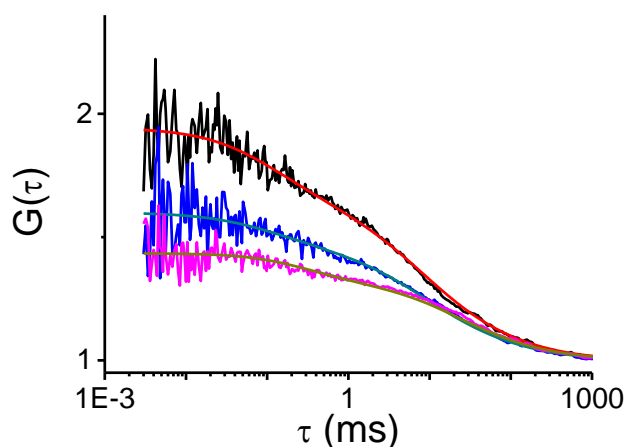


Figure 7.14 2fFCS measurement of Au-NP-I. Shown are the two auto correlation functions (black and blue), the cross correlation function (magenta) and the corresponding fits (red). The resulting diffusion coefficient is $D = 4.02 \mu\text{m}^2\text{s}^{-1}$. This leads to a hydrodynamic radius of $R_h = 60.8 \text{ nm}$.

The measurement of the Au-NP-I is shown in Figure 7.14. The resulting hydrodynamic radius (60.8 nm) is much larger than the expected radius (29 nm + 8.2 nm = 37.2 nm). We think that this is due to aggregation of Au-NP-I's. The surface coverage of the Au-NP-I's is not sufficient to avoid aggregation of low numbers of Au-NPs. Therefore the synthesis of the Au-NP-I's has to be improved.

7.3.1. References

1. Storhoff, J.J., et al., *Sequence-Dependent Stability of DNA-Modified Gold Nanoparticles*. *Langmuir*, 2002. **18**(17): p. 6666-6670.

7.4. Hydrogels made of star polymers

In cooperation with Konstantina Dyankova and Jürgen Groll we started to investigate hydrogels, formed quit of star polymers. This hydrogels should have a heterogeneous size distribution in mesh size. The approach was to synthesize gel films with a thickness of 12 less than 100 μm to measure the diffusion of different tracer molecules in water, above the gel film, near the interface of water and gel film (top of the gel film), in different heights inside the gel film and near the interface between gel film and cover slide glass (bottom of the gel film). The resulting diffusion coefficients should give us information about the influence of the hydrogel on the diffusion and therefore answer the question, if there is a spatial order in the mesh size inside the gel film, and dose the density of the star polymers inside the gel film show any spatial structure.

In a first approach, we synthesized the gel film in the sample cell, mount the sample cell on the 2fFCS and then added a solution containing the two fluorescence dyes AlexaFluor488 and AlexaFluor587 (both from Invitrogen, Germany) on top of the gel film. Then we measured a fluorescence microscopy image in z direction after equilibration for one hour, Figure 7.15.

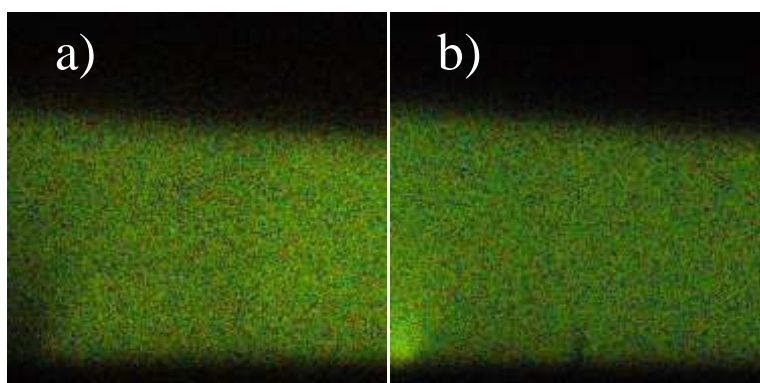


Figure 7.15 Fluorescence microscopy images of the hydrogel with added dye solution. a) Image of the AlexaFluor 488; b) image of the AlexaFluor 587.

The images show that we were able to control the thickness of the gel film. The next step was to calculate the intensity profile of both images (Figure 7.16) and compare them.

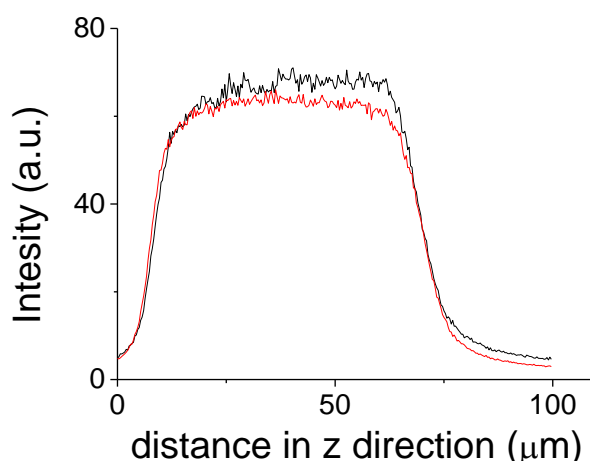


Figure 7.16 Intensity profile of the hydrogel filled with a solution of AlexaFluor488 and AlexaFluor587 dye. Red line indicates the intensity of the AlexaFluor 587 dye and black the intensity if the AlexaFluor 488 dye.

The two intensity distributions correlate well and demonstrate that we covered the complete gel film in the measurement.

Then, we repeated the experiment, without equilibration time and using bovine serum albumin (BSA) labeled with Atto655 (Atto-TEC GmbH, Germany) (Figure 7.17).

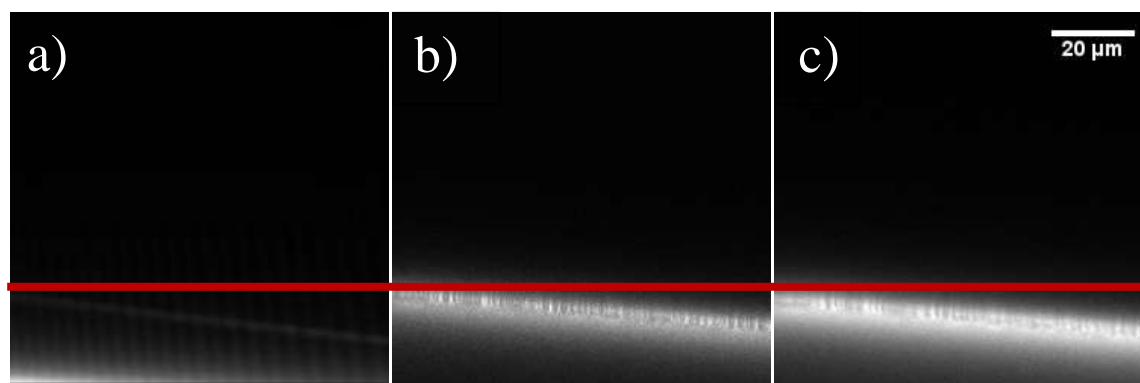


Figure 7.17 Fluorescence microscopy images of the pure gel (a), gel with added BSA direct after adding the BSA solution (b) and 2 min after adding the BSA solution. The red line indicate the highest point of the gel film.

The BSA diffuses into the hydrogel (Figure 7.17 b) and c)). The diffusion is hindered. Therefore the lower part of the hydrogel is not illuminated by labeled BSA. This indicates two things. First of all, the gel film again is prepared with a thickness of less than 100 μm . This is proven by the fact, that we are covering the range above the gel with no BSA. This is only possible if we are above the droplet with BSA, we added. The second is, that the diffusion of the BSA is hindered by the gel. Otherwise the gel film should be illuminated by the labeled BSA down to the bottom of the gel film, which is not the case. The intensity profiles of the images in figure 7.17 b) and c) are shown in Figure 7.18.

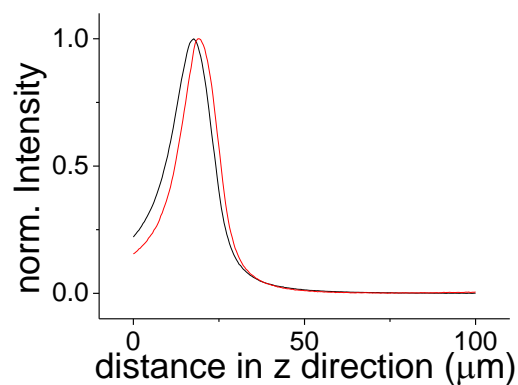


Figure 7.18 Intensity profile of the hydrogel with added solution of BSA. Red line indicates the intensity direct after adding the BSA solution and black the intensity 2 min after adding the BSA solution. The peak is slightly shifted to lower z value.

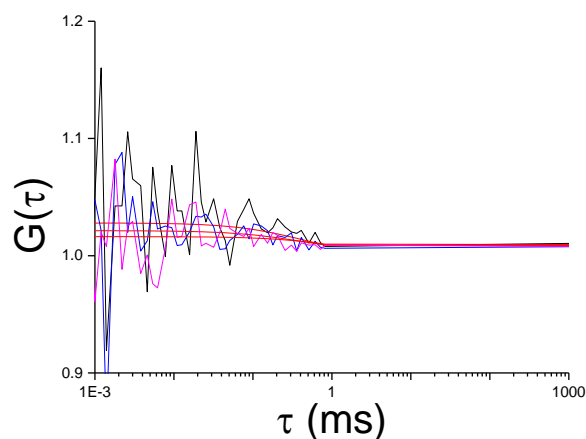


Figure 7.19 2f-FCS measurement of BSA in the hydrogel. The measurement shows the auto correlation functions of the two foci (black and blue) and the cross correlation of the two foci (red). The correlation in this measurement is very low. No reliable results can be taken from the measurement. Nevertheless the measurements show a correlation. The measurements work but have to be improved.

In the first diffusion measurements, we were able to measure a correlation function (Figure 7.19). Nevertheless the correlation is very low. Therefore the measurement has to be improved. The BSA was labeled by Konstantina herself. The BSA molecules are probably not sufficiently labeled and/or the labeled BSA has to be cleaned more efficiently to minimize the background in the measurement.

The measurements are promising to be accurate and may give the answers to the open questions. Therefore the measurements have to be repeated and improved.

7.5. Temperature-sensitive polymers from Renate Messing

We measured homemade model polymers of different polymerization degree from Renate Messing. The polymers were named R94.R-rein-a to e. The polymer was labeled with Rhodamine B and shows a lower critical solution temperature (LCST) of 28°C to 30°C. For the first test measurements, we choose a measurement temperature of 25°C, below the LCST.

First DLS measurements from Renate Messing gave us hydrodynamic radii which we can use to interpret our 2fFCS measurements (Table 7.5).

Table 7.5 Summary of the DLS measurement results for three different samples. r_i indicates the intensity weighted radii; r_v the volume weighted radii and r_n the number weighted radii; PDI is the polydispersity index.

Name	r_i / nm	r_v / nm	r_n / nm	PDI
R94.R-rein-a	3	1.4	1.9	0.29
R94.R-rein-b	2.8	1.6	2	0.228
R94.R-rein-c	3.1	1.7	2.2	0.284

The polymer was diluted in LiChroSolv water and measured in the temperature controlled sample cell for 2 hours. Each sample was measured in a series of 10 repetitions of measurement. The measurements of one sample series were compared.

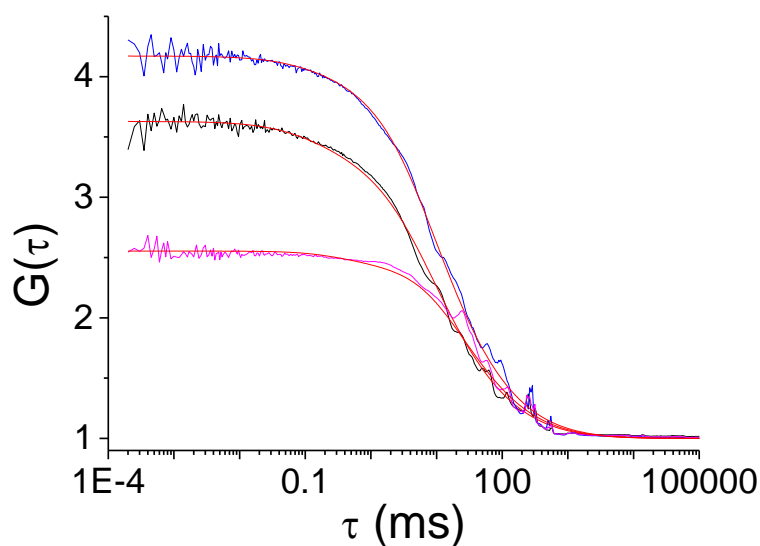


Figure 7.20 2fFCS measurement of the sample R94.R-rein-a. Black: auto correlation function of focus one; blue: auto correlation function of focus two; magenta: cross correlation function of the two foci; red: the corresponding fits. As fitting model we used a two particle model.

Figure 7.20 shows one of the measurement results of sample R94-a. The fitted diffusion coefficient of sample R94.R-rein-a is $D = 164.9 \mu\text{m}^2\text{s}^{-1}$. Calculating the hydrodynamic radius via Stokes-Einstein equation (Eq. 2.13) leads to $r_h = 1.5 \text{ nm}$. This radius is in good agreement with the volume weighted result of the DLS measurements. We had to fit the results of the sample using a two particle model. The diffusion coefficient of the second species is about one decade lower than the expected diffusion coefficient and can be explained by aggregates.

Sample R94.R-rein-b shows a similar behaviour as sample R94.R-rein-a (Figure 7.21). This again makes the fitting with a two particle model necessary. The fitted diffusion coefficient of the faster component was $D = 106.2 \mu\text{m}^2\text{s}^{-1}$. The slower species again can be explained by aggregates in the sample.

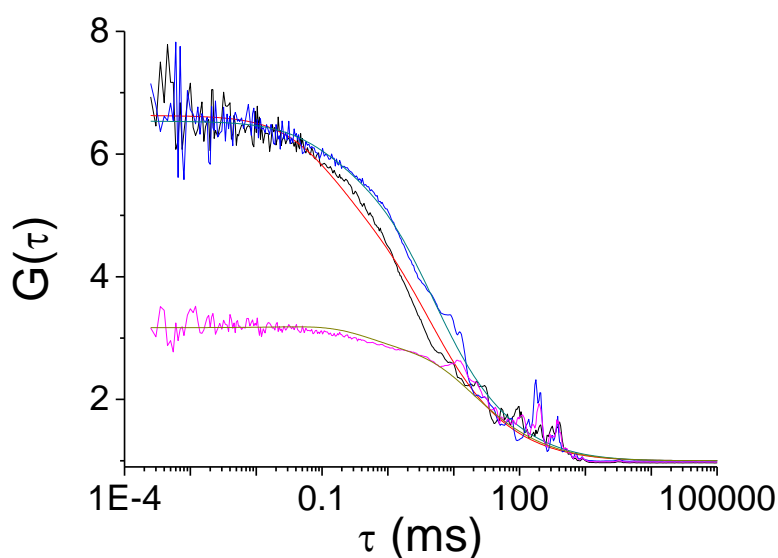


Figure 7.21 2fFCS measurement of the sample R94.R-rein-b. black: auto correlation function of focus one; blue: auto correlation function of focus two; magenta: cross correlation function of the two foci; red: the corresponding fits. As fitting model we used a two particle model.

The resulting hydrodynamic radius for the faster species was calculated to be $r_h = 2.3 \text{ nm}$. A decrease in the diffusion coefficient was expected. The increasing polymerization

degree leads to an increase in chain length and therefore an increase in the hydrodynamic radius. The radius is higher than from the DLS measurement predicted. This is maybe due to small aggregates in the sample, which disturb the results of the single polymers.

Sample R94.R-rein-c and R94.R-rein-e could not be evaluated. The samples had a too high polydispersity to be fitted sufficiently with our fitting models. Therefore we do not show results here.

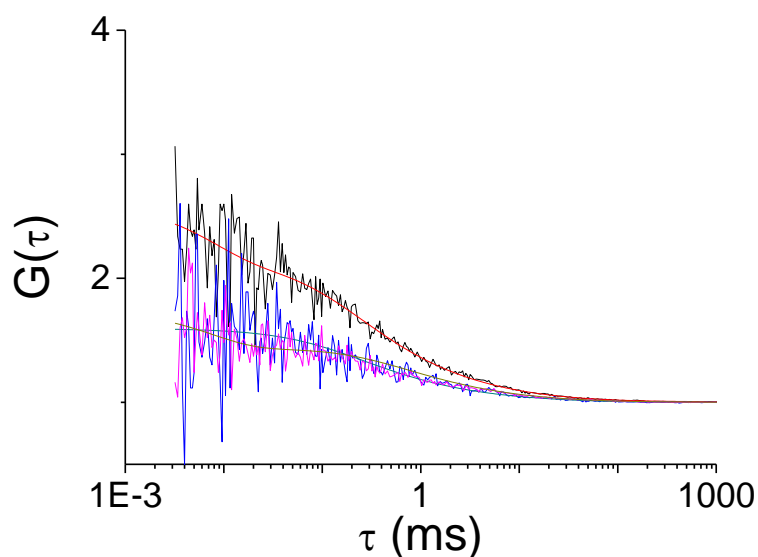


Figure 7.22 2fFCS measurement of the sample R94.R-rein-d. Black: auto correlation function of focus one; blue: auto correlation function of focus two; magenta: cross correlation function of the two foci; red: the corresponding fits. As fitting model we used a two particle model.

Sample R94.R-rein-d again shows evaluable results (Figure 7.22). The diffusion coefficient for the fast species was fitted to be $D = 103.5 \mu\text{m}^2\text{s}^{-1}$. The calculated radius was $r_h = 2.4 \text{ nm}$. The increase of the radius is smaller than expected, compared to the results from sample R94.R-rein-b. Nevertheless, taking into account that the results for sample R94.R-rein-b was too high, the resulting hydrodynamic radius of sample R94.R-rein-d is plausible.

The next step would be the investigation of the LCST behavior. The very small radii of the investigated polymers can be a problem for this investigation. The collapse of the polymer above the LCST is maybe too small to be detected by the 2fFCS. A much bigger polymer would be more sufficient for this investigation.

7.6. Galectin-1 – LacNAc Interaction

In cooperation with Christiane Römer and Claudia Rech, we wanted to measure the binding of N-acetyllactosamine (LacNAc) to Galectin-1. Therefore, we measured the diffusion coefficients of Galectin-1 labeled with Dylight649 and the LacNAc sugar labeled with Atto 488 in buffer solution at 25°C. The results are shown in figure 7.23.

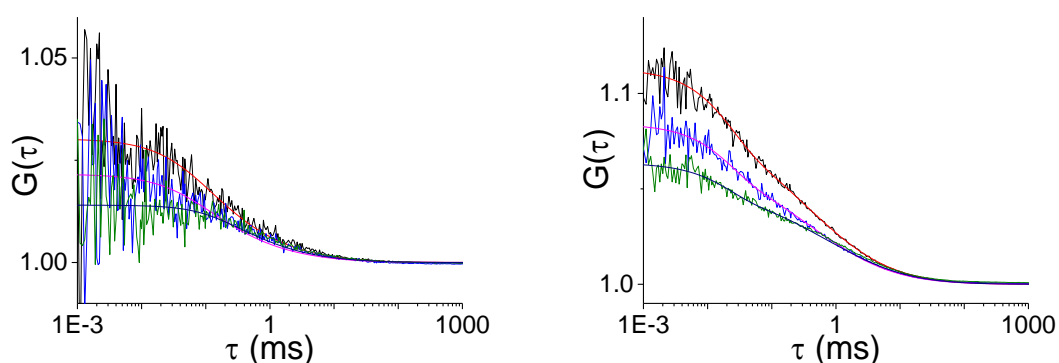


Figure 7.23 2fFCS measurements of LacNAc labeled with Atto 488 (left) and Galectin-1(right). The measurement results of Galectin-1 had to be fitted with a two species model. The slower species in this fit is addressed to aggregates inside the sample. The resulting diffusion coefficients are, for LacNAc: $D = 189.83 \mu\text{m}^2\text{s}^{-1}$; and for Galectin-1: $D = 118.46 \mu\text{m}^2\text{s}^{-1}$.

Calculating the hydrodynamic radius of galectin-1 from the diffusion coefficient using the Stokes-Einstein equation (Eq.2.13) leads to $R_h = 2.07 \text{ nm}$ which is in good agreement with literature[1].

To measure the binding of LacNAc to the Galectin-1, we performed a two colour-2fFCS measurement. Such an experiment is realized by measuring both components, LacNAc and Galectin-1 simultaneously using their specific excitation wavelengths and calculate the cross correlation for the two laser light colours. The resulting diffusion coefficients for the LacNAc should retain the diffusion of free LacNAc and additionally show the diffusion of the complex. The same should be for the Galectin-1 diffusion coefficients. In the colour cross correlation only the diffusion coefficient of the complex should be visible. The results of the experiment is shown in figure 7.24.

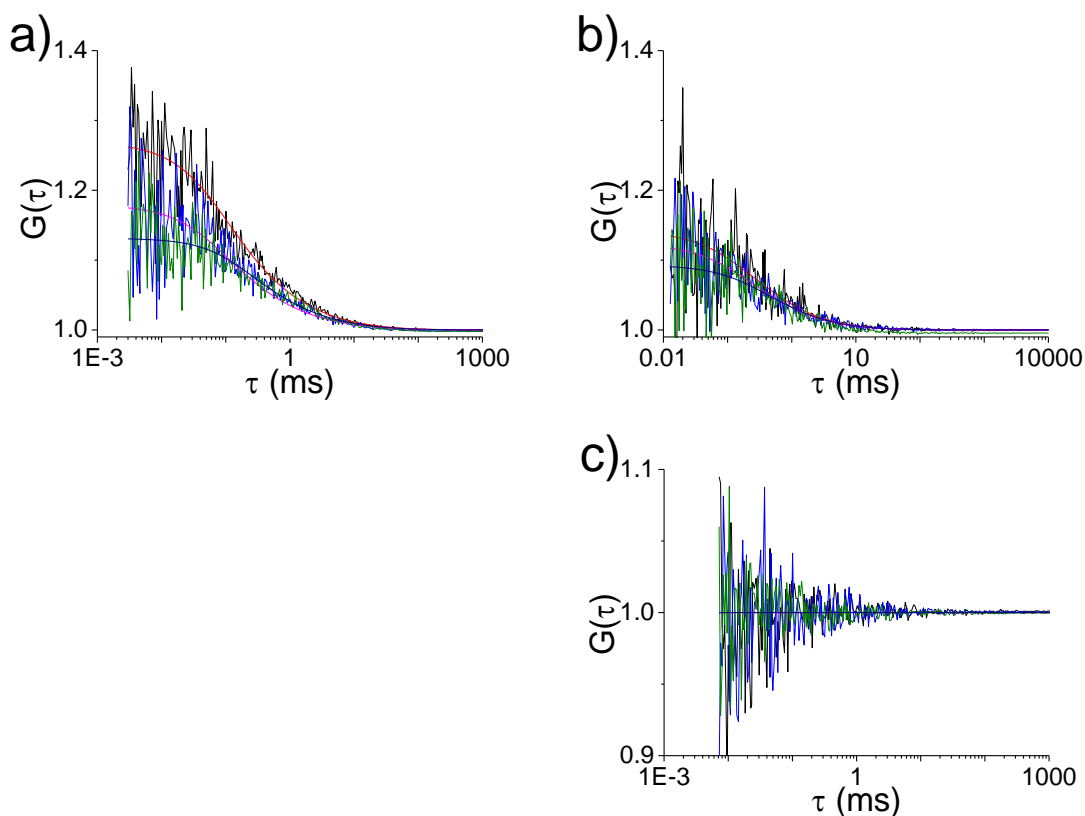


Figure 7.24 Two color-2fFCS measurement of LacNAc-Atto488 (a), Galectin-1-Dylight649(b). c) show the color cross correlation in this experiment.

The result of the LacNAc measurement channel (figure 7.24 a) is $D = 189 \mu\text{m}^2\text{s}^{-1}$, retains the diffusion coefficient of the measurement of figure 7.23 left. No other diffusion is

visible in this result. The measurement result for the Galectin-1 only shows a much slower diffusion ($D = 44.08 \mu\text{m}^2\text{s}^{-1}$) as the measurement of figure 7.23 right. The diffusion is of a factor of 2.7 slower than for free Galectin-1. Is this an indication for binding of LacNAc to the Galectin-1? A factor of 2.7 indicates that the complex has to consist out of more than one Galectin-1 and one LacNAc molecule. But if this is a complex of Galectin-1 and LacNAc and not only Galectin-1 aggregates why does one not see the complex in the LacNAc measurement? If there are complexes which show fluorescence for both labels, this complexes should be measured in the cross colour correlation, Figure 7.24 c).

The cross colour correlation shows no correlation at all. This proves that no complexes, which show fluorescence for both excitation wavelengths are measured.

Only one possibility for complexes is left, the fluorescence of the LacNAc label is quenched during the complexation. We started to proof this with a blind test by measuring the diffusion coefficient of the LacNAc labeled with Atto 488 with added unlabeled Galectin-1. The resulting diffusion coefficients are almost the same as in figure 7.23 left, and figure 7.24 a).

7.6.1. References

1. He, L., et al., *Detection of Ligand- and Solvent-Induced Shape Alterations of Cell-Growth-Regulatory Human Lectin Galectin-1 in Solution by Small Angle Neutron and X-Ray Scattering*. Biophysical Journal, 2003. **85**(1): p. 511-524.

7.7. Lysozyme labelled with Fluorescein and Rhodamin

In cooperation with Ilja Voets and Saskia Bucciarelli we measured home-labelled lysozyme proteins. Therefore we prepared stock solutions for both lysosymes in buffer. The concentration of the stock solutions is about 1×10^{-4} mol/L for the rhodamine-labelled and about 2×10^{-4} mol/L for the fluorescein-labelled lysozyme. The solutions where stored for 12h in the fridge. Before measuring we diluted the solutions to a concentration of about 2×10^{-9} mol/L, to be able to measure them in the 2fFCS.

The diluted solutions were filled in our temperature controlled sample cells and equilibrated at 25°C for approximately 30 min.

Afterwards we measured the samples for 1 h using proper laser colours and fluorescence filters.

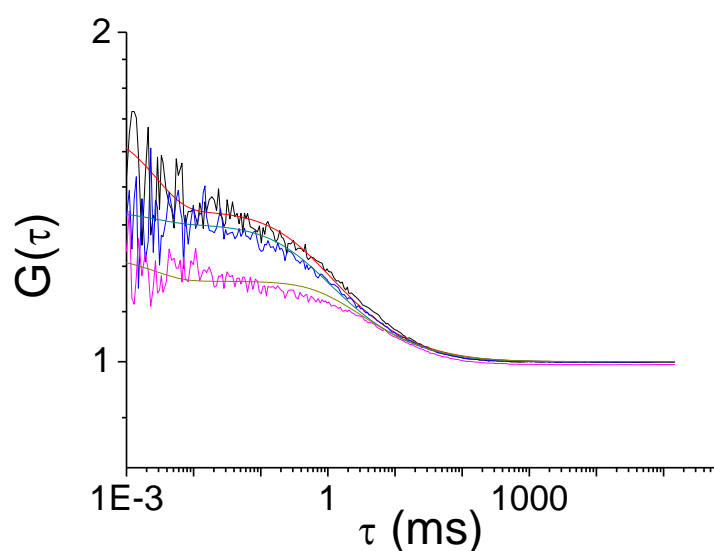


Figure 7.25 2f-FCS measurement of lysozyme labeled with fluorescein. The measurement shows the auto correlation functions of the two foci (black and blue) and the cross correlation of the two foci (magenta). All correlation functions had to be fitted with a single particle model including triplet state. The resulting Diffusion coefficient and radius is $D = 23.96 \mu\text{m}^2\text{s}^{-1}$, $R = 10.2 \text{ nm}$.

The results for the lysozyme labelled with fluorescein are shown in the figure 7.25. The measurement data were fitted with a single molecule model including triplet state. As one can see, the fit for the cross correlation of the two foci does not match properly. And the diffusion coefficient is about 10 times to high.

A fit, with a two component model, lead to senseless diffusion coefficients. We think this is maybe due to the fact of aggregation. We have to think about how to prevent this by achieving better dilution of the lysosyms.

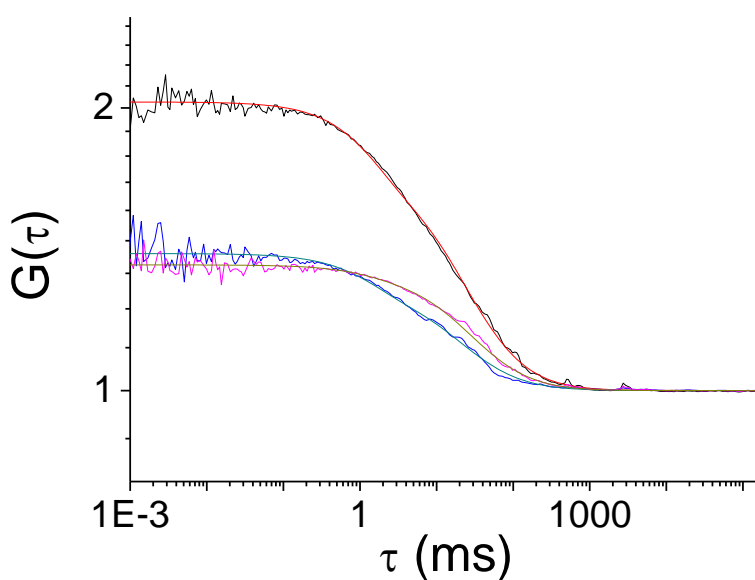


Figure 7.26 2f-FCS measurement of lysozyme labeled with fluorescein. The measurement shows the auto correlation functions of the two foci (black and blue) and the cross correlation of the two foci (magenta). All correlation functions had to be fitted with a single particle model including triplet state. The resulting Diffusion coefficient and radius is $D = 372.2 \mu\text{m}^2\text{s}^{-1}$, $R = 0.66 \text{ nm}$.

The results for the lysozyme labelled with Rhodamine are shown in the figure 7.26. The data were fitted as well by the one component model including triplet state.

Here, the fit for the cross correlation of the two foci matches much better with the data and the diffusion coefficient is too small only in a factor of 2. The sample seems to work much better than the other one. But here we see shoulders in the decay, which maybe cause the error in the diffusion coefficient and are as well due to aggregation.

We have to solve the problem with the aggregation, but then we are able to measure the lysosyms in our 2fFCS.

Is it possible to use ultra sound bath to desolve of the aggregates or do we have to prepare a stock solution with lower concentration, or do we have to use other techniques? These are the main questions which have to be solved.

7.8. Curriculum Vitae

Name:	Swen Lehmann
Address:	Baustraße 28A, 40723 Hilden (Germany) Tel. 02103 / 941352 Email: lehmann@pc.rwth-aachen.de
Family status:	married, two sons
<u>PhD Dissertation</u> 04/2008 – now	PhD-student at the Institute of Physical Chemistry at the RWTH Aachen, Germany, supervised by Prof. Dr. W. Richtering with the topic: „ Smart crowding in poly-Acrylamide/Poly(N-isopropylacrylamide) composite hydrogels, studied by two-focus fluorescence correlation spectroscopy “.
<u>University</u> 10/1999 – 07/2007	Academic studies (physics) at the „Heinrich-Heine-Universität Düsseldorf“ <u>Diploma</u> : 31 st July 2007
<u>Military service</u> 09/1998 – 06/1999	Staff soldier
<u>School</u> 08/1995 – 06/1998	School: „bischöfliche Marienschule Mönchengladbach“ 8 th June 1998 Abitur
09/1991 – 06/1995	School: „Städtische Realschule Korschenbroich“
08/1989 – 09/1991	School: „Gemeinschaftshauptschule Korschenbroich“

08/1985 – 06/1989

Elementary school: „Kath. Grundschule St. Maternus“ in
Korschenbroich

Hilden, 14th December 2014

List of publications

Articles

Charge-Induced Conformational Changes of Dendrimers,
Macromolecules 2008

DOI: 10.1021/ma800283z

The role of the N-terminal domain in dimerization and
nucleocytoplasmic shuttling of latent STAT3, *JCS* 2011

DOI: 10.1242/jcs.072520

Spatially Resolved Tracer Diffusion in Complex Responsive
Hydrogels, *JACS* 2012

DOI: 10.1021/ja306808j

Temperature-Sensitive Composite Hydrogels: Coupling Between
Gel Matrix and Embedded Nano- and Microgels, *Prog. Colloid
Polym. Sci.* 2013

DOI: 10.1007/978-3-319-01683-2_8

Diffusion of mesoscopic actives within sensitive core-shell
micogel carriers, *J. Colloid Interface Sci.* 2014

DOI: 10.1016/j.jcis.2014.06.014

Refractive index mismatch can misindicate anomalous diffusion in single-focus fluorescence correlation spectroscopy, *Macromol. Chem. Phys.* 2014

DOI: 10.1002/macp.201400349

Poster presentations

05/2009

108. Bunsentagung, Köln

Title: Tracer diffusion in acrylamide gels and filled acrylamide gels, an observation with two-foci-fluorescence-correlation-spectroscopy

09/2009

44. Hauptversammlung der Deutschen Kolloidgesellschaft, Hamburg

Title: Tracer Diffusion study in filled Acrylamide gels

Oral presentations

07/2011

Workshop of the SPP „intelligente Hydrogele“, Köln

Title: Diffusion measurements in hydrogels with switchable inhomogeneities

10/2010

Workshop of the SPP „intelligente Hydrogele“, Aachen

Title: Spatial resolved diffusion measurements on hydrogels with switchable inhomogeneities via two focus fluorescence correlation spectroscopy